

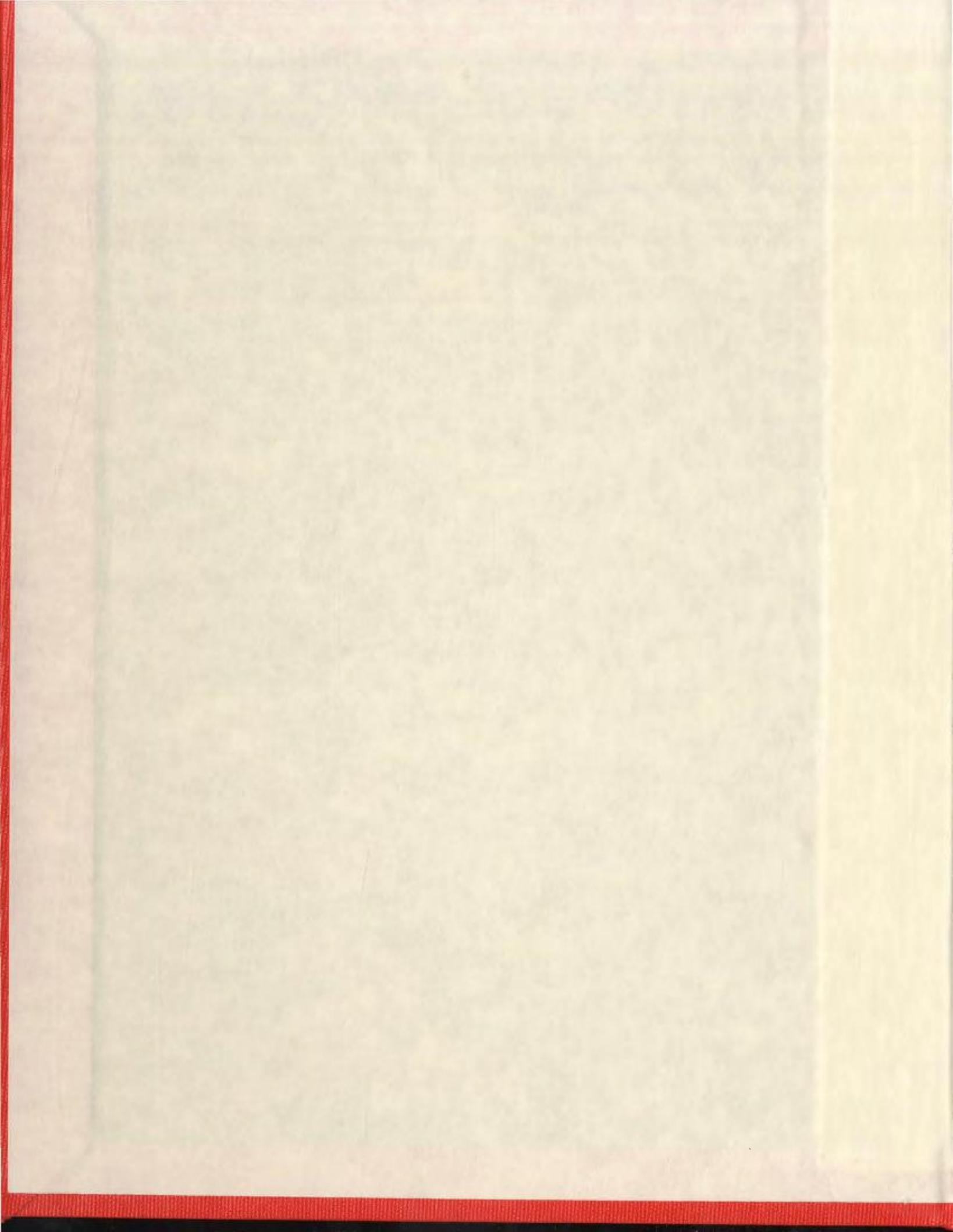
COMPUTATION OF STRESS INTENSITY FACTOR FOR  
THROUGH CRACKS IN PLATES AND BENDING OF  
SHELLS USING P-VERSION FINITE ELEMENT METHOD

CENTRE FOR NEWFOUNDLAND STUDIES

**TOTAL OF 10 PAGES ONLY  
MAY BE XEROXED**

(Without Author's Permission)

RAMALAKSHMI PULLELA





**COMPUTATION OF STRESS INTENSITY FACTOR FOR THROUGH CRACKS  
IN PLATES AND BENDING OF SHELLS USING P-VERSION FINITE  
ELEMENT METHOD**

**By**

**© Ramalakshmi Pullela, B.E.**

**A thesis submitted to the School of Graduate  
Studies in partial fulfilment of the  
requirements for the degree of  
(Master of Engineering)**

**Faculty of Engineering and Applied Science  
Memorial University of Newfoundland**

**September, 2005**

**St John's**

**Newfoundland**

**Canada**



# Abstract

The present study concerns the analysis of bending of plates and shells subjected to various boundary conditions and load. Bending stress intensity factors for plates containing through thickness crack under edge bending load are evaluated. To accomplish the task, hierarchical degenerated plate/shell element and hierarchical 18-node solid thick shell element are developed.

The hierarchical degenerated plate shell element has four corner nodes, four mid-side nodes and one central node on the mid-surface of the shell geometry with five degrees of freedom at each node. For defining the geometry, Lagrangian shape functions were employed. P-version shape functions upto order seven were used for defining the displacement field. Crack tip singular plate/shell element was developed by enriching the displacement field of the element with the asymptotic displacement field near the crack tip. A hierarchical 18-node solid thick shell element has been developed. Sixteen nodes consisting 8 corner nodes and 8 mid-side nodes are used to define the geometry and eighteen nodes for defining the displacement field. Each node has three degrees of freedom.

Some benchmark problems were analyzed in order to check correctness the elements of both plate/shell and thick solid elements. Analyses were performed to obtain the stress intensity factors of plate with through thickness crack using hierarchical degenerated plate/shell element. Numerical results obtained from the present element formulations are compared with analytical/numerical solutions available from literature. It is inferred that numerical results are in good agreement with the benchmark plate and shell problems.

# Acknowledgements

My sincere thanks to my supervisor Dr.K.Munaswamy for his guidance, advice, encouragement and financial support during my study at Memorial University of Newfoundland.

I also want to thank Dr. Ray Gosine, Dean, Faculty of Engineering and Applied Science for his encouragement through out my Masters program here. I would like to thank Dr.R.Venkatesan, Associate Dean, Graduate Studies and Research for the advice provided during my graduate program. I would like to thank Dr.Swamidas, Dr.Adhuri and Dr.Booton for their guidance during my course work.

I am grateful to my brother Dr. V.Rao Pullela and his family for their help and constant encouragement during my studies at Memorial University of Newfoundland.

I would like to thank Indian Community for their kind help during my stay in St.John's. Many thanks to my relatives and friends for their moral support. To my parents for their forbearance and love.

# CONTENTS

Abstract	ii
Acknowledgements	iii
List of Figures	vi
List of Tables	ix
List of Symbols and Abbreviations	x
Chapter 1 INTRODUCTION AND OVERVIEW	1
1.1 Finite Element Method.....	1
1.2 P-version Finite Element Method .....	3
1.3 Plate and Shell with through cracks .....	4
1.4 Objective of the thesis .....	5
1.5 Layout of the thesis .....	6
Chapter 2 BACKGROUND AND SCOPE OF WORK .....	7
2.1 Literature Review .....	7
2.1.1 Plate and Shell elements .....	7
2.1.2 P-version FEM .....	12
2.1.3 Crack tip element .....	14
2.2 Scope of the study .....	18
Chapter 3 ELEMENT FORMULATION	20
3.1 Hierarchical Degenerated Plate/Shell Element .....	20

	3.1.1	Geometric definition of the element .....	21
	3.1.2	Displacement field .....	23
	3.1.3	Stress Strain relationship .....	28
	3.1.4	Element Matrices Evaluation .....	29
	3.1.5	Displacement field near the crack tip for a plate with through thickness crack .....	33
	3.1.6	Enrichment of displacement field for plate element ..	37
	3.2	Hierarchical 18 node Solid Thick Shell Element .....	43
	3.2.1	Geometric definition of the element .....	43
	3.2.2	Displacement field .....	45
	3.2.3	Element Stiffness matrix generation .....	48
Chapter 4		COMPUTER IMPLEMENTATION	49
	4.1	Computer Program .....	49
	4.1.1	Input .....	49
	4.1.2	Shape Function Derivatives .....	52
	4.1.3	Element stiffness matrix evaluation and assembly ...	52
	4.2	Solution Procedure .....	54
	4.2.1	Preconditioned Conjugate Gradient Method .....	55
Chapter 5		NUMERICAL STUDIES AND DISCUSSIONS	58
	5.1	Square plate problem .....	58
	5.2	Barrel Vault problem .....	96
	5.3	Pinched Cylindrical Shell .....	100
	5.4	Stress Intensity Factors Evaluation for Plates subjected to	

	Bending Loads .....	104
	5.4.1 Benchmark problem .....	104
	5.4.2 Bending Stress Intensity factors for plate with central and edge cracks .....	107
Chapter 6	CONCLUSIONS AND RECOMMENDATIONS .....	112
	6.1 Conclusions .....	112
	6.2 Recommendations .....	115
	REFERENCES .....	116
	APPENDICES .....	122
	Shape functions .....	122
	A.1 Hierarchical degenerated plate element .....	122
	A.2 Displacement field shape functions for hierarchical degenerated plate/shell element .....	123
	A.3 Hierarchical 18 node solid plate element .....	124
	A.4 Displacement field shape functions for hierarchical 18 node solid plate element .....	125

# List of Figures

Figure 3.1: Hierarchical Degenerated plate shell element .....	22
Figure 3.2: Local polar coordinate system for through crack in plate .....	33
Figure 3.3: Modes of fracture .....	34
Figure 3.4: Geometry of plate element with through crack .....	37
Figure 3.5: Hierarchical 18 node solid plate element .....	44
Figure 4.1 Organization of the computer program .....	51
Figure 4.3 Pre-conditioned Conjugate Gradient Method.....	57
Figure 5.1: Square plate and meshes used for the analysis.....	61
Figure 5.2: Plot of deflection of SS plate under CL at $l/t$ equal to 66.67 for 4x4 refined mesh (w max is the central deflection according to thin plate theory) .....	63
Figure 5.3: Plot of deflection of SS plate under UDL for $l/t$ equal to 66.67 for 4x4 uniform mesh (w max is the central deflection according to thin plate theory) .	65
Figure 5.4: Plot of deflection of clamped plate under CL for $l/t$ equal to 66.67 for 4x4 uniform mesh (w max is the central deflection according to thin plate theory) .	67
Figure 5.5: Plot of deflection of clamped plate under UDL for $l/t$ equal to 66.67 for 4x4 uniform mesh (w max is central deflection according to thin plate theory) .....	69
Figure 5.6: Plot of deflection of SS plate under UDL for various $l/t$ ratios for 2x2 mesh	71
Figure 5.7: Plot of deflection of SS plate under UDL for various $l/t$ ratios for 4x4 mesh	73
Figure 5.8: Plot of deflection of clamped plate under UDL for various $l/t$ ratios for 2x2 mesh (w max is central deflection according to thin plate theory) .....	75

Figure 5.9: Plot of deflection of clamped plate under UDL for various $l/t$ ratios for 4x4 mesh (w max is central deflection according to thin plate theory).....	77
Figure 5.10: Plot of deflection of SS plate under CL for $l/t$ equal to 66.67 for 4x4 uniform mesh (w max is the central deflection according to thin plate theory).....	80
Figure 5.11: Plot of deflection of SS plate under UDL for $l/t$ equal to 66.67 for 4x4 uniform mesh (w max is the central deflection according to thin plate theory) ...	82
Figure 5.12: Plot of deflection of clamped plate under CL for $l/t$ equal to 66.67 for 4x4 uniform mesh (w max is the central deflection according to thin plate theory) ..	84
Figure 5.13: Plot of deflection of clamped plate under UDL for $l/t$ equal to 66.67 for 4x4 uniform mesh (w max is the central deflection according to thin plate theory) ..	86
Figure 5.14: Plot of deflection of SS plate under UDL for various $l/t$ ratios for 2x2 mesh (w max is the central deflection according to thin plate theory).....	88
Figure 5.15: Plot of deflection of SS plate under UDL for various $l/t$ ratios for 4x4 mesh (w max is the central deflection according to thin plate theory).....	90
Figure 5.16: Plot of deflection of clamped plate under UDL for various $l/t$ ratios for 2x2 mesh (w max is the central deflection according to thin plate theory).....	92
Figure 5.17: Plot of deflection of clamped plate under UDL for various $l/t$ ratios for 4x4 mesh (w max is the central deflection according to thin plate theory).....	94
Figure 5.18: Barrel vault and its finite element meshes.....	97
Figure 5.19: Pinched cylindrical shell, loading and dimensions. ....	101
Figure 5.20: Centre crack under bending moment.....	105
Figure 5.21: Plot of Bending Stress Intensity factor for centre-crack plate under bending moment for different crack lengths at $b/h$ equal to 10.....	107

Figure 5.22: Plot of Bending Stress Intensity factor for centre-crack plate under bending moment for different crack lengths at  $b/h$  equal to 2 ..... 108

Figure 5.23: Plot of Bending Stress Intensity factor for edge-crack plate under bending moment for different crack lengths at  $b/h$  equal to 10 ..... 109

Figure 5.24: Plot of Bending Stress Intensity factor for edge-crack plate under bending moment for different crack lengths at  $b/h$  equal to 2 ..... 110

# List of Tables

Table 5.1: SS Plate under CL: Displacements for different orders ( $l/t = 66.66$ ) .....	62
Table 5.2: SS Plate under UDL: Displacements for different orders ( $l/t = 66.66$ ) .....	64
Table 5.3: Clamped Plate under CL: Displacements for different orders ( $l/t = 66.66$ ) .....	66
Table 5.4: Clamped Plate under UDL: Displacements for different orders ( $l/t = 66.66$ ) ....	68
Table 5.5: SS Plate under UDL: Displacements for different orders for 2x2 mesh .....	70
Table 5.6: SS Plate under UDL: Displacements for different orders for 4x4 mesh .....	72
Table 5.7: Clamped Plate under UDL: Displacements for different orders for 2x2 mesh ..	74
Table 5.8: Clamped Plate under UDL: Displacements for different orders for 4x4 mesh ..	76
Table 5.9: SS Plate under CL: Displacements for different orders ( $l/t = 66.66$ ) .....	79
Table 5.10: SS Plate under UDL: Displacements for different orders ( $l/t = 66.66$ ) .....	81
Table 5.11: Clamped Plate under CL: Displacements for different orders ( $l/t = 66.66$ ) .....	83
Table 5.12: Clamped Plate under UDL: Displacements for different orders ( $l/t = 66.66$ ) ..	85
Table 5.13: SS Plate under UDL: Displacements for different orders for 2x2 mesh .....	87
Table 5.14: SS Plate under UDL: Displacements for different orders for 4x4 mesh .....	89
Table 5.15: Clamped Plate under UDL: Displacements for different orders for 2x2 mesh	91
Table 5.16: Clamped Plate under UDL: Displacements for different orders for 4x4 mesh	93
Table 5.17: Displacements at B and C of cylindrical roof.....	98
Table 5.18: Displacements at B and C of cylindrical roof.....	99
Table 5.19: Deflection under the load of Pinched cylinder .....	102
Table 5.20: Deflection under the load of Pinched cylinder .....	103
Table 5.21: Normalized Stress Intensity factors in a plate containing central crack subjected to uniform bending $M_0$ away from the crack region. $a/b = 0.1$ ...	106

# List of Symbols and Abbreviations

FEA	Finite Element Analysis
2D,3D	Two dimensional, three dimensional
{ }	Column vector
[ ]	Matrix
⟨ ⟩	Row vector
DOF	Degrees of Freedom
UDL	Uniformly Distributed load
CL	Concentrated Load
SS	Simply Supported
PCG	Pre conditioned conjugate gradient method
SIF	Stress Intensity factor
x,y,z	Cartesian coordinates
$\xi,\eta,\zeta$	Curvilinear coordinates
u,v,w	Displacement Components
$\alpha,\beta$	Rotations of normal to the plate/shell surface
h	Thickness of plate/shell
[K]	Global Stiffness matrix
{ $\delta$ }	displacement vector
{F}	Load Vector
N	Shape function

$\{\varepsilon\}$	Strain Vector
$\{\sigma\}$	Stress Vector
E	Young's modulus
$[D']$	Elasticity Matrix
$\gamma$	Poisson's ratio
J	Jacobian matrix
$[B]$	Strain displacement matrix
X,Y,Z	Local Cartesian coordinates of crack front
r, $\theta$	Local polar coordinates of located at the crack tip
$K_I, K_{II}, K_{III}$	Stress intensity factors for mode I, mode II and mode III

# Chapter 1

## INTRODUCTION AND OVERVIEW

### 1.1 Finite Element Method

The *finite element method* is a *numerical* approach by which general differential equations can be solved in an *approximate* manner. It is the characteristic feature of finite element method that instead of seeking approximations that hold directly over the entire region, the region is divided into smaller parts, called finite elements, and the approximation is carried out over each element. As the FE method is a numerical means of solving governing differential equations, it can be applied to various physical phenomena. Applications of finite element method include structural analysis, heat transfer, fluid flow, mass transfer and electromagnetic potential [1] etc. The steps involved in the FEM are: the discretization of the domain into a number of finite domains called elements, evaluation of element properties in the form of element stiffness and load matrices to obtain global stiffness and load matrices and finally solving the resulting linear algebraic equations to obtain the displacements at the nodes.

The discretization process divides the domain into small units, each represented by an element. The discretization is suitably carried out to improve the accuracy and convergence of the solution. The density of the elements at a location in the domain depends upon the geometry and the external load distribution. A sub-domain where there is a complex geometry and sharp edges or stress raiser needs a finer mesh i.e.

higher element density. The discretization should be optimal. It should not lead to too many elements, which increases computational effort. Once the elements are created, element matrices are calculated and then assembled. The resulting system of equations is solved to obtain the solution. Since Finite Element Method is an approximate method, the solution for any analysis is not exact, unavoidable modeling and numerical errors are introduced. Therefore a systematic approach must be implemented to determine the accuracy of the analysis in the finite element solutions.

The most effective approach for determining the accuracy of the solution in finite element solution is to perform 'extensions'. Extensions are step by step changes in the finite element discretization that cause the number of degrees-of-freedom (DOF) to increase at each step, with the goal of reducing numerical error in the solution. DOF can be increased by increasing the number of elements or the polynomial levels of the elements. Reduction of error can be accomplished in  $h$ -refinement or  $h$ -extension and  $p$ -extension. The  $h$ -extension is carried out by increasing the number or density of the finite elements while holding the polynomial order constant. In the second approach ( $p$ -extension) the order of the approximation polynomial for the unknown displacement field is increased while maintaining the number and density of element constant. In practice, the  $h$ -extension process is the least efficient numerically (lowest convergence rates) and the most cumbersome to implement. The  $p$ -refinement can be done for the domain or selectively for few elements where there is a high strain gradient.

## 1.2 P-version Finite Element Method

P-version finite element refinement can be performed by two methods. In the first method regular interpolation functions of higher order are employed by increasing the number of nodes in each element. The second method uses hierarchical interpolation functions as shape functions. The lower order hierarchical shape functions are the subset of the higher order functions. This property of hierarchical shape functions enables the enhancement of computational effort. The element matrices required for the additional degrees of freedom are only needed to be evaluated and assembled thus reducing computational effort. As the regular interpolation functions in the first method do not exhibit this hierarchical property, the element matrices need to be evaluated afresh and assembled.

The hierarchical elements [2] have many advantages over the h-version. The p-version element shows good numerical convergence and the mesh design is less critical because there is always a possibility to increase the element order without changing the mesh division. In h-version, mesh modification by element division is necessary to achieve convergence. Hierarchical shape functions allow more accurate mapping of geometry shapes such as circles. In h-version geometry shapes are mapped with quadratic functions. The size of the input file is small in p-version, as there are fewer elements. These merits contribute to the reduced computational effort and time. The resulting matrices are better conditioned and hence they converge for solving. Also it provides an immediate estimation of the error by comparing successive solutions.

## 1.3 Plate and Shell with through cracks

Plate and curved structural elements in the form of general shells are common in engineering practice. They are observed in pressure vessels, nuclear reactors, aircraft and roof structures. Hence, a significant effort has been directed to the development of a suitable finite element procedure for the analysis of general shell structures. Over the years, hundreds of elements have been developed.

A number of plate elements are available in the literature, which does not use the concept of hierarchical analysis. These elements employ h-version analysis for convergence, which demands more computational effort. Moreover many of these elements suffer from a problem called “Shear locking”. These elements become too stiff and produce displacements far less than the actual value when the thickness is small. This problem is overcome chiefly by modifying the transverse shear strain field, which is cumbersome and involves additional computational effort.

Structural shells [3] are widely used in a broad spectrum of industries e.g. aerospace, automotive, power generation, railroad, ship building and chemical. Very often the usage is characterized by irregularities in the form of discontinuities, complex loading and support conditions over the surface and at the edges.

In the design of such shells it is necessary to account for the aforementioned irregularities, which become the source of singularities in the stress field and hence the potential seat for crack initiation and propagation, affect the fatigue life of the shell under cyclic loading conditions.

The sources of singularities can be classified under three headings

1. Geometric: Re-entrant corners, cracks, cutouts with sharp corners, discontinuities in curvature and thickness, presence of stiffeners, mixed boundary conditions etc.
2. Loading: concentrated sources over the surface and at the edges line sources over the surface, and sudden changes in the intensity of the external sources.
3. Material: Sudden changes in material properties, as in the case of laminated materials.

The stress intensity factors for plane extension and plate bending problems are often useful in discussing the fracture of various structures. For the plane extension problem of cracked plates, many effective finite element codes have been developed and some of them are available for engineers [4] and [5]. For the plate-bending problem of cracked plates, on the other hand, only a few finite element methods have been published [6]. Some investigators [7] and [8] have obtained the singularity solutions for problems based on classical bending theory for stress intensity factors. These values cannot be combined in plane extension and plate bending problems, as the angular distributions of the stress fields in these problems are different around the crack tip [9].

## **1.4 Objective of the thesis**

The objective of this work is to,

- Develop a hierarchical nine-node degenerated plate/shell element, incorporating through thickness crack singularity, with inplane displacement  $u$  and  $v$ , out of plane displacement  $w$  and rotations of normal to the mid surfaces as degrees of freedom for obtaining the stress intensity factors.

- To develop solid thick shell element with in plane displacement  $u$  and  $v$ , and out of plane displacement  $w$  as degrees of freedom for the analysis of thick/ thin plates and shells.
- Demonstrate the advantage of the singular element over the existing ones in the development of finite element code.

To accomplish these objectives, the major requirement is the development of a finite element program for the developed singular shell element. A computer program is developed for obtaining SIF for through cracks in plates and shells. A number of benchmark problems are solved to show the effectiveness and use of the element.

## **1.5 Layout of the thesis**

The first chapter gives an introduction to the various concepts and terminologies relevant to the present work. Chapter two gives a detailed review of the literature and defines the scope of the study. Chapter three gives the formulation of the 9-node hierarchical plate/shell and 18-node solid thick shell elements. It also includes the derivation of various equations and matrices for stress intensity factor evaluation. The computer implementation of the finite element formulation using objected oriented approach is discussed in chapter four. Chapter five presents the numerical results obtained from the analysis of test problems. Conclusions and recommendations are given in chapter six.

# Chapter 2

## BACKGROUND AND SCOPE OF WORK

### 2.1 Literature Review

Finite element analysis is widely applied in many fields of engineering. Almost all finite element problems include the following steps: 1. Data input 2. Calculation of element stiffness matrix and load vectors 3. Assembly of global stiffness and load matrices 4. Application of boundary conditions 5. Solution of equations 6. Post processing the solutions and results output.

These fundamentals are very well explained in the textbooks by many authors like Zienkiewicz [10], Bathe [11] etc. The following sections give a detailed account of literature relevant to the current work.

#### 2.1.1 Plate and Shell elements

Plates and Shells [12] are three-dimensional bodies characterized by the fact that one of the dimensions is much smaller than the other two. The various theories of plates and shells recognize and exploit this. These theories are useful because the quantities of interest in the analyses of plates and shells, such as membrane forces, bending moments and shear forces, are related to certain averages of the displacement across the small dimensions of these three dimensional bodies. This permits reduction of the dimensions in the case of plates and shells from three to two.

Usually plates and shells are stiffened and/or joined with solid bodies. If we have to ensure the reliability and accuracy of computed data without sacrificing computational efficiency then we must be able to model these parts of the structure with three dimensional theories while retaining the simplified assumptions incorporated in plate and shell theories where those assumptions hold.

Several plate and shell theories have been developed by two approaches. The first approach, favored in the engineering literature [13-15] is by prior assumptions concerning the mode of deformation. The second approach is that the solution of the three dimensional differential equations of elasticity expanded by power series so that the powers of thickness parameters are factored. There are several possible variants for this approach [16-19]. The power series expansion can be applied to the differential equations of elasticity or any of the variational formulations of the differential equations of elasticity.

The most widely used conventional plate and shell theories are Kirchoff's plate theory and Reissner-Mindlin theory. In Kirchoff's plate theory transverse shear strains and normal strains are neglected; whereas Reissner-Mindlin theory takes into account deformations caused by transverse shear forces. Over the years, hundreds of plate and shell elements have been developed. They are put into three categories depending upon the mathematical principles employed.

Bathe and Ho [20] suggested that were three approaches were being followed in the development of plate and shell elements.

1. A particular shell theory is used and discretized.
2. Three dimensional continuum equations were used and discretized.

3. Plate bending and membrane element stiffness were superimposed and assembled in a global co-ordinate system.

The three approaches have advantages and disadvantages, and it is still difficult to state which of the three approaches is most effective based on criteria combining accuracy, computational cost and simplicity in use. Considering approach three, triangular flat elements having displacements and rotations at the corner nodes as degrees of freedom are particularly appealing for many practical reasons; for example, arbitrary shell geometries, general supports and cut outs, and beam stiffeners can be modeled. Alternative formulations of three noded triangular plate-bending elements have been presented in the literature vide; a DKT (Discrete Kirchhoff theory) element, a HSM (Hybrid Stress Model) element and a SRI (Selective reduced integration) element.

Displacement based Kirchhoff plate theory element formulation [21 and 22] was based on the principle of minimum potential energy, where the compatibility requirements involve displacements and rotations. Their ineffectiveness is due to incompleteness, incompatibility, and lack of invariance with regard to element orientation and singularity. It was then realized that it is impossible to formulate a compatible triangular element with nine degrees of freedom with a single-field polynomial expansion for  $w$ . One of the first compatible triangular elements is the well-known HCT element. Its formulation was based on the subdivision of the complete element into three sub triangles. An incomplete cubic (9- term) polynomial was used in each sub region for the displacement  $w$ , and the normal slope along the exterior edge of each region varies linearly. The HCT element has frequently been regarded as a reference element for bending analysis of plates, mainly because of the extensive numerical results presented

with its formulation. However, the formulation involves cumbersome algebraic manipulations and the element is rather stiff.

The hybrid stress method [23] was developed to overcome the difficulties that were encountered in the development of pure displacement models due to element compatibility requirements. The most effective and also simplest element is called the HSM element. This triangular bending element was derived from Kirchhoff plate theory. The element has a linear distribution of bending moments in the interior and a cubic displacement variation with a linear normal slope variation along the edges of the element. The derivation of the stiffness matrices of hybrid stress elements appears to be rather cumbersome, and the evaluation of the element matrices appears to involve more algebraic manipulations and computer storage than comparative displacement models.

The formulation of elements based on the discrete Kirchhoff theory for bending of thin plates was obtained by first considering theory of plates including transverse shear deformations. The transverse shear energy is neglected altogether and the Kirchhoff hypothesis is introduced in a discrete way along the edges of the element to relate the rotations to the transverse displacements. This approach has been used to formulate effective nine degrees of freedom triangular bending elements that converge to the classical thin plate solution. The final result is that the DKT element has not received widespread adoption and has also not been implemented in any major computer code.

Recent and somehow successful developments of a beam element, quadrilateral plate elements and axisymmetric shell elements, based on selective reduced integration concepts and the theory of plates including transverse shear effects, suggest that a simple selectively integrated triangular plate element with 9 degrees of freedom may be

effective. Based on the results employing this element, it was concluded that the element is not effective when compared with the HSM and DKT elements.

The theory of plates with transverse shear deformations included (the plate theory of Reissner or Mindlin) uses a generalization of the Kirchhoff hypothesis 'a point of the plate originally on the normal to the undeformed middle surface'. For thin plates the transverse shear strains and therefore the transverse shear strain energy  $U_s$  are negligible compared to the bending energy.

Cook [24] developed a 24-degree of freedom quadrilateral shell element by the very simple process of combining standard membrane and bending formulation with a device for membrane-bending coupling and a device for inclusion of warping effects. The membrane element is of the isoparametric type and is numerically integrated using a 2x2 Gauss rule. For membrane action there is three DOF at each corner  $i$ , consisting of x and y translations  $u_i$  and  $v_i$  and drilling rotation  $\theta_{zi}$ , positive counter clockwise.

Roufaeil [25] developed three rectangular plate-bending elements. They have 14 and 16 degrees of freedom and are displacement based Mindlin plate theory elements. The shape functions of the displacement and rotations are not completely independent. Numerical results were presented for problems involving rectangular plates of different aspect ratios and support conditions. The elements perform quite well for the class of problems studied and do not show any sign of the 'shear locking' phenomenon for thin plates.

## 2.1.2 P-version FEM

The concept of p-version finite element analysis is relatively new. A large number of papers have been published on this subject and its merits over h-version are well proved. One of the first works on p-version FEM is by Peano [26]. New hierarchies of this family of the finite element is that the shape functions corresponding to an interpolation of order  $p$ , constitute the subset of higher order interpolation functions greater than  $p$ . Hence the stiffness matrix of the element of order  $p$ , forms the subset of stiffness matrices of higher orders greater than  $p$ . This development gives rise to new families of finite elements, which are computationally efficient.

The elemental arrays of higher polynomial order can be efficiently computed using hierarchical elements with precomputed arrays. These precomputed arrays are computed once and stored in a permanent file, which can be used in all subsequent applications of the program. Rossow and Kutz [27] showed that the use of hierarchical elements with precomputed arrays are competitive in terms of computational efficiency compared to conventional finite element method.

The advantages of the hierarchical approach are presented by Zienkiewicz et al [28]. They showed the hierarchical nature of the stiffness matrices. The condition of the stiffness matrix increases because of the appearance of hierarchical variables as a perturbation on the original solution. This ensures a faster rate of iteration convergence. The perturbation nature of the hierarchical form has a further merit of providing an immediate measure of the error in the solution, by analyzing the displacement solutions of successive orders.

A proper mesh design increases the performance of p-refinement attainable by the finite element method. Szabo [29] gives the guidelines for prior mesh design for the P-version FEM. Babuska et al [30] discuss the optimal selection of shape functions for p-type finite elements. They also discuss the efficacy of the conjugate gradient and multilevel iteration methods for solving the linear system.

The hierarchical linear equation sets can be efficiently solved by using a proper solution strategy. Morris et al [31] developed an algorithm, which has the ability to choose dynamically between iterative and direct solvers. It can also adjust the preconditioning in iterative solvers dynamically. The combination of direct and iterative solvers gives an efficient solution path, combining the advantages of both the solvers.

Woo and Basu [32] presented a new hierarchical p-version cylindrical shell element for the analysis of singular cylindrical shells. They used the Legendre polynomial shape functions for the approximation of the displacement field. A blend mapping function exactly maps the curved boundaries using the exact geometric parameters. The Legendre polynomials are able to oscillate with increased frequency near the end points and thus are better suited to approximating singular behavior. The stiffness matrix based on this element is well conditioned even at higher p-levels and hence gives faster convergence. This p-version cylindrical shell element is very efficient in terms of accuracy and computational efficiency compared to h-version cylindrical elements.

Szabo and Sahrman [33] presented a 4-node 2-D element and an 8-node 3-D solid element for the analysis of shells. The work done by Surana and Sorem [34] is of special interest here. They developed hierarchical three-dimensional curved shell element

based on the p-version concept. The geometry of the element is described by the coordinates of the nodes in its middle surface and nodal vectors describing its top and bottom surfaces. The element displacement function can be of any arbitrary and different polynomial order. The approximation functions and their corresponding hierarchical variables are obtained by first constructing the approximation functions and nodal variables for each of the three directions and then taking the tensor product. Here both the displacement functions and nodal variables are hierarchical and hence so are the element matrices. The formulation is effective for both thin and thick plates. The usage of hierarchical variables in the thickness direction increases the number of degrees of freedom greatly, which increases the computational burden. Sethuramalingam [35] has used similar concept to develop plate/shell element for analyzing plate and shell problems and showed the advantages of using p-version FEM.

### **2.1.3 Crack tip element**

Plate and shell formulations are widely used to analyze thin-walled structures such as aircraft fuselages subjected to bending and pressure loads. Through-the-thickness cracks (often called as through cracks) may develop when these structures are subjected to cyclic loads, and the determination of mixed-mode stress intensity factors is critical to the modeling of fatigue crack propagation. Despite the practical importance, relatively little research has focused on developing robust numerical methods to determine fracture parameters and simulate crack growth in thin plates.

The finite element method has been used extensively in fracture mechanics and numerous singular elements have been developed. The analysis of plate members

containing through thickness flaws and subjected to bending load has been a subject of controversy during the past decade. Unlike the case of thin plates acted on by in-plane loads, where the use of two dimensional elasticity theory, provides an effective means of deriving stress intensity factor solutions predictions of elastic fields for comparable structures subjected to bending loads is influenced by the specific plate theory by which the analysis is performed [extended finite element method].

Ganti [36] has developed two dimensional crack tip p-version plane elements incorporating near crack tip displacement field to obtain stress intensity factors of plane elasticity problems. Ahmad and Loo [37] developed a special crack-tip finite element to obtain the bending and shear stress intensity factors for thin elastic plates containing crack. The bending and shear stress intensity factors were then used to compute the Strain Energy Density factor and the direction of crack initiation. A triangular crack tip element, which was based on a displacement function derived from William's expansion [7], was developed. The crack tip elements were used only in the vicinity of the tip of the crack while conventional 9 degrees of freedom triangular plate bending elements were used in the rest of the domain. Yagawa and Nishioka [38] analyze stress intensity factors for plates in bending where the displacement field was made up of terms from the isoparametric shell element of Zienkiewicz, Taylor and Loo [39], supplemented by terms from the crack tip solution of Williams. They employed singular element where behavior of the in plane displacements is based on transverse shear while out-of-plane displacements were governed by classical plate theory. Reasonable results were obtained despite the apparent conflict of physical theories.

Chen and Chen [40] proposed a hybrid-displacement finite element model for the bending analysis of thin cracked plates subjected to static and dynamic loading. The variational principle, governing the assumed hybrid displacement finite element model for the fracture mechanics of the singular region, is the modified Hamilton's principle. In this functional the transverse shear effect is ignored due to the use of Kirchoff's hypothesis.

Ye and Gallagher [41] created yet another singularity element based on classical plate theory for analysis of plate bending problems. Singularity formulation of a triangular plate-bending element is by approximation of the displacement field by the combination of the singular solutions of the plate bending equation. The bending intensity factor  $K_B$  for a rectangular plate containing a center crack and subjected to purely cylindrical bending was studied. Singular elements were used only in the region surrounding the crack tip while the DKT element was used in the rest of the plate. Explicit integration was carried out to compute the stiffness matrix terms.

Watanabe et.al [42] proposed a new evaluation method using thick shell elements to calculate the distribution of the J-integral values along crack fronts of through-wall cracks in plate and shell structures. Dividing tentatively the thick shell element into several layers in the thickness direction, integral paths were defined at each layer to obtain the thickness distributions of the J-integral values of through-wall cracks in plate and shell structures. Curved quadrilateral reduced integration thick shell element derived from 20-node isoparametric solid element proposed by Ahmad et.al [43] was employed to analyze the stress of plate and shell structure. Stiffness matrix was evaluated using reduced integration technique. The distributions of the J-integral values along the crack

fronts are compared between the present method using the thick shell element and that using the three-dimensional solid elements.

Go et al [44] formulated a super-element for the dynamic problem of a cracked plate by considering a geometric series of similar elements. This group of elements was generated layer-by-layer approaching infinitely small size around the point of singularity.

Ehlers [45] used eight-noded isoparametric shell element with three translational and two rotational degrees of freedom. Due to the rotational degrees of freedom the element is capable of transverse deformation; thus its formulation corresponds to a general thin shell theory. Results for stress intensity factors derived from shallow shell theory are rigorously valid only for very short cracks.

Agnihotri [46] proposed a two-dimensional finite element model to study the stress distribution of a cracked plate subjected to mechanical “mode I” loading and a plane strain constraint. The effect of singularity near the crack tip has been examined and is overcome by introducing 12-noded cubic isoparametric elements. The cubic isoparametric element is collapsed into a triangular element by placing the two side nodes of a side at  $1/9$  and  $4/9$  of the length of the side from the crack tip.

Vafai and Estekanchi [47] studied the overall behavior of plates and shells as affected by the presence of a through crack in the elastic range. This overall view is important if the general stability and integrity of the structure as a whole is to be investigated. Due attention has been focused on FE modeling of the problem and the significance of various parameters such as the order of mesh refinement at the crack tip area and the effect of the boundary conditions on the results obtained from the analysis.

The effect of Poisson's ratio and geometric parameters such as crack length and shell curvature were also studied.

Murthy et al [48] developed a general solution to the symmetric bending stress distribution at the tip of a crack in a plate taking shear deformation into account through Reissner's theory. The solution was obtained in terms of polar coordinates at the crack tip and includes the complete class of solutions satisfying all the three boundary conditions along the crack. Analysis in their work took finiteness of the plate into account. The aim was to develop a general solution, which could be readily applied to wide class of problems. While the analysis in earlier studies was based on the integral equation approach, this analysis used the differential equation approach.

The complete class of possible solutions was obtained for symmetric bending stresses in the vicinity of a crack tip in a plate taking shear deformation into account through the use of Reissner's theory.

The analysis was carried out for the case of symmetric bending of the plate with respect to the crack. Also, the analysis was carried out for the case where there was no normal loading on the plate. In other words, the solutions obtained could be used in a situation where the plate is subjected only to known edge loads or known kinematic constraints on the exterior boundary.

## **2.2 Scope of the study**

P-version hierarchical crack tip element and plate shell element is developed using OOP concept. The plate shell element has five degrees of freedom, three translations in the global cartesian directions and two rotations in the local axes.

Isoparametric element is used to define the geometry of the element having nodal coordinates and the nodal vector perpendicular to the midplane. The displacement approximation functions are hierarchical in nature and derived from Lagrangian family. The degrees of freedom at mid nodes are hierarchical in nature. The degrees of freedom at the corner nodes are the displacements  $u$ ,  $v$ , and  $w$  in the global  $X$ ,  $Y$ ,  $Z$ -axes and the rotations in the local axes. The element matrices are evaluated by using both full integration ( $p+1$ ) and reduced integration ( $p$ ) techniques.

The element matrices are evaluated using numerical integration. As the order of the approximation polynomial function increases, the number of Gaussian points has to be increased to obtain the element matrices. This increases the computational effort required for element generation.

Standard example problems from references are chosen for verifying the performance of the element. A square isotropic plate subjected to different boundary and loading conditions is analyzed. The plate is also analyzed by varying the thickness. Results are compared with the analytical solutions. A cylindrical barrel vault under self-weight is analyzed. This is a test example for shells in which the bending action is severe. A pinched cylindrical shell is also analyzed. Bending Stress intensity factor for an infinite plate with a through-thickness central crack subjected to a far end moment is determined. For rectangular plate subjected to edge moment away from the crack region, bending stress intensity factors are evaluated for various crack length to width ratios. The results are compared with the reference values from the literature. The effectiveness of the element is demonstrated.

# Chapter 3

## ELEMENT FORMULATION

The present work discusses the isoparametric formulation of the plate and shell element including geometric definition of the element, shape functions, displacement fields, Jacobian matrix, strain-displacement matrix and stress-strain matrix. The principle of displacement finite element approach is used to determine the stiffness matrix and nodal force vector. Solution method involves finding the displacements from the equation  $[K]\{\delta\} = \{F\}$  where  $[K]$  is the global stiffness matrix,  $\{\delta\}$  is displacement vector and  $\{F\}$  is load vector. The analysis includes development of p-version finite element model for the bending of thin/moderately thick plates by enriching the displacement field with nearfield crack displacements and bending of shells.

### 3.1 Hierarchical Degenerated Plate/Shell Element

In this study, the displacement finite element approach is used. In this formulation, it is assumed that the normal to the middle surface remains practically normal after deformation. This assumption permits the shear deformation, which is very important in the thick shell situation. The strain energy corresponding to the strain perpendicular to the middle surface is ignored for simplification. The element has four corner nodes, four mid side nodes and one central node with five degrees of freedom at each node. The degrees of freedom consist of displacements in the X, Y, Z directions and

rotations of vector normal to the middle surface about two orthogonal directions normal to it.

### 3.1.1 Geometric definition of the element

Consider a typical shell element in Figure 3.1. The geometry of the element is defined using eight nodes as shown in figure. The nodes are located at the middle surface. The external surfaces of the element are curved and the sections across the thickness are straight. Two curvilinear coordinates  $\xi, \eta$  in the middle plane and a linear coordinate  $\zeta$  in the thickness direction are used to define the geometry. The local coordinates  $\xi, \eta$  and  $\zeta$  vary between -1 and 1. The top and bottom coordinates define the shape of the element. The relationship between the cartesian coordinates and the curvilinear coordinates for any point in the element is given by:

$$\begin{Bmatrix} x \\ y \\ z \end{Bmatrix} = \sum_{i=1}^8 N_i(\xi, \eta) \begin{Bmatrix} x_i \\ y_i \\ z_i \end{Bmatrix}_{mid} + \sum_{i=1}^8 N_i(\xi, \eta) \frac{\zeta}{2} v_{3i} \quad (3.1)$$

where,

$$v_{3i} = \begin{Bmatrix} x_i \\ y_i \\ z_i \end{Bmatrix}_{mid} - \begin{Bmatrix} x_i \\ y_i \\ z_i \end{Bmatrix}_{bottom} \quad (3.2)$$

$N_i(\xi, \eta)$  is a serendipity approximation shape function. The subscript *top*, *bottom* and *mid* indicates top, bottom and mid planes respectively. The subscript *i* refer to the element node number. The mid-plane coordinates are evaluated from the average of top and bottom co-ordinates.

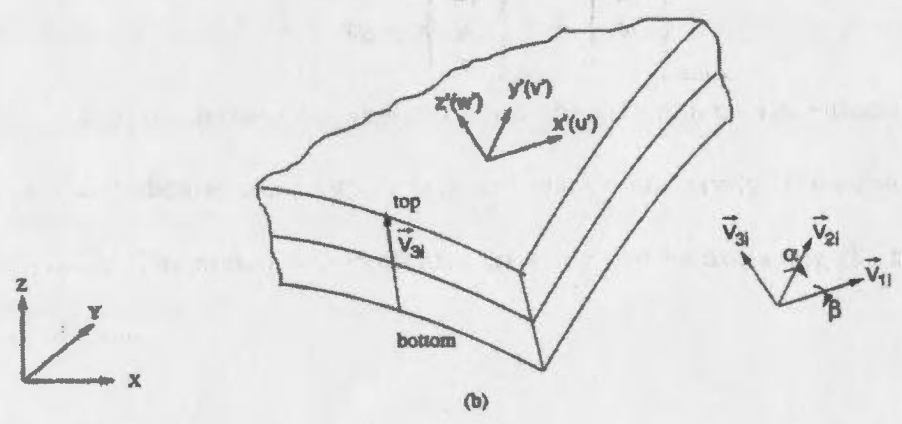
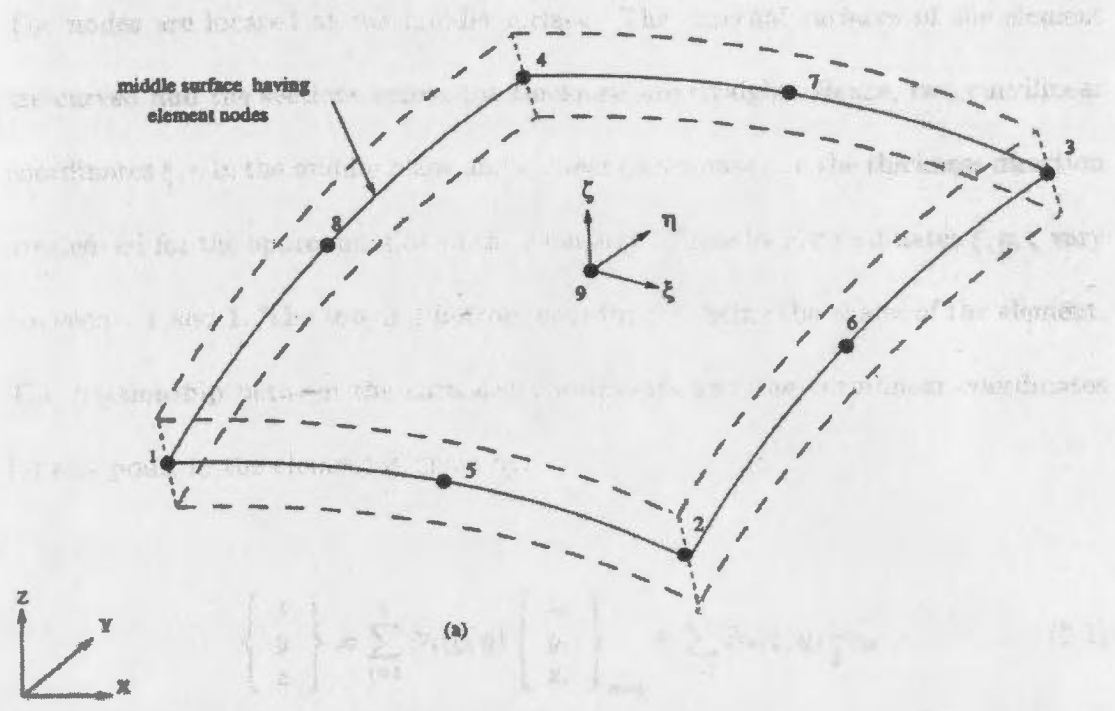


Figure 3.1: Hierarchical Degenerated plate shell element

### 3.1.2 Displacement field

The inplane displacements  $u(\zeta)$  and  $v(\zeta)$  and out of plane displacements  $w(\zeta)$  along the thickness direction at each node is given as

$$\begin{aligned} u_i(\zeta) &= u_{oi} + \zeta \frac{h_i}{2} (v_{1i}^1 \alpha_i - v_{2i}^1 \beta_i) \\ v_i(\zeta) &= v_{oi} + \zeta \frac{h_i}{2} (v_{1i}^2 \alpha_i - v_{2i}^2 \beta_i) \\ w_i(\zeta) &= w_{oi} + \zeta \frac{h_i}{2} (v_{1i}^3 \alpha_i - v_{2i}^3 \beta_i) \end{aligned} \quad (3.3)$$

where  $u_{oi}$ ,  $v_{oi}$  and  $w_{oi}$  are displacement components at node  $i$  on mid-surface,  $h_i$ , thickness of the plate/shell at node  $i$ ,  $\alpha_i$  and  $\beta_i$  are rotations of normal to the surface about  $x$  and  $y$  axes respectively,  $v_{1i}^j$  is the  $j^{\text{th}}$  component of vector  $\{v_{1i}\}$  at node  $i$  and  $v_{2i}^j$  is the  $j^{\text{th}}$  component of vector  $\{v_{2i}\}$  at node  $i$  and  $\zeta$  is the curvilinear co-ordinate along the normal to mid surface. The vectors  $\overline{v_{1i}}$  and  $\overline{v_{2i}}$  are normal to the vector  $\overline{v_{3i}}$ .  $\overline{v_{3i}}$  is the vector normal to the middle surface as defined in equation (3.2). The vectors  $\overline{v_{1i}}$  and  $\overline{v_{2i}}$  are uniquely defined as:

$$\begin{aligned} \overline{v_{1i}} &= \frac{j \times \overline{v_{3i}}}{|j \times \overline{v_{3i}}|} \\ \overline{v_{2i}} &= \frac{\overline{v_{3i}} \times \overline{v_{1i}}}{|\overline{v_{3i}} \times \overline{v_{1i}}|} \end{aligned}$$

The membrane displacement  $u(\zeta)$  within the element in terms of curvilinear coordinates  $\xi$  and  $\eta$  can be written as

$$\begin{aligned}
u(\zeta) &= a_1 + a_2\xi + a_3\eta + a_4\xi\eta + a_5\xi^2 + a_6\eta^2 + a_7\xi^2\eta + a_8\xi\eta^2 + a_9\xi^2\eta^2 \\
&= [P]\{a\}
\end{aligned} \tag{3.4}$$

The displacement components at the nodes are determined by substituting appropriate curvilinear co-ordinates of the nodes. At the corner nodes, the displacement components  $u, v$  and  $w$  and rotations of the normal to the mid-surface are the degrees of freedom. The hierarchical degrees of freedom of the displacement components and rotations used as degrees of freedom at the mid-side nodes and central node are as follows:

$$\frac{\partial^2 u_i(\zeta)}{\partial \xi^2}, \frac{\partial^2 v_i(\zeta)}{\partial \xi^2}, \frac{\partial^2 w_i(\zeta)}{\partial \xi^2} \text{ at nodes 5 and 7}$$

$$\frac{\partial^2 u_i(\zeta)}{\partial \eta^2}, \frac{\partial^2 v_i(\zeta)}{\partial \eta^2}, \frac{\partial^2 w_i(\zeta)}{\partial \eta^2} \text{ at nodes 6 and 8}$$

$$\frac{\partial^4 u_i(\zeta)}{\partial \xi^2 \partial \eta^2}, \frac{\partial^4 v_i(\zeta)}{\partial \xi^2 \partial \eta^2}, \frac{\partial^4 w_i(\zeta)}{\partial \xi^2 \partial \eta^2} \text{ at central node 9}$$

By substituting appropriate curvilinear co-ordinates at the nodes, into equation (3.4), we get

$$\{\delta(\zeta)\} = [C]\{a\} \tag{3.5}$$

$$\{a\} = [C]^{-1} \{\delta(\zeta)\} \tag{3.6}$$

where  $\{\delta(\zeta)\}$  is given by

$$\delta_i = u_{oi} + t \frac{h_i}{2} (v^1_{1i} \alpha_i - v^1_{2i} \beta_i) \quad \text{for } i = 1, 2, 3, 4$$

$$\delta_i = \frac{\partial^2 u_{oi}}{\partial \xi^2} + \zeta \frac{h_i}{2} \left( v^1_{1i} \frac{\partial^2 \alpha_i}{\partial \xi^2} - v^1_{2i} \frac{\partial^2 \beta_i}{\partial \xi^2} \right) \quad \text{for } i = 5 \text{ and } 7$$

$$\delta_i = \frac{\partial^2 v_{oi}}{\partial \eta^2} + \zeta \frac{h_i}{2} \left( v^1_{1i} \frac{\partial^2 \alpha_i}{\partial \eta^2} - v^1_{2i} \frac{\partial^2 \beta_i}{\partial \eta^2} \right) \quad \text{for } i = 6 \text{ and } 8$$

$$\delta_i = \frac{\partial^4 u_{oi}}{\partial \xi^2 \partial \eta^2} + \zeta \frac{h_i}{2} \left( v^1_{1i} \frac{\partial^4 \alpha_i}{\partial \xi^2 \partial \eta^2} - v^1_{2i} \frac{\partial^4 \beta_i}{\partial \xi^2 \partial \eta^2} \right) \quad \text{for } i = 9$$

Substituting equation (3.6) into equation (3.4) we get

$$u(\zeta) = [P][C]^{-1} \{\delta\} \quad (3.7)$$

Instead of inverting  $[C]$  matrix and pre-multiplying with  $[P]$  matrix, we can rewrite the equation (3.7) using standard procedure involving shape functions as

$$u(\zeta) = [N] \{\delta\} \quad (3.8)$$

where  $[N]$  is the hierarchical shape function (see Appendix ). Substituting for  $\{\delta\}$  in terms of displacement degrees of freedom, we can write second order displacement interpolation function for  $u(\xi, \eta, \zeta)$  as

$$u(\xi, \eta, \zeta) = \sum_{i=1}^4 N_i u_{oi} + \sum_{i=1}^4 \zeta \frac{h_i}{2} N_i (v^1_{1i} \alpha_i - v^1_{2i} \beta_i) \\ + \sum_{i=5}^9 N_i u_{oi} + \sum_{i=5}^9 \zeta \frac{h_i}{2} N_i (v^1_{1i} \alpha_i - v^1_{2i} \beta_i) \quad (3.9)$$

where

Defining  $N_{gi} = \zeta \frac{h_i}{2} N_i$

The equation (3.9) can be rewritten as

$$\begin{aligned}
 u(\xi, \eta, \zeta) = & \sum_{i=1}^4 N_i u_{oi} + \sum_{i=1}^4 N_{gi} (v^1_{1i} \alpha_i - v^1_{2i} \beta_i) \\
 & + \sum_{i=5}^9 N_i u''_{oi} + \sum_{i=5}^9 N_{gi} (v^1_{1i} \alpha_i'' - v^1_{2i} \beta_i'')
 \end{aligned} \tag{3.10}$$

where ( )'' denotes the partial derivative with respect to  $\xi, \eta$  at the respective nodes on mid sides

Similarly the displacement distribution for  $v$  and  $w$  can be written as

$$\begin{aligned}
 v(\xi, \eta, \zeta) = & \sum_{i=1}^4 N_i v_{oi} + \sum_{i=1}^4 N_{gi} (v^2_{1i} \alpha_i - v^2_{2i} \beta_i) \\
 & + \sum_{i=5}^9 N_i v''_{oi} + \sum_{i=5}^9 N_{gi} (v^2_{1i} \alpha_i'' - v^2_{2i} \beta_i'')
 \end{aligned} \tag{3.11}$$

$$\begin{aligned}
 w(\xi, \eta, \zeta) = & \sum_{i=1}^4 N_i w_{oi} + \sum_{i=1}^4 N_{gi} (v^3_{1i} \alpha_i - v^3_{2i} \beta_i) \\
 & + \sum_{i=5}^9 N_i w''_{oi} + \sum_{i=5}^9 N_{gi} (v^3_{1i} \alpha_i'' - v^3_{2i} \beta_i'')
 \end{aligned} \tag{3.12}$$

Following the same procedure higher order displacement functions can be written as

$$\begin{aligned}
 u(\xi, \eta, \zeta) = & \sum_{i=1}^4 N_i u_{oi} + \sum_{i=1}^4 N_{gi} (v^1_{1i} \alpha_i - v^1_{2i} \beta_i) \\
 & + \sum_{p=2}^{p_{\max}} \sum_{i=5}^9 N_{pi} u'^p_{oi} + \sum_{p=2}^{p_{\max}} \sum_{i=5}^9 N_{gpi} (v^1_{1i} \alpha_i'^p - v^1_{2i} \beta_i'^p)
 \end{aligned} \tag{3.13}$$

where  $u'_{oi}$  = mid surface displacement at the corner nodes 'i'

$$u'_{oi}{}^p = \frac{\partial^p u_{oi}}{\partial \xi^p} \quad \text{at node } i \text{ for } i = 5 \text{ and } 7$$

$$\begin{aligned}
&= \frac{\partial^p u_{oi}}{\partial \eta^p} \quad \text{at node } i \text{ for } i = 6 \text{ and } 8 \\
&= \frac{\partial^{2p} u_{oi}}{\partial \xi^p \partial \eta^p} \quad \text{at central node } i = 9
\end{aligned}$$

$\alpha_i, \beta_i$  = Rotation of normal about x and y axes at corner nodes i, i = 1 to 4

$$\alpha_i'^p = \frac{\partial^p \alpha_i}{\partial \xi^p} \quad \text{at node } i, i = 5 \text{ and } 7$$

$$= \frac{\partial^p \alpha_i}{\partial \eta^p} \quad \text{at node } i, i = 6 \text{ and } 8$$

$$= \frac{\partial^{2p} \alpha_i}{\partial \xi^p \partial \eta^p} \quad \text{at central node } i = 9$$

$$\beta_i''^p = \frac{\partial^p \beta_i}{\partial \xi^p} \quad \text{at node } i, i = 5 \text{ and } 7$$

$$= \frac{\partial^p \beta_i}{\partial \eta^p} \quad \text{at node } i, i = 6 \text{ and } 8$$

$$= \frac{\partial^{2p} \beta_i}{\partial \xi^p \partial \eta^p} \quad \text{at central node } i = 9$$

Similarly, the other displacement components can be written as

$$\begin{aligned}
v(\xi, \eta, \zeta) &= \sum_{i=1}^4 N_i v_{oi} + \sum_{i=1}^4 N_{gi} (v_{1i}^2 \alpha_i - v_{2i}^2 \beta_i) \\
&\quad + \sum_{p=2}^{p_{\max}} \sum_{i=5}^9 N_{pi} v_{oi}'^p + \sum_{p=2}^{p_{\max}} \sum_{i=5}^9 N_{gpi} (v_{1i}^2 \alpha_i'^p - v_{2i}^2 \beta_i''^p)
\end{aligned} \tag{3.14}$$

$$\begin{aligned}
w(\xi, \eta, \zeta) &= \sum_{i=1}^4 N_i w_{oi} + \sum_{i=1}^4 N_{gi} (v_{1i}^3 \alpha_i - v_{2i}^3 \beta_i) \\
&\quad + \sum_{p=2}^{p_{\max}} \sum_{i=5}^9 N_{pi} w_{oi}'^p + \sum_{p=2}^{p_{\max}} \sum_{i=5}^9 N_{gpi} (v_{1i}^3 \alpha_i'^p - v_{2i}^3 \beta_i''^p)
\end{aligned} \tag{3.15}$$

### 3.1.3 Stress Strain relationship

The strain [10] components in directions of orthogonal axes related to the surface where  $\zeta$  is constant are essential if account is to be taken of the basic shell assumptions. Thus the strain components normal to this surface  $z'$  and along the two orthogonal axes  $x'$  and  $y'$  are given simply with strain in direction  $z'$  neglected.

The strain matrix is given by

$$\left\{ \varepsilon' \right\} = \begin{Bmatrix} \varepsilon_{x'} \\ \varepsilon_{y'} \\ \gamma_{x'y'} \\ \gamma_{x'z'} \\ \gamma_{y'z'} \end{Bmatrix} = \begin{Bmatrix} \frac{\partial u'}{\partial x'} \\ \frac{\partial v'}{\partial y'} \\ \frac{\partial u'}{\partial y'} + \frac{\partial v'}{\partial x'} \\ \frac{\partial w'}{\partial x'} + \frac{\partial u'}{\partial z'} \\ \frac{\partial w'}{\partial y'} + \frac{\partial v'}{\partial z'} \end{Bmatrix} \quad (3.16)$$

To derive the properties of a finite element the essential strains and stresses have to be defined. If the element is assumed to be a basic shell element, the strain component along  $z'$  direction (normal to the surface  $\zeta = \text{constant}$ ) is assumed to be zero or neglected. Thus at any point in this surface ( $\zeta = \text{constant}$ ) if we erect a normal  $z'$  with two other orthogonal axes  $x'$  and  $y'$  tangent to it, the strain components are simply given by the three-dimensional relationships. Neglecting normal strain in direction  $z'$  in accordance with shell assumption. The stress-strain relationships can now be written as

$$\left\{ \sigma' \right\} = \begin{Bmatrix} \sigma_{x'} \\ \sigma_{y'} \\ \tau_{x'y'} \\ \tau_{x'z'} \\ \tau_{y'z'} \end{Bmatrix} = [D'] \left\{ \varepsilon' \right\} \quad (3.17)$$

where  $D'$  is the isotropic material property matrix and is given by

$$[D'] = \frac{E}{1-\nu^2} \begin{bmatrix} 1 & \nu & 0 & 0 & 0 \\ \nu & 1 & 0 & 0 & 0 \\ 0 & 0 & \frac{1-\nu}{2} & 0 & 0 \\ 0 & 0 & 0 & \frac{1-\nu}{2k} & 0 \\ 0 & 0 & 0 & 0 & \frac{1-\nu}{2k} \end{bmatrix} \quad (3.18)$$

Here  $E$  and  $\nu$  are Young's modulus and Poisson's ratio. The factor  $k$  is included to improve shear displacement approximation. The value of  $k$  is 6/5 and it is the ratio of relevant strain energies.

### 3.1.4 Element Matrices Evaluation

The derivatives of the displacement with respect to the global  $X, Y, Z$  coordinates are given by the relation,

$$\begin{bmatrix} u_{,x} & v_{,x} & w_{,x} \\ u_{,y} & v_{,y} & w_{,y} \\ u_{,z} & v_{,z} & w_{,z} \end{bmatrix} = [J]^{-1} \begin{bmatrix} u_{,\xi} & v_{,\xi} & w_{,\xi} \\ u_{,\eta} & v_{,\eta} & w_{,\eta} \\ u_{,\zeta} & v_{,\zeta} & w_{,\zeta} \end{bmatrix} \quad (3.19)$$

where  $[J]$  is the Jacobian matrix given by:

$$[J] = \begin{bmatrix} x_{,\xi} & y_{,\xi} & z_{,\xi} \\ x_{,\eta} & y_{,\eta} & z_{,\eta} \\ x_{,\zeta} & y_{,\zeta} & z_{,\zeta} \end{bmatrix} \quad (3.20)$$

Here a comma (,) followed by a subscript indicates the partial differentiation with respect to the subscript. These derivatives of the displacements are transformed to the local displacement directions  $x', y', z'$  for the evaluation of strains. The directions of the local axes are established by the following method.

A vector normal to the shell surface is found by the cross product of two vectors tangential to the surface and it is given by:

$$V_3 = \begin{Bmatrix} x_{,\xi} \\ y_{,\xi} \\ z_{,\xi} \end{Bmatrix} \times \begin{Bmatrix} x_{,\eta} \\ y_{,\eta} \\ z_{,\eta} \end{Bmatrix} \quad (3.21)$$

The other two directions are uniquely defined as:

$$V_1 = \frac{j \times V_3}{|j \times V_3|}$$

$$V_2 = \frac{V_3 \times V_1}{|V_3 \times V_1|}$$

The  $x', y', z'$  directions are obtained by reducing the above vectors to unit magnitude.

$$[\theta] = [\bar{V}_1, \bar{V}_2, \bar{V}_3] \quad (3.22)$$

The local derivatives of the displacement are given by

$$\begin{bmatrix} u'_{,x'} & v'_{,x'} & w'_{,x'} \\ u'_{,y'} & v'_{,y'} & w'_{,y'} \\ u'_{,z'} & v'_{,z'} & w'_{,z'} \end{bmatrix} = [\theta]^T \begin{bmatrix} u_{,x} & v_{,x} & w_{,x} \\ u_{,y} & v_{,y} & w_{,y} \\ u_{,z} & v_{,z} & w_{,z} \end{bmatrix} [\theta] \quad (3.23)$$

Substitution of these components in equation (3.16) gives the strain components in terms of displacement degrees of freedom of the element as,

$$\{\varepsilon'\} = [B'] \{\delta\} = [B'] \begin{Bmatrix} \{\delta_1\} \\ \{\delta_2\} \\ \vdots \\ \{\delta_n\} \end{Bmatrix} \quad (3.24)$$

$$\{\varepsilon'\} = [B'_1 \quad B'_2 \quad B'_3 \dots B'_{n-1} \quad B'_n] \{\delta\}$$

$$\text{where } \{\delta_i\} = \begin{Bmatrix} u_i \\ v_i \\ w_i \\ \alpha_i \\ \beta_i \end{Bmatrix} \text{ for corner nodes}$$

and

$$\{\delta_i\} = \begin{Bmatrix} u_i^{p} \\ v_i^{p} \\ w_i^{p} \\ \alpha_i^{p} \\ \beta_i^{p} \end{Bmatrix} \text{ for hierarchical nodes}$$

where the matrix  $[B']$  is called the strain displacement matrix. The displacement matrix  $\{\delta\}$  is partitioned into sub-matrices containing the nodal variables corresponding to the particular node  $i$ . The value of  $n$  depends upon the number of nodes in the element including the hierarchical nodes.

The element stiffness matrix and load vector is evaluated by the following definitions.

$$[K^e] = \int_{\Omega} [B]^T [D][B] d\Omega \quad (3.25)$$

$$\{F^e\} = \int_{\Gamma} [N]^T \{f_s\} d\Gamma + \int_{\Gamma} [N]^T \{f_b\} d\Gamma \quad (3.26)$$

The integration process is done in the local coordinate system. Changing the limits to local coordinate system gives,

$$[K^e] = \int_{-1}^1 \int_{-1}^1 \int_{-1}^1 [B]^T [D][B] |J(\xi, \eta, \zeta)| d\xi d\eta d\zeta \quad (3.27)$$

Gauss quadrature rule is used to numerically integrate the element stiffness matrix.

Gaussian integration using  $NG^k \times NG^j \times NG^i$  points is given by

$$[K^e] = \sum_{k=1}^{NG^k} \sum_{j=1}^{NG^j} \sum_{i=1}^{NG^i} [B(\xi_i, \eta_j, \zeta_k)]^T [D][B(\xi_i, \eta_j, \zeta_k)] |J(\xi_i, \eta_j, \zeta_k)| w_i w_j w_k \quad (3.28)$$

where  $w_i, w_j$  and  $w_k$  are the Gaussian weights corresponding to the  $i, j$  and  $k^{th}$  gauss points.  $NG^i, NG^j$  and  $NG^k$  are number of Gaussian points along  $\xi, \eta$  and  $\zeta$  directions. Two-point integration is used along the  $\zeta$  direction, as  $\zeta$  is a linear coordinate. The order of integration along the  $\xi$  and  $\eta$  directions depends upon the hierarchical order chosen along the respective directions.

Once the stiffness and load matrices for all the elements are evaluated, they are assembled to form the global stiffness matrix and load matrix.

$$[K^G]\{\delta\} = \{F^G\} \quad (3.29)$$

The above equation is solved to get the global vector of nodal displacements  $\{\delta\}$ .

The stresses evaluated by equation are in the local coordinate system. Since the stresses in the local coordinate system are not easily visualized, it is conveniently transformed to the global system using the following expression.

$$\begin{bmatrix} \sigma_x & \tau_{xy} & \tau_{xz} \\ \tau_{xy} & \sigma_y & \tau_{yz} \\ \tau_{xz} & \tau_{yz} & \sigma_z \end{bmatrix} = [\theta] \begin{bmatrix} \sigma_{x'} & \tau_{x'y'} & \tau_{x'z'} \\ \tau_{x'y'} & \sigma_{y'} & \tau_{y'z'} \\ \tau_{x'z'} & \tau_{y'z'} & 0 \end{bmatrix} [\theta]^T \quad (3.30)$$

### 3.1.5 Displacement field near the crack tip for a plate with through thickness crack

Consider the problem of a through crack in a plate shown in the figure 3.2, where for convenience a local polar co-ordinate system centered at the crack tip was adopted. As opposed to the stress intensity factors obtained in classical elasticity, in plate theory the quantities of interest are moment and shear intensity factors.

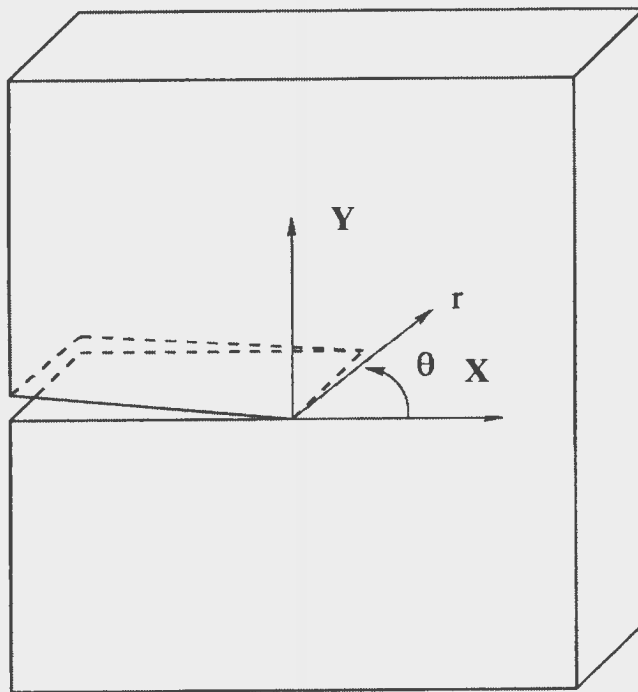


Figure 3.2: Local polar coordinate system for through crack in plate

Considering variation in stress components through the plate thickness a link to the stress intensity factors of three-dimensional elasticity is made. There are five crack modes in plate bending and tension analysis as shown in the figure 3.3. The stress resultant intensity factor  $K_I$ ,  $K_2$  and  $K_3$  are usually used instead of  $K_I$ ,  $K_{II}$  and  $K_{III}$ . The

relationship between the stress resultant intensity factors and stress intensity factors are given by [49].

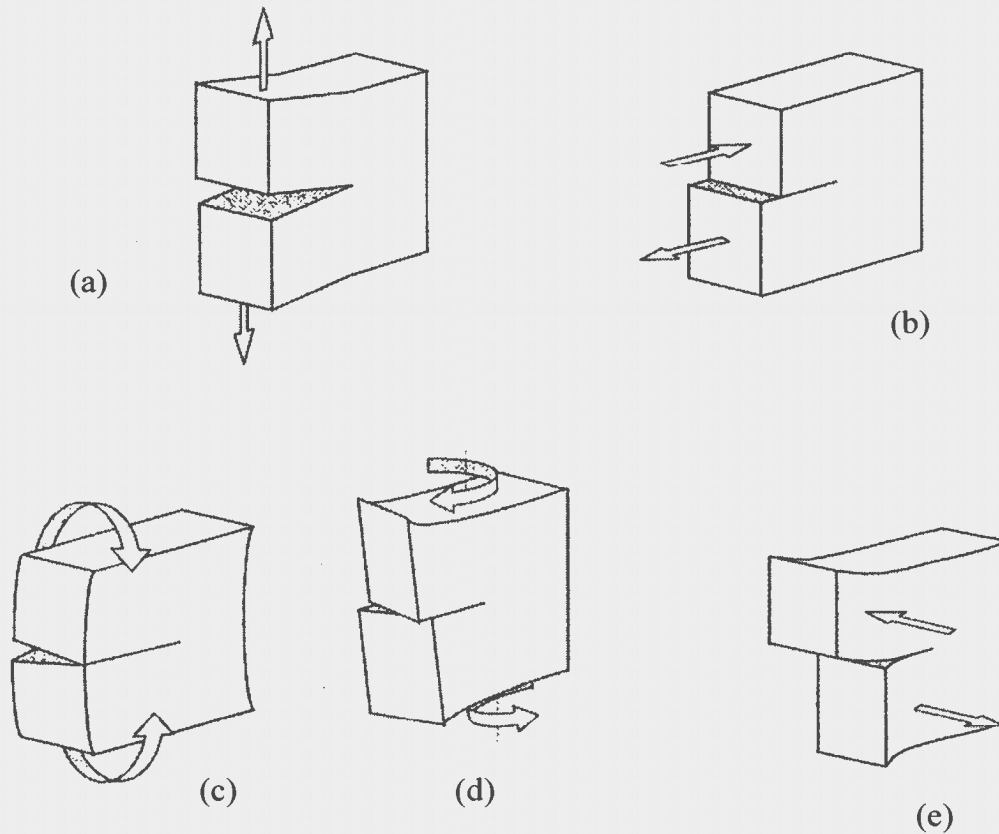


Figure 3.3: Modes of fracture

(a) mode I due to membrane load (b) mode II due to membrane load (c) mode I due to bending (d) mode II due to torsion load and (e) mode III due transverse shear load [49]

The in plane stresses are constant throughout the thickness of the plate. The bending stresses vary linearly through the plate thickness, where as the transverse shear stresses vary parabolically. These considerations typically motivate the following relationships.

$$K_{Ib} = \frac{12Z}{h^3} K_{Ib}, K_{IIb} = \frac{12Z}{h^3} K_{2b}, K_{IIIb} = \frac{3}{2h} \left[ 1 - \left( \frac{Z}{h} \right)^2 \right] K_{3b}$$

where  $Z$  is coordinate in thickness direction and membrane stress resultant intensity factors are given by

$$K_{Im} = \frac{1}{h} K_{1m}, K_{IIIm} = \frac{1}{h} K_{2m}$$

The “membrane” in-plane shear [50], “bending”, “twisting” and “transverse shear” components are related to the modes I, II and III stress intensity factors at any point in through thickness direction along the crack front are given by

$$\begin{aligned} K_I(Z) &= K_{1m} + K_{1b}Z \\ K_{II}(Z) &= K_{2m} + K_{2b}Z \\ K_{III}(Z) &= \frac{3}{2} \left[ 1 - \left( \frac{2Z}{h} \right)^2 \right] K_{3b} \end{aligned}$$

In crack problems, the most information is in the asymptotic solution around the crack tip. It would be preferable that the approximate theory used satisfies certain minimum requirements namely the asymptotic results given by the plate theory (i.e. the singularity and the angular distribution of stresses) should be compatible with the corresponding plane and anti plane elasticity solutions.

The local polar co-ordinate axes are shown in the Figure 3.2 with origin coincident with the crack tip. The  $Z$ -axis crack edge is parallel to global  $z$ -axis coinciding with the normal to the mid surface of the plate. The near crack tip displacements  $u_c, v_c$  and  $w_c$  along  $X, Y$  and  $Z$  directions and rotations of normal to the mid-plane at the vicinity of crack tip are given as follows.

The in plane displacements  $u_c$  and  $v_c$  along the mid-surface is given [51] as

$$\begin{aligned} u_c &= K_{1m} f_1(r, \theta) + K_{2m} g_1(r, \theta) \\ v_c &= K_{1m} f_2(r, \theta) + K_{2m} g_2(r, \theta) \end{aligned} \tag{3.31}$$

where

$$f_1 = \left( \frac{1}{4G} \sqrt{\frac{r}{2}} \right) \left\{ (2\gamma - 1) \cos\left(\frac{\theta}{2}\right) - \cos\left(\frac{3\theta}{2}\right) \right\}$$

$$g_1 = \left( \frac{1}{4G} \sqrt{\frac{r}{2}} \right) \left\{ (2\gamma + 3) \sin\left(\frac{\theta}{2}\right) - \sin\left(\frac{3\theta}{2}\right) \right\}$$

$$f_2 = \left( \frac{1}{4G} \sqrt{\frac{r}{2}} \right) \left\{ (2\gamma + 1) \sin\left(\frac{\theta}{2}\right) - \sin\left(\frac{3\theta}{2}\right) \right\}$$

$$g_2 = \left( \frac{1}{4G} \sqrt{\frac{r}{2}} \right) \left\{ (2\gamma - 3) \cos\left(\frac{\theta}{2}\right) + \cos\left(\frac{3\theta}{2}\right) \right\}$$

and transverse displacement  $w_c$  and rotations of normal to the mid surface is given [52] as

$$w_c = K_{1b} f_3(r, \theta) + K_{2b} g_3(r, \theta) + K_3 h_3(r, \theta)$$

$$\alpha_c = K_{1b} F_1(r, \theta) + K_{2b} G_1(r, \theta) \quad (3.32)$$

$$\beta_c = K_{1b} F_2(r, \theta) + K_{2b} G_2(r, \theta)$$

where

$$F_1 = \frac{6\sqrt{2r}}{Et^3} \cos\left(\frac{\theta}{2}\right) [4 - (1 + \nu)(1 + \cos(\theta))]$$

$$G_1 = \frac{6\sqrt{2r}}{Et^3} \sin\left(\frac{\theta}{2}\right) [4 + (1 + \nu)(1 + \cos(\theta))]$$

$$F_2 = \frac{6\sqrt{2r}}{Et^3} \left[ 4 \sin\left(\frac{\theta}{2}\right) - (1 + \nu) \left( \cos\left(\frac{\theta}{2}\right) \sin(\theta) \right) \right]$$

$$G_2 = \frac{6\sqrt{2r}}{Et^3} \left[ -2 \cos\left(\frac{\theta}{2}\right) (1 - \nu) + (1 + \nu) \sin\left(\frac{\theta}{2}\right) \sin(\theta) \right]$$

$$f_3 = \frac{6\sqrt{2}r^{\frac{3}{2}}}{Et^3} \left[ \frac{1}{3}(7+\nu)\cos\left(\frac{3\theta}{2}\right) - (1-\nu)\cos\left(\frac{\theta}{2}\right) \right]$$

$$g_3 = \frac{6\sqrt{2}r^{\frac{3}{2}}}{Et^3} \left[ -\frac{1}{3}(5+3\nu)\sin\left(\frac{3\theta}{2}\right) + (1-\nu)\sin\left(\frac{\theta}{2}\right) \right]$$

$$h_3 = \frac{6\sqrt{2}r}{5t\mu} \sin\left(\frac{\theta}{2}\right)$$

### 3.1.6 Enrichment of displacement field for plate element

The geometry of a typical plate element with through crack located at one of the corner node is shown in figure number 3.4.

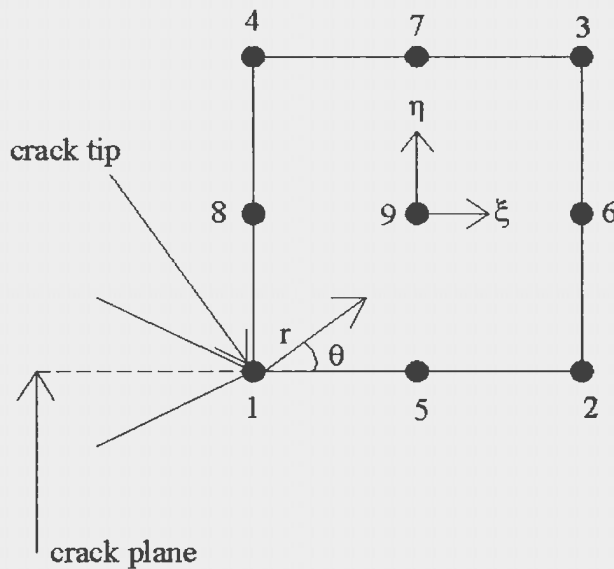


Figure 3.4: Geometry of plate element with through crack

The displacement field of plate element described in earlier section is enriched by augmenting the equations such as (3.4) with the near crack tip displacement field described in the earlier section.

The membrane displacement field  $u(\zeta)$ , equation (3.4) is enriched by the near field crack displacement functions (Eqns 3.31 to 3.32) as

$$\begin{aligned} u_{en}(\zeta) &= u(\zeta) + K_{1m}f_1 + K_{2m}g_1 + K_{1b}\zeta\frac{h}{2}F_1 + K_{2b}\zeta\frac{h}{2}G_1 \\ v_{en}(\zeta) &= v(\zeta) + K_{1m}f_2 + K_{2m}g_2 + K_{1b}\zeta\frac{h}{2}F_2 + K_{2b}\zeta\frac{h}{2}G_2 \\ w_{en}(\zeta) &= w(\zeta) + K_{1b}F_3 + K_{2b}G_3 + K_3H_3 \end{aligned} \quad (3.33)$$

where  $K_{1m}$  is the mode I membrane stress intensity factor,  $K_{2m}$  is the mode II membrane stress intensity factor,  $K_{1b}$  is the mode I bending stress intensity factor,  $K_{2b}$  is the mode II bending stress intensity factor and  $K_3$  is the shear stress intensity factor.

Considering the membrane displacement  $u_{en}(\zeta)$  within the element in terms of curvilinear coordinates  $\xi$  and  $\eta$  can be written as

$$u_{en}(\zeta) = [P]\{a\} + K_{1m}f_1 + K_{2m}g_1 + \zeta\frac{h}{2}K_{1b}F_1 + \zeta\frac{h}{2}K_{2b}G_1 \quad (3.34)$$

Proceeding in a similar way as described in section 3.3, the constants in vector  $\{a\}$  can be determined as described below. The displacement components at the nodes are determined by substituting appropriate curvilinear coordinates of nodes to obtain  $\{\delta(\zeta)\}$  and are given below for second order:

$$\delta_i = u_{oi} + \zeta\frac{h_i}{2}(v_{1i}^1\alpha_i - v_{2i}^1\beta_i) + K_{1m}f_{1i} + K_{2m}g_{1i} + \zeta\frac{h}{2}K_{1b}F_1|i + \zeta\frac{h}{2}K_{2b}G_1|i$$

for  $i = 1$  to  $4$  (3.35)

$$\begin{aligned}
\delta_i &= \frac{\partial^2 u_{oi}}{\partial \xi^2} + \zeta \frac{h_i}{2} \left( v^1_{1i} \frac{\partial^2 \alpha_i}{\partial \xi^2} - v^1_{2i} \frac{\partial^2 \beta_i}{\partial \xi^2} \right) + \\
&K_{1m} \frac{\partial^2 f_1}{\partial \xi^2} \Big|_i + K_{2m} \frac{\partial^2 g_1}{\partial \xi^2} \Big|_i + \zeta \frac{h}{2} K_{1b} \frac{\partial^2 F_1}{\partial \xi^2} \Big|_i + \zeta \frac{h}{2} K_{2b} \frac{\partial^2 G_1}{\partial \xi^2} \Big|_i \quad \text{for } i = 5 \text{ and } 7 \\
\delta_i &= \frac{\partial^2 v_{oi}}{\partial \eta^2} + \zeta \frac{h_i}{2} \left( v^1_{1i} \frac{\partial^2 \alpha_i}{\partial \eta^2} - v^1_{2i} \frac{\partial^2 \beta_i}{\partial \eta^2} \right) + \quad (3.36) \\
&K_{1m} \frac{\partial^2 f_1}{\partial \eta^2} \Big|_i + K_{2m} \frac{\partial^2 g_1}{\partial \eta^2} \Big|_i + \zeta \frac{h}{2} K_{1b} \frac{\partial^2 F_1}{\partial \eta^2} \Big|_i + \zeta \frac{h}{2} K_{2b} \frac{\partial^2 G_1}{\partial \eta^2} \Big|_i \quad \text{for } i = 6 \text{ and } 8 \\
\delta_i &= \frac{\partial^4 u_{oi}}{\partial \xi^2 \partial \eta^2} + \zeta \frac{h_i}{2} \left( v^1_{1i} \frac{\partial^4 \alpha_i}{\partial \xi^2 \partial \eta^2} - v^1_{2i} \frac{\partial^4 \beta_i}{\partial \xi^2 \partial \eta^2} \right) + \\
&K_{1m} \frac{\partial^4 f_1}{\partial \xi^2 \partial \eta^2} \Big|_i + K_{2m} \frac{\partial^4 g_1}{\partial \xi^2 \partial \eta^2} \Big|_i + \zeta \frac{h}{2} K_{1b} \frac{\partial^4 F_1}{\partial \xi^2 \partial \eta^2} \Big|_i + \zeta \frac{h}{2} K_{2b} \frac{\partial^4 G_1}{\partial \xi^2 \partial \eta^2} \Big|_i \quad \text{for } i = 9
\end{aligned}$$

Substituting (3.33,3.34) into (3.1), we get

$$u(\zeta) = [P][C]^{-1} \{ \delta(\zeta) \} \quad (3.37)$$

Following the procedure explained in section 3.1, the displacement function  $u(\zeta)$

can be written as

$$u(\zeta) = [N] \{ \delta \} + K_{1m} f_{1m} + K_{2m} g_{1m} + \zeta \frac{h}{2} K_{1b} F_1 + \zeta \frac{h}{2} K_{2b} G_1 \quad (3.38)$$

where  $[N]$  is the hierarchical shape function. Substituting for  $\{ \delta(\zeta) \}$  in terms of

displacement degrees of freedom, we can write displacement interpolation function for

$u_{en}(\xi, \eta, \zeta)$  as

$$u_{en}(\xi, \eta, \zeta) = \sum_{i=1}^4 N_i u_{oi} + \sum_{i=1}^4 \zeta \frac{h_i}{2} N_i (v^1_{1i} \alpha_i - v^2_{2i} \beta_i) \quad (3.39)$$

$$\begin{aligned}
& + \sum_{i=5}^9 N_i u_{oi}'' + \sum_{i=5}^9 \zeta \frac{h_i}{2} N_i (v_{1i}^1 \alpha_i'' - v_{2i}^2 \beta_i'') \\
& + K_{1m} \left( f_1 - \sum_{i=1}^4 N_i f_{1i} - \sum_{i=5}^9 N_i f_{1i}'' \right) + K_{2m} \left( g_1 - \sum_{i=1}^4 N_i g_{1i} - \sum_{i=5}^9 N_i g_{1i}'' \right) \\
& + K_{1b} \zeta \frac{h_i}{2} \left( F_1 - \sum_{i=1}^4 N_i F_{1i} - \sum_{i=5}^9 N_i F_{1i}'' \right) + K_{2b} \zeta \frac{h_i}{2} \left( G_1 - \sum_{i=1}^4 N_i G_{1i} - \sum_{i=5}^9 N_i G_{1i}'' \right)
\end{aligned}$$

Defining

$$F_{1m} = f_1 - \sum_{i=1}^4 N_i f_{1i} - \sum_{i=5}^9 N_i f_{1i}''$$

$$G_{1m} = g_1 - \sum_{i=1}^4 N_i g_{1i} - \sum_{i=5}^9 N_i g_{1i}''$$

and

$$F_{1B} = \zeta \frac{h_i}{2} \left( F_1 - \sum_{i=1}^4 N_i F_{1i} - \sum_{i=5}^9 N_i F_{1i}'' \right)$$

$$G_{1B} = \zeta \frac{h_i}{2} \left( G_1 - \sum_{i=1}^4 N_i G_{1i} - \sum_{i=5}^9 N_i G_{1i}'' \right)$$

The enriched form of equation (3.9) can be rewritten as

$$\begin{aligned}
u_{en}(\xi, \eta, \zeta) &= \sum_{i=1}^4 N_i u_{oi} + \sum_{i=5}^9 N_{gi} (v_{1i}^1 \alpha_i - v_{2i}^2 \beta_i) \\
&+ \sum_{i=5}^9 N_i u_{oi}'' + \sum_{i=5}^9 N_{gi} (v_{1i}^1 \alpha_i'' - v_{2i}^2 \beta_i'') + K_{1m} F_1 + K_{2m} G_1 \\
&+ K_{1b} F_{1B} + K_{2b} G_{1B}
\end{aligned} \tag{3.40}$$

where ( )'' denotes the partial derivative with respect to  $\xi, \eta$  at the respective nodes on mid sides

Similarly the displacement distribution for  $v$  and  $w$  can be written as

$$v(\xi, \eta, \zeta) = \sum_{i=1}^4 N_i v_{oi} + \sum_{i=5}^9 N_{gi} (v_{1i}^1 \alpha_i - v_{2i}^2 \beta_i)$$

$$\begin{aligned}
& + \sum_{i=5}^9 N_i v_{oi}'' + \sum_{i=5}^9 N_{gi} (v_{1i}^1 \alpha_i'' - v_{2i}^2 \beta_i'') + K_{1m} F_2 + K_{2m} G_2 \\
& + K_{1b} F_{2B} + K_{2b} G_{2B}
\end{aligned} \tag{3.41}$$

$$\begin{aligned}
w(\xi, \eta, \zeta) &= \sum_{i=1}^4 N_i w_{oi} + \sum_{i=5}^9 N_{gi} (v_{1i}^1 \alpha_i - v_{2i}^1 \beta_i) \\
& + \sum_{i=5}^9 N_i w_{oi}'' + \sum_{i=5}^9 N_{gi} (v_{1i}^1 \alpha_i'' - v_{2i}^2 \beta_i'') + K_{1b} F_3 + K_{2b} G_3 + K_3 H_3
\end{aligned} \tag{3.42}$$

Following the same procedure higher order displacement functions can be written as

$$\begin{aligned}
u(\xi, \eta, \zeta) &= \sum_{i=1}^4 N_i u_{oi} + \sum_{i=1}^4 N_{gi} (v_{1i}^1 \alpha_i - v_{2i}^1 \beta_i) \\
& + \sum_{p=2}^{p_{\max}} \sum_{i=5}^9 N_{pi} u_{oi}^{1p} + \sum_{p=2}^{p_{\max}} \sum_{i=5}^9 N_{gpi} (v_{1i}^1 \alpha_i^{1p} - v_{2i}^1 \beta_i^{1p}) \\
& + K_{1m} F_1 + K_{2m} G_1 + K_{1b} F_{1B} + K_{2b} G_{1B}
\end{aligned} \tag{3.43}$$

Similarly, the other displacement components can be written as

$$v(\xi, \eta, \zeta) = \sum_{i=1}^4 N_i v_{oi} + \sum_{i=1}^4 N_{gi} (v_{1i}^2 \alpha_i - v_{2i}^2 \beta_i) \tag{3.44}$$

$$\begin{aligned}
& + \sum_{p=2}^{p_{\max}} \sum_{i=5}^9 N_{pi} v_{oi}^{2p} + \sum_{p=2}^{p_{\max}} \sum_{i=5}^9 N_{gpi} (v_{1i}^2 \alpha_i^{2p} - v_{2i}^2 \beta_i^{2p}) \\
& + K_{1m} F_2 + K_{2m} G_2 + K_{1b} F_{2B} + K_{2b} G_{2B}
\end{aligned}$$

$$\begin{aligned}
w(\xi, \eta, \zeta) &= \sum_{i=1}^4 N_i w_{oi} + \sum_{i=1}^4 N_{gi} (v_{1i}^3 \alpha_i - v_{2i}^3 \beta_i) \\
& + \sum_{p=2}^{p_{\max}} \sum_{i=5}^9 N_{pi} w_{oi}^{3p} + \sum_{p=2}^{p_{\max}} \sum_{i=5}^9 N_{gpi} (v_{1i}^3 \alpha_i^{3p} - v_{2i}^3 \beta_i^{3p}) + K_{1b} F_3 + K_{2b} G_3 + K_3 H_3
\end{aligned} \tag{3.45}$$

Using the above equation, the strain-displacement relations are evaluated as

$$\{\varepsilon'_{en}\} = [B'_1 \ B'_2 \ B'_3 \ \dots \ B'_n \ B'_k] \{\delta\}$$

where the vector  $\{\delta\}$  is given as

$$\{\delta\} = \begin{Bmatrix} (\delta_1) \\ (\delta_2) \\ (\delta_n) \\ (\delta_k) \end{Bmatrix}$$

$\{\delta_i\}$  are defined in equation (3.24) and  $\{\delta_k\}$  consist of stress intensity factor as given

below.

$$\{\delta_k\} = \begin{Bmatrix} K_{1m} \\ K_{2m} \\ K_{1b} \\ K_{2b} \\ K_3 \end{Bmatrix}$$

The stiffness matrix for the enriched plate element is then evaluated using the standard procedure described in previous section.

## **3.2 Hierarchical 18 node Solid Thick Shell Element**

Review of the literature on analysis of plate bending problems indicates, the effect of crack closure on the compressive side in plate bending problems are not included in the analysis [38]. Almost all the researchers assumed that there is no crack surface interference (on compression side) in the bending problem [50]. Thus, the results published in literature should be considered together with the solutions corresponding to generalized plane stress problems. The crack closure effect on bending can only be studied by considering the combined effect of membrane and bending singularities across the thickness without separately considering membrane, bending stress intensity factors. Keeping this in view, plate with crack problems can be analyzed using 18-node solid plate element that is presented in this section.

The idea proposed here is to use 18-noded solid element by removing mid-side nodes from 20-noded solid element. The basic solid element with 18 nodes for general plates and shells is shown in the figure 3.5. The element properties are derived by prescribing linear displacement variations across the thickness of the element and the strain energy due to stress normal to the shell mid plane is neglected. Thus the element avoids the Kirchoff's assumption and agrees with higher order theories for thick shells and plates.

### **3.2.1 Geometric definition of the element**

A typical shell element is shown in the Figure 3.5. The geometry of the element is defined using sixteen nodes. The nodes are located at top and bottom surface. The external surfaces of the element are curved and the sections across the thickness are

straight. Two curvilinear coordinates  $\xi, \eta$  in the middle plane and a linear coordinate  $\zeta$  in the thickness direction are used to define the geometry. The local coordinates  $\xi, \eta$  and  $\zeta$  vary between -1 and 1. The top and bottom coordinates define the shape of the element. The relationship between the cartesian coordinates and the curvilinear coordinates for any point in the element is given by:

$$\begin{Bmatrix} x \\ y \\ z \end{Bmatrix} = \sum_{i=1}^{16} N_i(\xi, \eta, \zeta) \begin{Bmatrix} x_i \\ y_i \\ z_i \end{Bmatrix} \quad (3.46)$$

$N_i(\xi, \eta, \zeta)$  is a serendipity approximation shape function (see Appendix). The subscript  $i$  refer to the element node number.

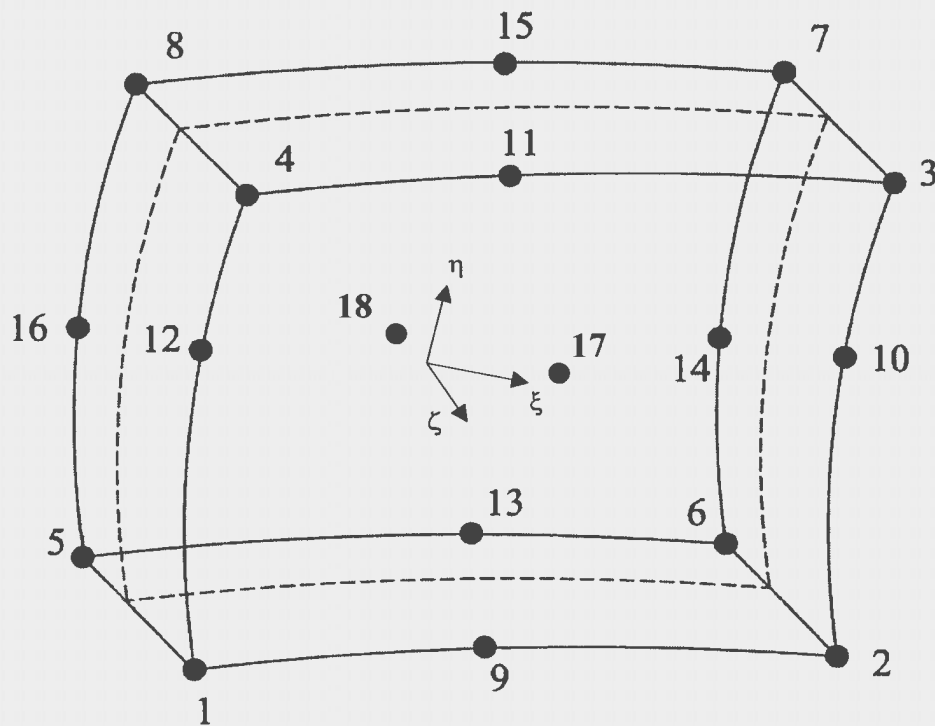


Figure 3.5: Hierarchical 18 node solid plate element

### 3.2.2 Displacement field

The higher order finite element approach for three-dimensional thin and thick-walled structures is based on a hierarchical element, applying the shape functions proposed by Szabo and Babuska [53]. The figure 3.5 depicts a hexahedral shell-like solid element. This element may be doubly curved with a non-constant thickness. The shell-like solid may be doubly curved with a non-constant thickness. When thin-walled structures are to be discretized it is important to treat the in-plane direction and thickness direction differently. Since the p-version is less prone to locking effects [53,54,55] a pure, strictly three-dimensional displacement formulation can be applied. Once the shape functions have been defined, the element formulation follows the procedure described in earlier section.

Let  $\xi, \eta$  be two curvilinear coordinates on the mid surface of the shell,  $\zeta$  orthogonal to  $\xi$  and  $\eta$ . The basic property of the hierarchic shell model is that the kinematics of lower order model are fully embedded in the definition of the higher model. The polynomial expansion of the displacements are given by

$$\begin{aligned}
 u(\xi, \eta, \zeta) &= \sum_o^{nk} (\zeta)^k u(\xi, \eta) \\
 v(\xi, \eta, \zeta) &= \sum_o^{nk} (\zeta)^k v(\xi, \eta) \\
 w(\xi, \eta, \zeta) &= \sum_o^{nk} (\zeta)^k w(\xi, \eta)
 \end{aligned} \tag{3.47}$$

where  $nk$  denoted highest order of polynomials in thickness direction. As  $nk$  approaches  $\infty$ , the solution converges to the exact three-dimensional solution. The displacement components of  $u(\xi, \eta), v(\xi, \eta)$  and  $w(\xi, \eta)$  can be approximated by any suitable shape

functions. The present implementation for hierarchical shell model is based on quadrilateral element formulation using shape functions developed in earlier sections. Following the procedure explained in the earlier section the displacement polynomial expression can be written as described below.

All the displacement components are assumed to vary linearly in  $\zeta$  direction. At corner nodes, the displacement components  $u$ ,  $v$  and  $w$  are the degrees of freedom. The hierarchical degrees of freedom of the displacement components are higher order derivatives with respect to  $\xi$ ,  $\eta$  directions at mid-side nodes on top and bottom surface edges. At central nodes on the top and bottom surfaces, higher order derivatives taken in  $\xi$ ,  $\eta$  are used as degrees of freedom. For second order, hierarchical degrees of freedom are as follows:

$$\frac{\partial^2 u_i}{\partial \xi^2}, \frac{\partial^2 v_i}{\partial \xi^2}, \frac{\partial^2 w_i}{\partial \xi^2} \quad \text{at nodes 9, 11, 13 and 15}$$

$$\frac{\partial^2 u_i}{\partial \eta^2}, \frac{\partial^2 v_i}{\partial \eta^2}, \frac{\partial^2 w_i}{\partial \eta^2} \quad \text{at nodes 10, 12, 14 and 16}$$

$$\frac{\partial^4 u_i}{\partial \xi^2 \partial \eta^2}, \frac{\partial^4 v_i}{\partial \xi^2 \partial \eta^2}, \frac{\partial^4 w_i}{\partial \xi^2 \partial \eta^2} \quad \text{at central nodes 17 and 18}$$

Following the similar proceeding described earlier, in plane displacement  $u(\xi, \eta, \zeta)$  can

$$\text{be given as } u(\xi, \eta, \zeta) = [N] \{ \delta \}$$

where for second order, the  $\{ \delta \}$  and  $[N]$  are given as below and

$$\delta_i = u_i \quad \text{for } i = 1, 2, 3 \text{ and } 4$$

$$\delta_i = \frac{\partial^2 u_i}{\partial \xi^2} \quad \text{for } i = 9, 11, 13 \text{ and } 15$$

$$\delta_i = \frac{\partial^2 u_i}{\partial \eta^2} \quad \text{for } i = 10, 12, 14 \text{ and } 16$$

$$\delta_i = \frac{\partial^4 u_i}{\partial \xi^2 \partial \eta^2} \quad \text{for } i = 17 \text{ and } 18$$

The equation (3.52) can be rewritten as

$$u(\xi, \eta, \zeta) = \sum_{i=1}^8 N_i u_i + \sum_{i=9}^{18} N_i u_i'' \quad (3.48)$$

where  $( )''$  denotes the partial derivative with respect to  $\xi, \eta$  at the respective nodes on mid sides

Similarly the displacement distribution for  $v$  and  $w$  can be written as

$$v(\xi, \eta, \zeta) = \sum_{i=1}^8 N_i v_i + \sum_{i=9}^{18} N_i v_i'' \quad (3.49)$$

$$w(\xi, \eta, \zeta) = \sum_{i=1}^8 N_i w_i + \sum_{i=9}^{18} N_i w_i'' \quad (3.50)$$

Following the same procedure higher order displacement functions can be written as

$$u(\xi, \eta, \zeta) = \sum_{i=1}^8 N_i u_i + \sum_{p=2}^{p_{\max}} \sum_{i=9}^{18} N_{pi} u_i'^p \quad (3.51)$$

where  $u_i$  = in plane displacement along X-direction at the corner nodes 'i'

$$\begin{aligned} u_{oi}'^p &= \frac{\partial^p u_i}{\partial \xi^p} \quad \text{at node } i \text{ for } i = 9, 11, 13 \text{ and } 15 \\ &= \frac{\partial^p u_i}{\partial \eta^p} \quad \text{at node } i \text{ for } i = 10, 12, 14 \text{ and } 16 \\ &= \frac{\partial^{2p} u_i}{\partial \xi^p \partial \eta^p} \quad \text{at central node } i = 17 \text{ and } 18 \end{aligned}$$

Similarly, the other displacement components can be written as

$$v(\xi, \eta, \zeta) = \sum_{i=1}^8 N_i v_{oi} + \sum_{p=2}^{p_{\max}} \sum_{i=9}^{18} N_{pi} v_i'^p \quad (3.52)$$

$$w(\xi, \eta, \zeta) = \sum_{i=1}^8 N_i w_{oi} + \sum_{p=2}^{p_{\max}} \sum_{i=9}^{18} N_{pi} w_i'^p \quad (3.53)$$

### 3.2.3 Element Stiffness matrix generation

As regards the material properties, the continuum mechanics of hierarchic shell models are based completely on a three-dimensional theory. Consequently, hierarchical shell models can be combined with arbitrary material laws. Since, in this formulation, displacement components vary linearly across the thickness, the same material law that is used in section 3.1.3 is used assuming basic shell assumption. Thus, the strain components normal to the shell surface are neglected and strain-correction factor  $k$  is used.

Thus, the stiffness matrix is obtained using the methods as described in sections 3.1.3, 3.1.4. But in this case displacement vectors at each node are given as

$$\{\delta_i\} = \begin{Bmatrix} u_i \\ v_i \\ w_i \end{Bmatrix} \quad \text{for corner nodes}$$

and

$$\{\delta_i\} = \begin{Bmatrix} u_i'^p \\ v_i'^p \\ w_i'^p \end{Bmatrix} \quad \text{for hierarchical nodes at mid-sides}$$

# Chapter 4

## COMPUTER IMPLEMENTATION

### 4.1 Computer Program

Most of the programs that were developed in the past were written in FORTRAN, which lacks many of the new features available in the present day computer languages. Object oriented programming has brought some new frontiers in the field of computer programming. The modern day computer programming languages use object-oriented approach that has many advantages compared to other programming languages.

A p-version finite element analysis program is developed in JAVA programming language. The capabilities include analysis of general plate and shell structures subjected to various loading conditions and stress intensity factor evaluation of plates containing through thickness cracks.

The hierarchical 9-node plate/shell and 18 node solid thick elements are used in the program development. The three main segments of the program are: Element stiffness matrix formulation, Global assembly of element stiffness matrices and load vectors and the solution routine.

The program is organized in various steps

- 1) Main program
- 2) Input

- 3) Calculation of shape functions its derivatives with respect to local coordinates
- 4) Formulation of stiffness matrix
- 5) Assembly of stiffness matrices
- 6) Solving the global stiffness matrix

The flow chart of the complete program organization is given in figure 4.1. The program code in the main file coordinates with other parts of the program.

### **4.1.1 Input**

The input obtains the data required for modeling and analysis of the problem such as the order of polynomial, type of element, the total number of nodes and elements, boundary conditions, loading information etc. and allocates memory required for element stiffness, global matrices and load vectors. Location vectors required for the assembly of sky line diagonal and compact off-diagonal matrices are also generated.

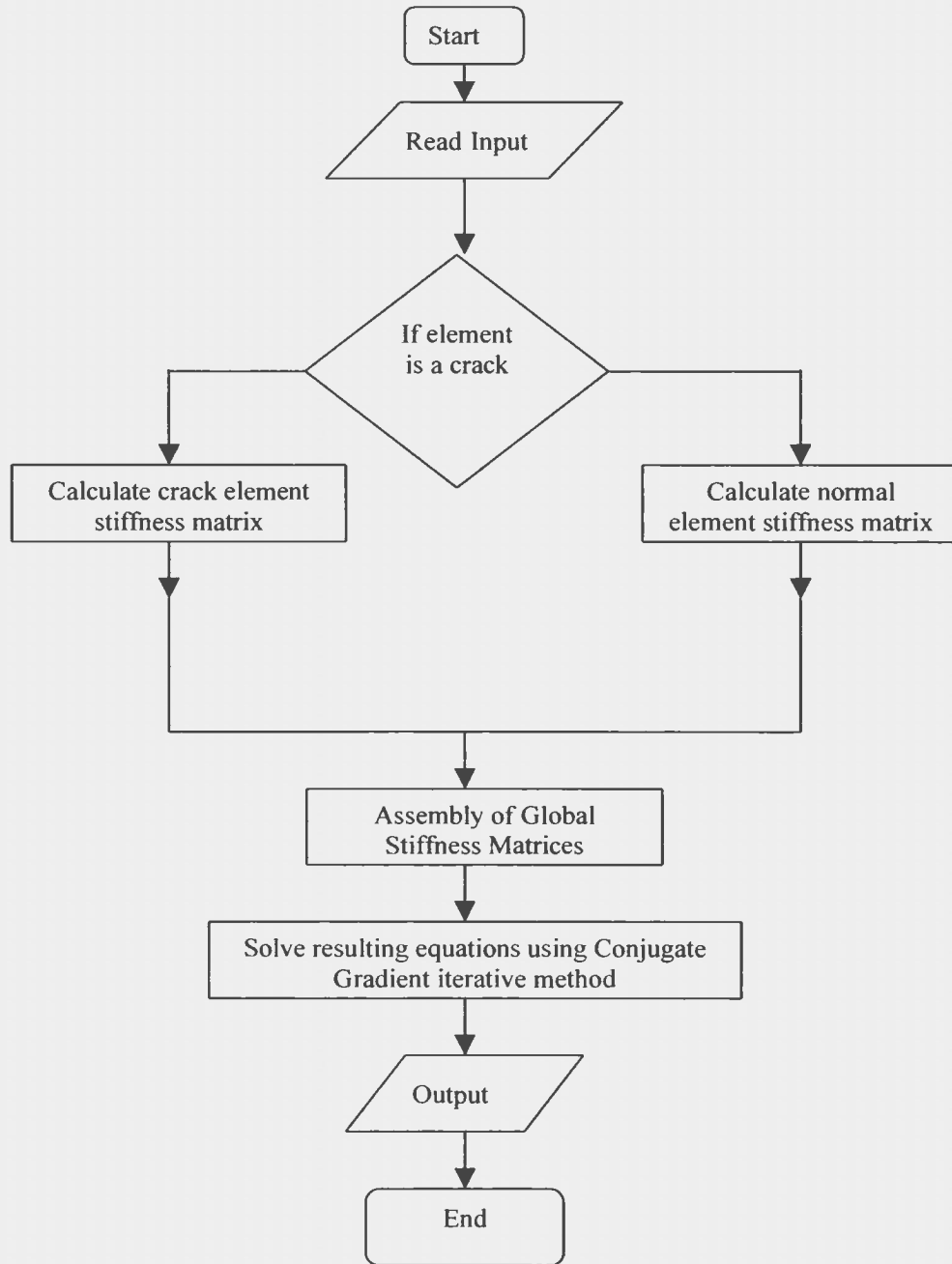


Figure 4.1 Organization of the computer program

## 4.1.2 Shape Function Derivatives

The derivatives of the shape functions are done in the starting of the analysis. For convenience, the code for the calculation of the derivatives of shape functions is written in a separate file.

The number of Gaussian points of integration and Gaussian weight at these points are chosen depending on the order of the elements. The inputs to the methods in this file are the polynomial order and element type. Based on the element used in the analysis it calculates the shape functions, and its derivatives at all the Gaussian integration points. The values of the derivatives and shape functions are stored in arrays and they are returned to the program for the calculation of the local stiffness matrices.

## 4.1.3 Element stiffness matrix evaluation and assembly

The order of the element is always greater than unity as  $p$  is successively increased. A geometric shape function of order two is used to model the element. Gaussian integration is employed for the evaluation of stiffness matrices. The  $(p+1)$  integration rule is used along the local  $\xi$  and  $\eta$  direction on the mid surface and two-point integration is used in the thickness direction. Since diagonal and off diagonal matrices are assembled in order to use Conjugate gradient method for the solution, the element matrices are generated as partitioned matrices. For example the element stiffness matrix for the order 3 is partitioned as given below.

$$[K]_e = \begin{bmatrix} K_{11}^e & K_{12}^e & K_{13}^e \\ & K_{22}^e & K_{23}^e \\ Sym & & K_{33}^e \end{bmatrix} \quad (4.1)$$

where  $K_{11}^e$ ,  $K_{22}^e$  and  $K_{33}^e$  are diagonal matrices corresponding to order 1, 2 and 3 and  $K_{12}^e$  is off diagonal matrix corresponding to order 1 and 2 and  $K_{13}^e$  is off diagonal matrix corresponding to order 1 and 3 and so on.

The diagonal matrices of all the elements are assembled into global diagonal matrix as a skyline matrices corresponding to each order. Similarly each off diagonal matrix of all the elements are assembled into global-off diagonal matrices in compact form including only non zero element in order to avoid the multiplication or division on non zero elements. The assembled matrices are as shown below:

$$\begin{bmatrix} K_{11}^g & K_{12}^g & K_{13}^g \\ & K_{22}^g & K_{23}^g \\ Sym & & K_{33}^g \end{bmatrix} \begin{Bmatrix} \delta_1 \\ \delta_2 \\ \delta_3 \end{Bmatrix} = \begin{Bmatrix} F_1 \\ F_2 \\ F_3 \end{Bmatrix} \quad (4.2)$$

$K_{11}^g, K_{22}^g \dots$  are skyline global diagonal stiffness matrices corresponding to the order 1, 2 and so on.  $K_{ij}^g$  are the global-off diagonal compact matrices corresponding to order  $i$  and  $j$ .  $\delta_1$  corresponds to nodal displacement vector corresponding to first order for the entire structure and  $\delta_2$  corresponds to nodal displacement vector corresponding to hierarchical degrees of freedom for order 2 and so on. Similarly, the load vector  $F_1$  corresponds to force components of first order and  $F_2, F_3, \dots$  etc for higher orders.

## 4.2 Solution Procedure

The use of hierarchical elements results in an improved stiffness matrix that contain lower order stiffness as sub-matrix. The improved stiffness matrix differs from the previous lower stiffness matrix in that it contains rows and columns corresponding to additional nodal variables. Hence the effort spent in triangularizing the previous stiffness matrix is entirely saved and improved solutions are obtained by iterative procedures. It is time consuming and costly to solve the simultaneous linear equations of equation 4.2 by direct methods such as Gaussian elimination or any other method. Therefore an iterative technique is employed to solve the equation of type in Equation (4.2). A large number of iterative techniques are available that use successive approximations in order to obtain more accurate solution.

There are many iterative techniques, which have advantages over others.

Iterative techniques are classified as

- a) Stationary iterative methods
- b) Non-stationary iterative methods.

Stationary iterative methods perform the same operations on current iterative vectors/approximations and some of the methods used in this category are Jacobi method, Gauss-Seidel method, successive over relaxation method, symmetric successive over relaxation method etc.

Non-stationary methods use the transformation matrix that is referred as preconditioner and perform operations on iterative vector and this method may even fail

to converge without preconditioner. Some of the common examples of this category are Conjugate Gradient method (CG), Conjugate gradient on normal equations, generalized Minimal residual (GMRES), Bi-conjugate gradient method (BiCG), Conjugate gradient squared method (CGS), Preconditioned conjugate gradient method (PCG) etc. In the present work preconditioned conjugate gradient method is employed for solving the equations.

### 4.2.1 Preconditioned Conjugate Gradient Method

The iterative method used in the present solution procedure is preconditioned Conjugate gradient method. In this method the preconditioned matrix

$$[M] = \begin{bmatrix} K_{11} & 0 & 0 \\ 0 & K_{22} & 0 \\ 0 & 0 & K_{33} \end{bmatrix} \text{ is used where } K_{11}, K_{22} \text{ and } K_{33} \text{ are the diagonal global stiffness}$$

matrices for the order 1, 2 and 3 respectively. The preconditioner is a transformation matrix, which transforms the coefficient matrix into one of the favorable spectrum on which the convergence rate depends. In this method successive vector sequences or successive approximations are generated and residuals corresponding to iterates are used in updating the iterates. The main concept is to find the search direction vectors  $P_i$  for  $i = 1, 2, 3, \dots, n$  which satisfies the condition and as efficiency is concerned, only small number of approximations are stored in the memory which increases the performance of the computer

The linear system that has to be solved is represented as  $[K]\{\delta\} = \{F\}$ . Usually 'K' has a large condition number when used in conjugate gradient method and so it is preconditioned. Preconditioning essentially means to replace the system with an equivalent system  $[M][K]\{\delta\} = [M]\{F\}$

The Preconditioned conjugate gradient method consists of essentially 5 steps:

1. Initialization
2. Begin Iteration
3. Perform Updates
4. Check for Convergence
5. Prepare for next CG update

The Preconditioned conjugate gradient method starts with an initial guess  $\{\delta\}^0$  of the results and then it is multiplied by the preconditioned conjugate gradient matrix. Even though the matrices  $[K]$  and  $[M]$  are symmetric it is not necessary that  $[MK]$  be a symmetric matrix. A good preconditioner is the starting point in the PCG method, which should satisfy two criteria a) It should be able to contract the eigen spectrum of the original system. b) It should be easy to factorize relative to the original system. c) It should be cheap for storage and fast to evaluate.

In this implementation diagonal matrices of global stiffness matrix is used as a preconditioner and it was observed that convergency of the results was good.

A pseudo code for preconditioned conjugate gradient method is given below:

$$\{r\}^0 = \{F\} - [K]\{\delta\}^0 \text{ for some initial guess } \{\delta\}^0$$

for  $i = 1, 2, 3, \dots$

Solve

$$[M]\{z\}^{i-1} = \{r\}^{i-1} \text{ where } [M] \text{ is a preconditioned matrix}$$

$$\rho^{i-1} = \{r\}^{(i-1)T} \{z\}^{i-1}$$

if  $i = 1$

$$\{p\}^1 = \{z\}^0$$

else

$$\beta_{i-1} = \frac{\{\rho_{i-1}\}}{\{\rho_{i-2}\}}$$

$$\{p\}^i = \{z\}^{i-1} + \beta_{i-1} \{p\}^{i-1}$$

end if

$$\{q\}^i = [K]\{p\}^i$$

$$\alpha_i = \frac{\{\rho_{i-1}\}}{\{\rho^i\}^T \{q\}^i}$$

$$\{\delta\}^i = \{\delta\}^{i-1} + \alpha_i \{p\}^i$$

$$\{r\}^i = \{r\}^{i-1} - \alpha_i \{q\}^i$$

Check convergence and continue if necessary

Figure 4.3 Pre-conditioned Conjugate Gradient Method

# Chapter 5

## Numerical Studies and Discussions

In order to verify the correctness of the element formulation and the software written, various benchmark plate and shell problems are analyzed.

1. Square plate under concentrated and distributed load with different boundary conditions.
2. A Barrel vault (Cylindrical roof) loaded by its self-weight.
3. A Pinched Cylindrical shell problem.
4. Infinite plate with central crack
5. Rectangular plate with central and edge crack

The numerical results obtained from the present work are compared with the analytical solutions and the results available in the literature. The results obtained are in excellent agreement with the reference values and they are sometimes more accurate with fewer degrees of freedom.

### 5.1 Square plate problem

An isotropic square plate shown in the Figure 5.1 is analyzed under different loading and boundary conditions. Using the symmetry, only one quarter of the plate is modeled for the analysis. The plate deforms under bending action and the inplane displacements are constrained in the tangential directions. The analysis is carried out for various thickness ratios to study the element behavior under thick and thin shell situations. The analysis is also carried out for different meshes. The results are compared with the exact

values given by Zienkiewicz [10]. Different cases considered in the analysis of the plate are:

1. Simply supported plate under concentrated load at the center.
2. Simply supported plate under uniformly distributed load.
3. Clamped plate under concentrated load at the center.
4. Clamped plate under uniformly distributed load.

All the four cases are analyzed for different thickness using 2x2, 3x3 and 4x4 meshes for orders upto seven. For the cases where concentrated load is applied at the center of the plate, the analysis are carried out with uniform mesh and refined mesh with element sizes in the ratio of 3 to 7.

The displacement solutions obtained are normalized using the following formulae.

$$\alpha = \frac{W_{\max} D}{q a^4} \text{ for a uniformly distributed load } q.$$

$$\beta = \frac{W_{\max} D}{P a^2} \text{ for a central concentrated load } P.$$

where

$W_{\max}$  is the maximum displacement at the center of the plate,

$D$  -Flexural rigidity and

$a$  - length of the plate.

A square plate with  $a/t$  equal to 66.66 was considered first to compare the numerical results with reference values. Numerical results obtained using Hierarchical degenerated plate/shell element for concentrated load and uniformly distributed load is presented in tables 5.1 to 5.5. The result show that numerical results obtained agree very well with the reference values. In order to study the effect of  $a/t$  on the results, the same

square plate is analyzed for various thickness ratios vide  $a/t$  equal to 10, 20, 100 and 200. The resulting numerical results are presented in tables 5.5 to 5.8.

For all the cases graphs (Figures 5.2 to 5.11) showing the variation of deflection along the central line as a ratio of  $w/w_{\max}$  vs. coordinate distance along the central line were presented.  $w_{\max}$  is the central deflection obtained from thin plate theory. From Figures 5.2 to 5.5 we see that the present analysis will give consistent results and agree very well with reference values. Figures 5.5 to 5.9 show the variation of deflection along the central line as a ratio of  $w/w_{\max}$  Vs. coordinate distance along the central line for different thickness to span ratios. From these graphs one can see that for thin plate situations ( $a/t = 100$  and  $200$ ) the results agree very well and no shear locking is observed. For reasonably thick situations ( $a/t = 10$  and  $20$ ) the results are similar and give the additional shear deformation not available by thin plate theory.

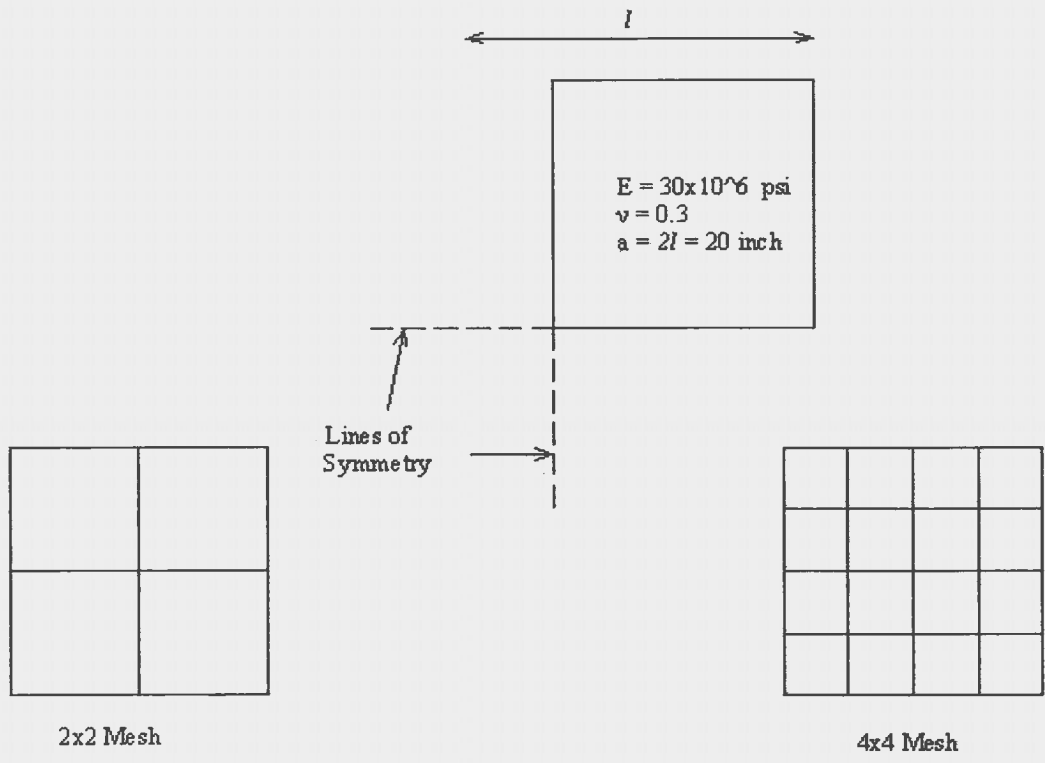


Figure 5.1: Square plate and meshes used for the analysis

Table 5.1: SS Plate under CL: Displacements for different orders ( $a/t = 66.66$ )

(Hierarchical nine noded Degenerated Plate/Shell Element)

Mesh	Order	DOF	$\beta = \frac{W_{\max} D}{Pa^2}$
2x2	2	125	0.01429
	3	205	0.01067
	4	285	0.011308
	5	365	0.011601
	6	445	0.01143
	7	525	0.01183
3x3	2	245	0.02833
	3	410	0.01163
	4	575	0.01162
	5	740	0.01162
	6	905	0.01163
	7	1070	0.01159
4x4	2	405	0.01135
	3	685	0.01165
	4	965	0.01078
	5	1245	0.01165
	6	1525	0.01164
	7	1805	0.01165
Reference value [10]			0.01160

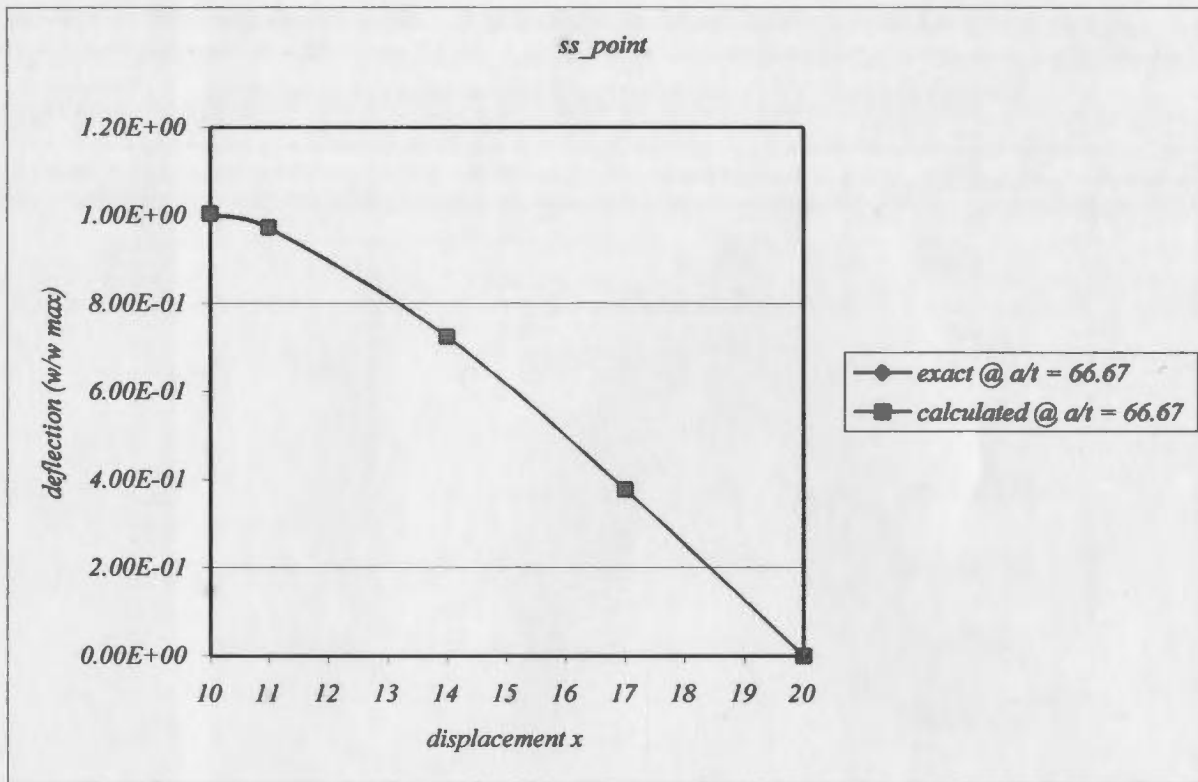


Figure 5.2: Plot of deflection of SS plate under CL at  $a/t$  equal to 66.67 for 4x4 refined mesh ( $w_{max}$  is the central deflection according to thin plate theory)

Table 5.2: SS Plate under UDL: Displacements for different orders ( $a/t = 66.66$ )

(Hierarchical nine noded Degenerated Plate/Shell Element)

Mesh	Order	DOF	$\alpha = \frac{W_{\max} D}{qa^4}$
2x2	2	125	0.004142
	3	205	0.004085
	4	285	0.004083
	5	365	0.0040819
	6	445	0.004083
	7	525	0.004083
3x3	2	245	0.0040807
	3	410	0.004071
	4	575	0.004072
	5	740	0.004072
	6	905	0.004072
	7	1070	0.0040719
4x4	2	405	0.004071
	3	685	0.004069
	4	965	0.004069
	5	1245	0.004069
	6	1525	0.004069
	7	1805	0.004069
Reference value [10]			0.004062

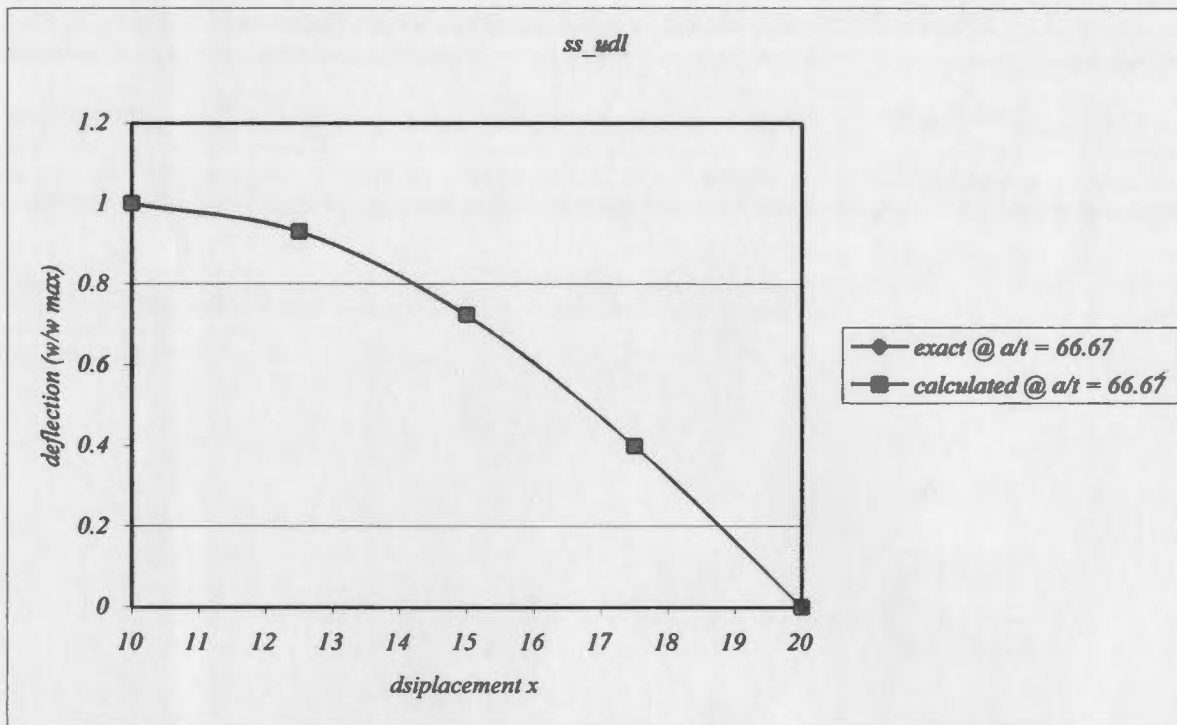


Figure 5.3: Plot of deflection of SS plate under UDL for  $a/t$  equal to 66.67 for 4x4 uniform mesh (w max is the central deflection according to thin plate theory)

Table 5.3: Clamped Plate under CL: Displacements for different orders ( $a/t = 66.66$ )

(Hierarchical nine noded Degenerated Plate/Shell Element)

Mesh	Order	DOF	$\beta = \frac{W_{\max} D}{Pa^2}$
2x2	2	125	1.0275e-4
	3	205	0.005591
	4	285	0.005569
	5	365	0.0055507
	6	445	0.005522
	7	525	0.005545
3x3	2	245	2.1862e-4
	3	410	0.005629
	4	575	0.004339
	5	740	0.005523
	6	905	0.005473
	7	1070	0.005619
4x4	2	405	3.8044e-4
	3	685	0.005629
	4	965	0.005488
	5	1245	0.005655
	6	1525	0.005637
	7	1805	0.005668
Reference value [10]			0.0056

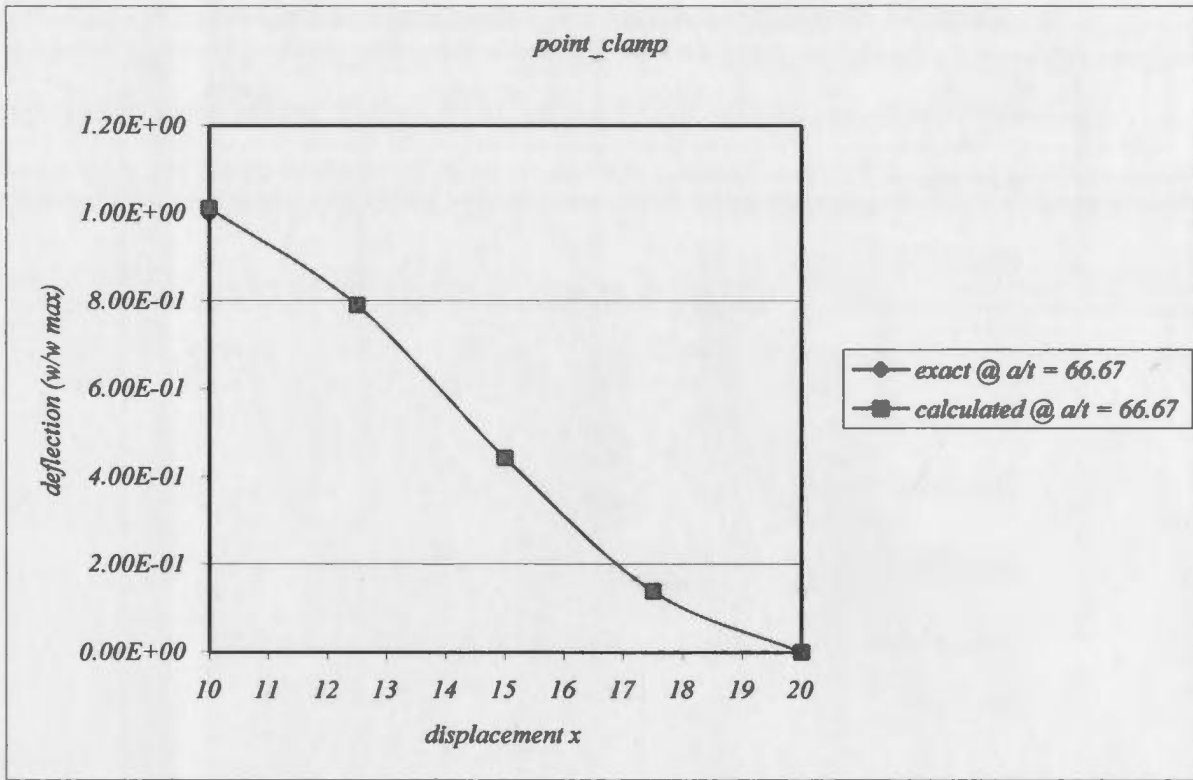


Figure 5.4: Plot of deflection of clamped plate under CL for  $a/t$  equal to 66.67 for 4x4 uniform mesh (w max is the central deflection according to thin plate theory)

Table 5.4: Clamped Plate under UDL: Displacements for different orders ( $a/t = 66.66$ )

(Hierarchical nine noded Degenerated Plate/Shell Element)

Mesh	Order	DOF	$\alpha = \frac{W_{\max} D}{qa^4}$
2x2	2	125	0.001284
	3	205	0.001266
	4	285	0.0012609
	5	365	0.001262
	6	445	0.001261
	7	525	0.001262
	3x3	2	245
3		410	0.0012708
4		575	0.0012705
5		740	0.0012706
6		905	0.0012705
7		1070	0.0012706
4x4		2	405
	3	685	0.0012709
	4	965	0.0012709
	5	1245	0.0012709
	6	1525	0.0012709
	7	1805	0.0012709
	Reference value [10]		

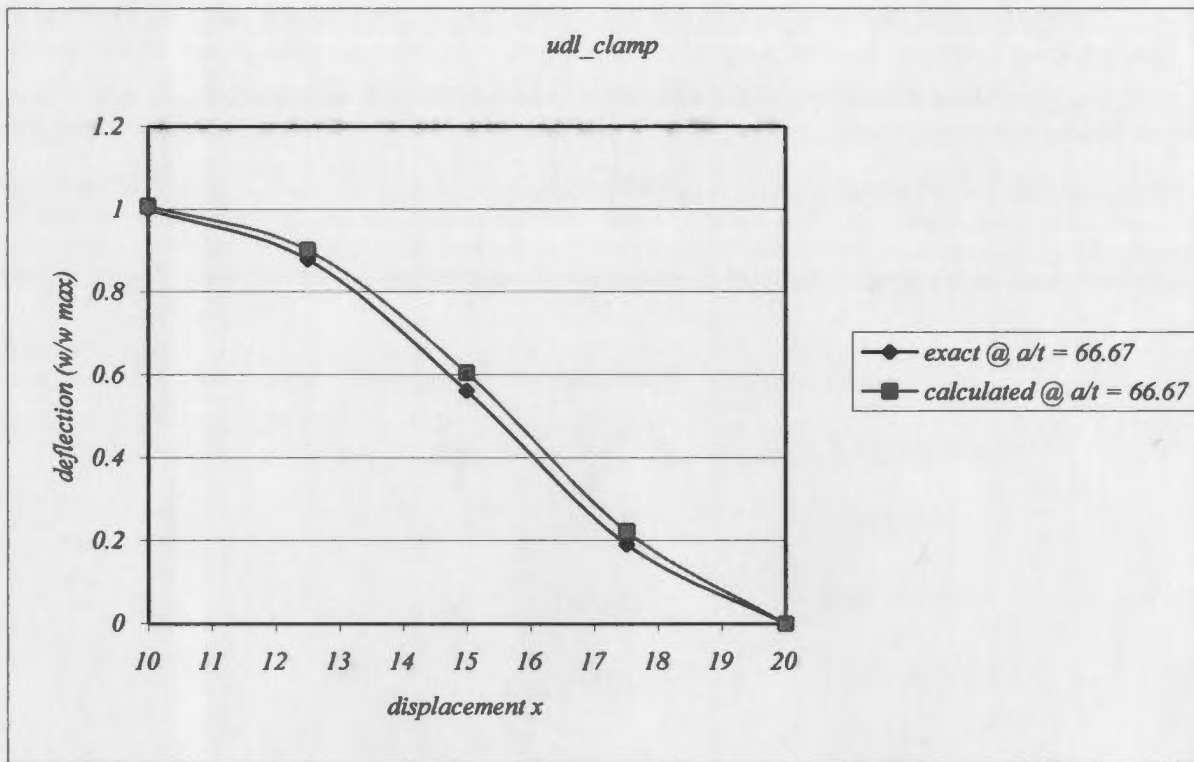


Figure 5.5: Plot of deflection of clamped plate under UDL for  $a/t$  equal to 66.67 for 4x4 uniform mesh ( $w_{max}$  is central deflection according to thin plate theory)

Table 5.5: SS Plate under UDL: Displacements for different orders for 2x2 mesh

(Hierarchical nine noded Degenerated Plate/Shell Element)

$a/t$	Order	DOF	$\alpha = \frac{W_{\max} D}{qa^4}$	$a/t$	$\alpha = \frac{W_{\max} D}{qa^4}$
20	2	125	0.004233	200	0.004135
	3	205	0.004189		0.0040705
	4	285	0.004188		0.004064
	5	365	0.004188		0.004066
	6	445	0.004188		0.0040602
	7	525	0.004188		0.004061
10	2	125	0.004492	100	0.004139
	3	205	0.004462		0.004076
	4	285	0.004452		0.004073
	5	365	0.004454		0.004072
	6	445	0.004454		0.004073
	7	525	0.004454		0.004074
Reference value [10]				0.004062	

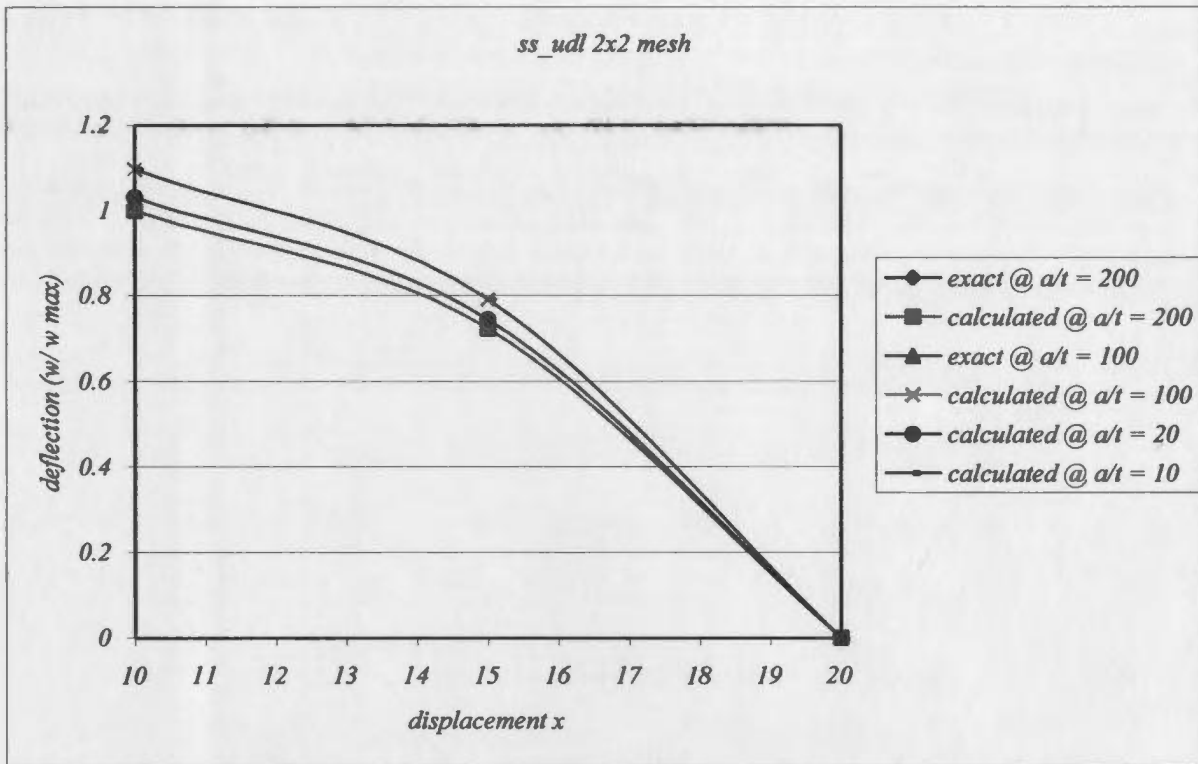


Figure 5.6: Plot of deflection of SS plate under UDL for various  $a/t$  ratios for 2x2 mesh  
 (w max is central deflection according to thin plate theory)

Table 5.6: SS Plate under UDL: Displacements for different orders for 4x4 mesh

(Hierarchical nine noded Degenerated Plate/Shell Element)

$a/t$	Order	DOF	$\alpha = \frac{W_{\max} D}{qa^4}$	$a/t$	$\alpha = \frac{W_{\max} D}{qa^4}$
20	2	405	0.004128	200	0.004065
	3	685	0.004128		0.004063
	4	965	0.004126		0.004063
	5	1245	0.004126		0.004063
	6	1525	0.004126		0.004064
	7	1805	0.004126		0.004063
	10	2	405		0.004304
3		685	0.004305	0.004066	
4		965	0.004302	0.004066	
5		1245	0.004303	0.004065	
6		1525	0.004303	0.004065	
7		1805	0.004303	0.0040659	
Reference value [10]					0.004062

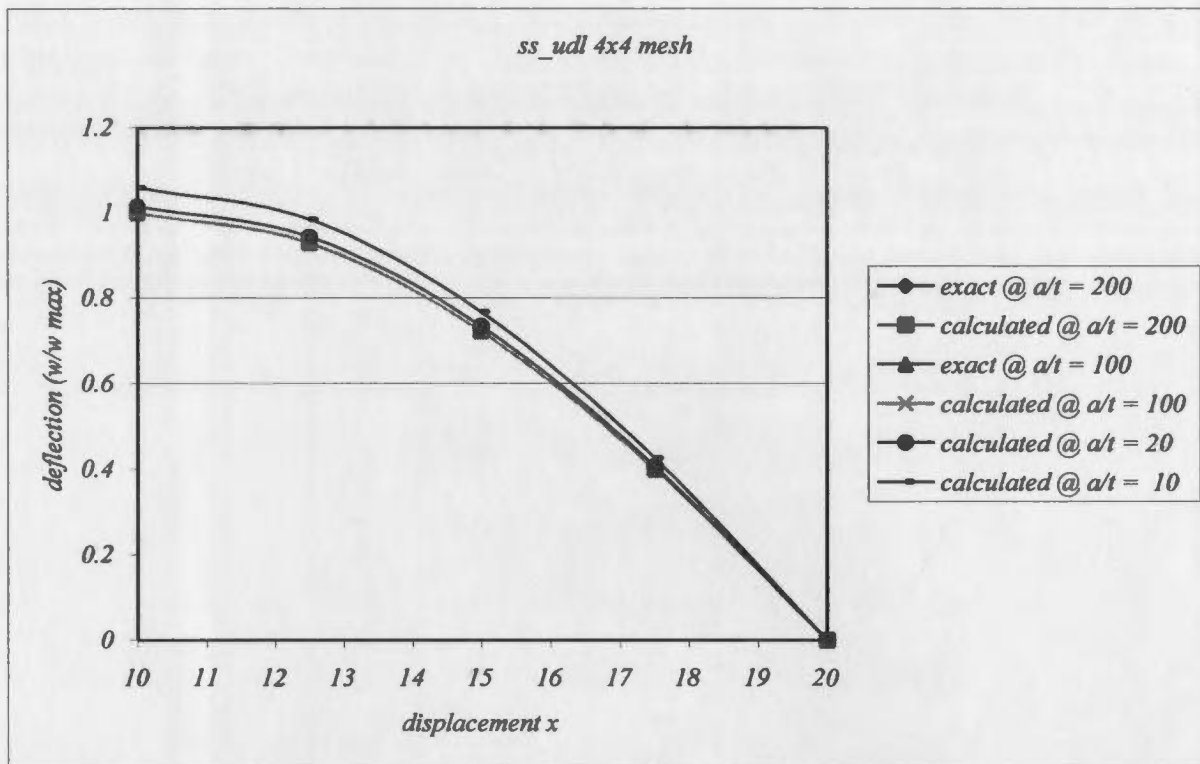


Figure 5.7: Plot of deflection of SS plate under UDL for various  $a/t$  ratios for 4x4 mesh

( $w_{max}$  is central deflection according to thin plate theory)

Table 5.7: Clamped Plate under UDL: Displacements for different orders for 2x2 mesh

(Hierarchical nine noded Degenerated Plate/Shell Element)

$a/t$	Order	DOF	$\alpha = \frac{W_{\max} D}{qa^4}$	$a/t$	$\alpha = \frac{W_{\max} D}{qa^4}$
20	2	125	0.001341	200	0.001279
	3	205	0.001325		0.001258
	4	285	0.001324		0.001229
	5	365	0.001324		0.001235
	6	445	0.001324		0.0012306
	7	525	0.001324		0.001231
	10	2	125		0.001581
3		205	0.001503	0.001262	
4		285	0.001503	0.0012507	
5		365	0.001503	0.001254	
6		445	0.001503	0.001252	
7		525	0.001503	0.001253	
Reference value [10]					0.00126

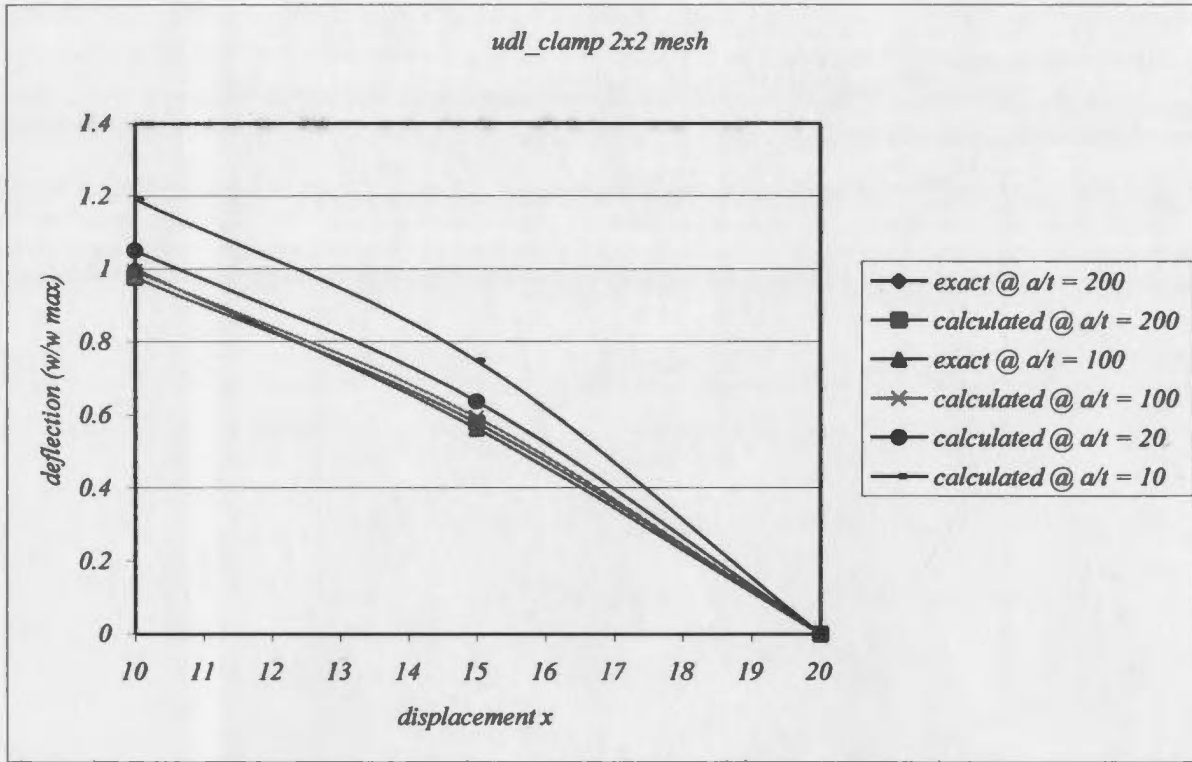


Figure 5.8: Plot of deflection of clamped plate under UDL for various  $a/t$  ratios for 2x2 mesh ( $w_{max}$  is central deflection according to thin plate theory)

Table 5.8: Clamped Plate under UDL: Displacements for different orders for 4x4 mesh

(Hierarchical nine noded Degenerated Plate/Shell Element)

$a/t$	Order	DOF	$\alpha = \frac{W_{\max} D}{qa^4}$	$a/t$	$\alpha = \frac{W_{\max} D}{qa^4}$
20	2	405	0.001328	200	0.001266
	3	685	0.001327		0.001265
	4	965	0.001327		0.001265
	5	1245	0.001327		0.001265
	6	1525	0.001327		0.001265
	7	1805	0.001327		0.001265
10	2	405	0.001505	100	0.001268
	3	685	0.001504		0.001267
	4	965	0.001504		0.001267
	5	1245	0.001504		0.001267
	6	1525	0.001504		0.001267
	7	1805	0.001504		0.001267
Reference value [10]					0.00126

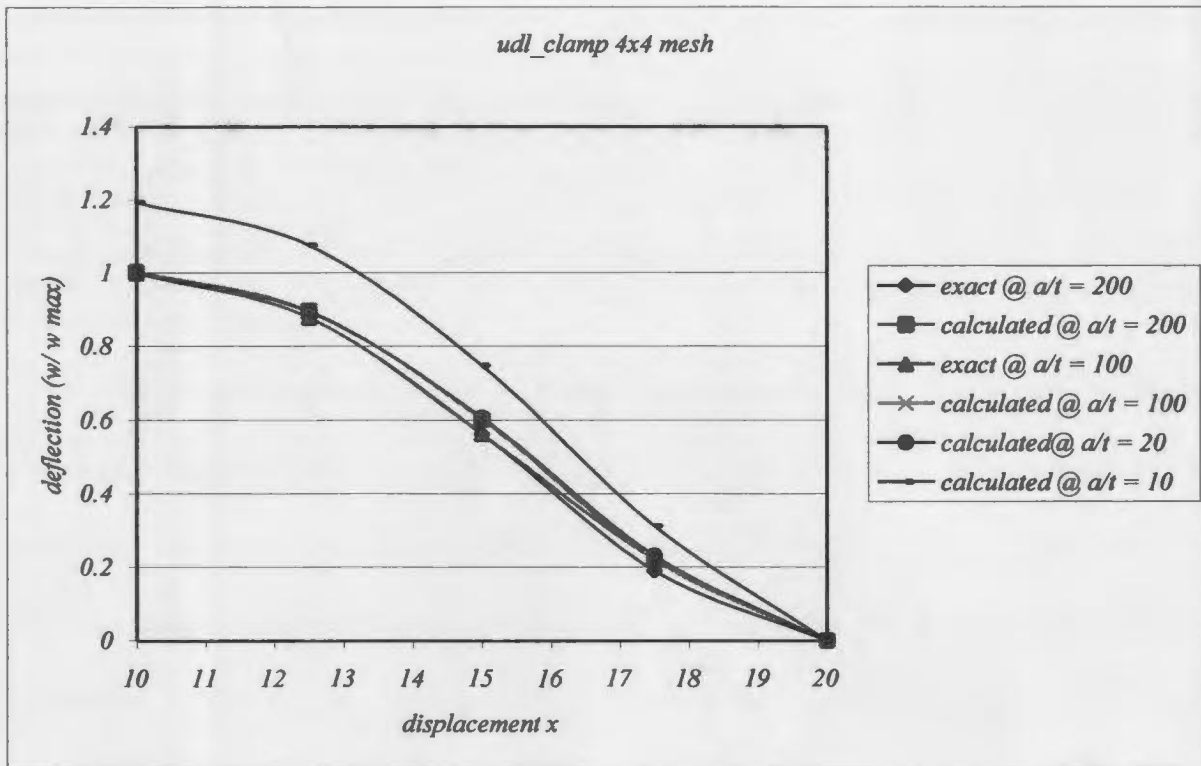


Figure 5.9: Plot of deflection of clamped plate under UDL for various  $a/t$  ratios for 4x4 mesh ( $w_{max}$  is central deflection according to thin plate theory)

The bench mark problems were also analyzed using 18 noded hierarchical solid thick shell elements using the same mesh divisions as were used with degenerated plate/shell element. The results are presented in tables and graphs. The results obtained for thickness to span ratio of 66.66 are presented in tables 5.9 to 5.12 for three different meshes. These tables compare the central deflection with reference values for both central concentrated load and uniformly distributed load cases for both simply supported and clamped cases. For all the cases uniform meshes were considered. From these tables it can be seen the results obtained from the 18 noded thick solid shell agree very well. The plots of deflection along the central line (Figures 5.10 to 5.13) for all boundary conditions and load cases show a very good agreement with thin plate theory. For

concentrated load uniform mesh is used. The deflections obtained for simply supported square plate with central concentrated load agree very well. In the case of degenerated plate/shell element a refined mesh is necessary for concentrated load case. From this it can be inferred that solid thick shell element perform very well compared to degenerated plate/shell element.

The central deflection for various thicknesses to span ratios with uniformly distributed load were presented in Tables 5.13 to 5.16. It can be seen that the results agree very well with reference values for thin plate situations for the maximum order of five. As noted by some authors that for higher orders, there will be some oscillations in the results. But this was not observed in the case of hierarchical plate/shell element. Figures 5.14 to 5.17 show the variation of deflection along the central line. The results are plotted for the order five. It can be seen that the results obtained agree very well with thin plate theory and as expected for thick plate situations the results show an additional shear deformation not available from thin plate theory.

Table 5.9: SS Plate under CL: Displacements for different orders ( $a/t = 66.66$ )

(Hierarchical 18 node solid thick shell element)

Mesh	Order	DOF	$\beta = \frac{W_{\max} D}{Pa^2}$
2x2	2	150	0.01043
	3	246	0.01149
	4	342	0.01158
	5	438	0.01161
	6	534	0.011603
	7	630	0.01161
3x3	2	294	0.01105
	3	492	0.011607
	4	345	0.01164
	5	444	0.01165
	6	543	0.01165
	7	642	0.01165
4x4	2	486	0.01133
	3	822	0.01164
	4	1158	0.01166
	5	1494	0.01166
	6	1830	0.01166
	7	2166	0.01166
Reference value [10]			0.0116

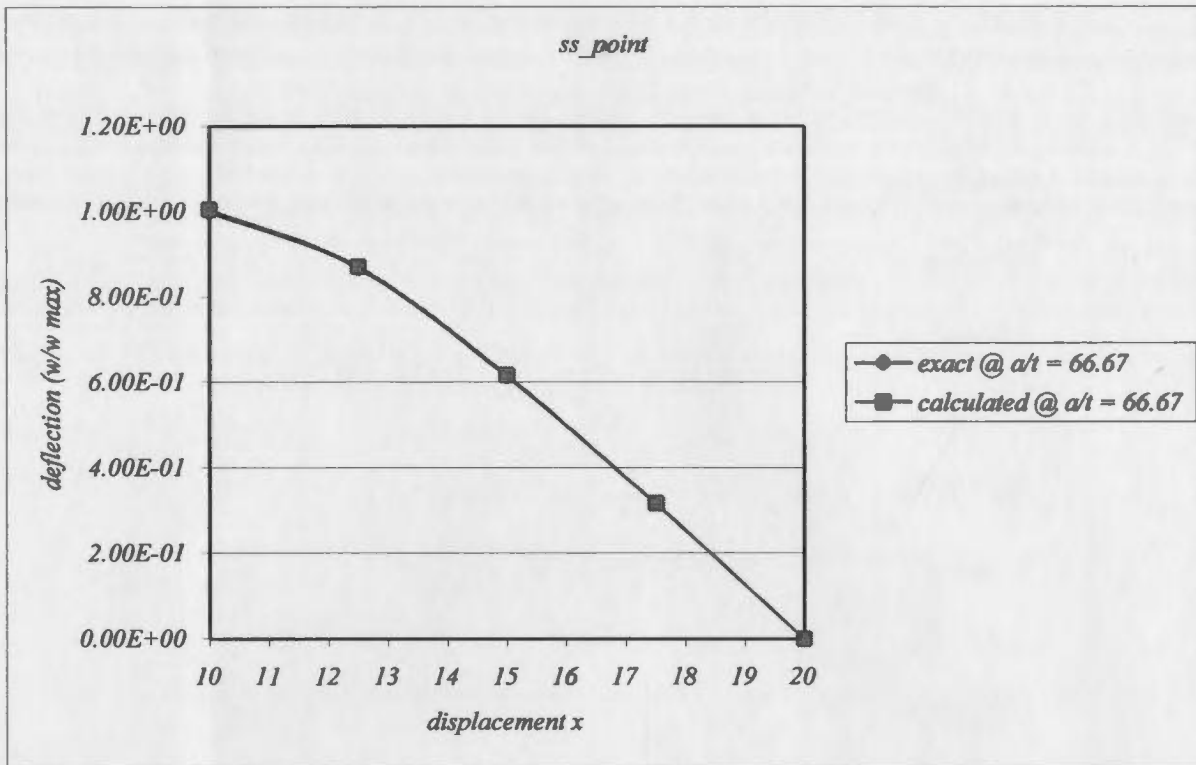


Figure 5.10: Plot of deflection of SS plate under CL for  $a/t$  equal to 66.67 for 4x4 uniform mesh (w max is the central deflection according to thin plate theory)

Table 5.10: SS Plate under UDL: Displacements for different orders ( $a/t = 66.66$ )

(Hierarchical 18-node solid thick shell element)

Mesh	Order	DOF	$\alpha = \frac{W_{\max} D}{qa^4}$
2x2	2	125	0.0040095
	3	205	0.004093
	4	285	0.004095
	5	365	0.004101
	6	445	0.00410
	7	525	0.004101
	3x3	2	245
3		410	0.004091
4		575	0.004095
5		740	0.004099
6		905	0.004099
7		1070	0.004099
4x4		2	405
	3	685	0.004091
	4	965	0.004094
	5	1245	0.004097
	6	1525	0.004097
	7	1805	0.004097
	Reference value [10]		

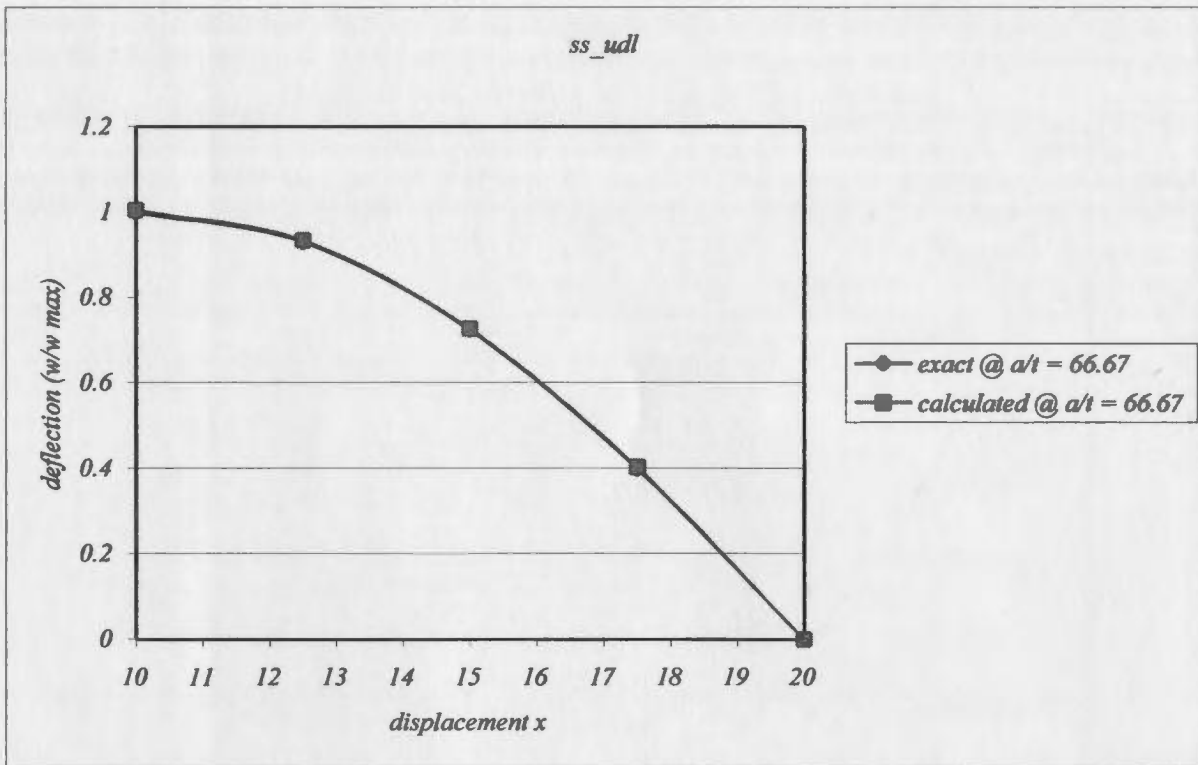


Figure 5.11: Plot of deflection of SS plate under UDL for  $a/t$  equal to 66.67 for 4x4 uniform mesh ( $w_{max}$  is the central deflection according to thin plate theory)

Table 5.11: Clamped Plate under CL: Displacements for different orders ( $a/t = 66.66$ )

(Hierarchical 18-node solid thick shell element)

Mesh	Order	DOF	$\beta = \frac{W_{\max} D}{Pa^2}$
2x2	2	125	0.004105
	3	205	0.005457
	4	285	0.005529
	5	365	0.005557
	6	445	0.005551
	7	525	0.00557
3x3	2	245	0.004936
	3	410	0.005601
	4	575	0.005631
	5	740	0.005637
	6	905	0.005632
	7	1070	0.005637
4x4	2	405	0.005263
	3	685	0.005636
	4	965	0.0056508
	5	1245	0.005653
	6	1525	0.005648
	7	1805	0.005653
Reference value [10]			0.0056

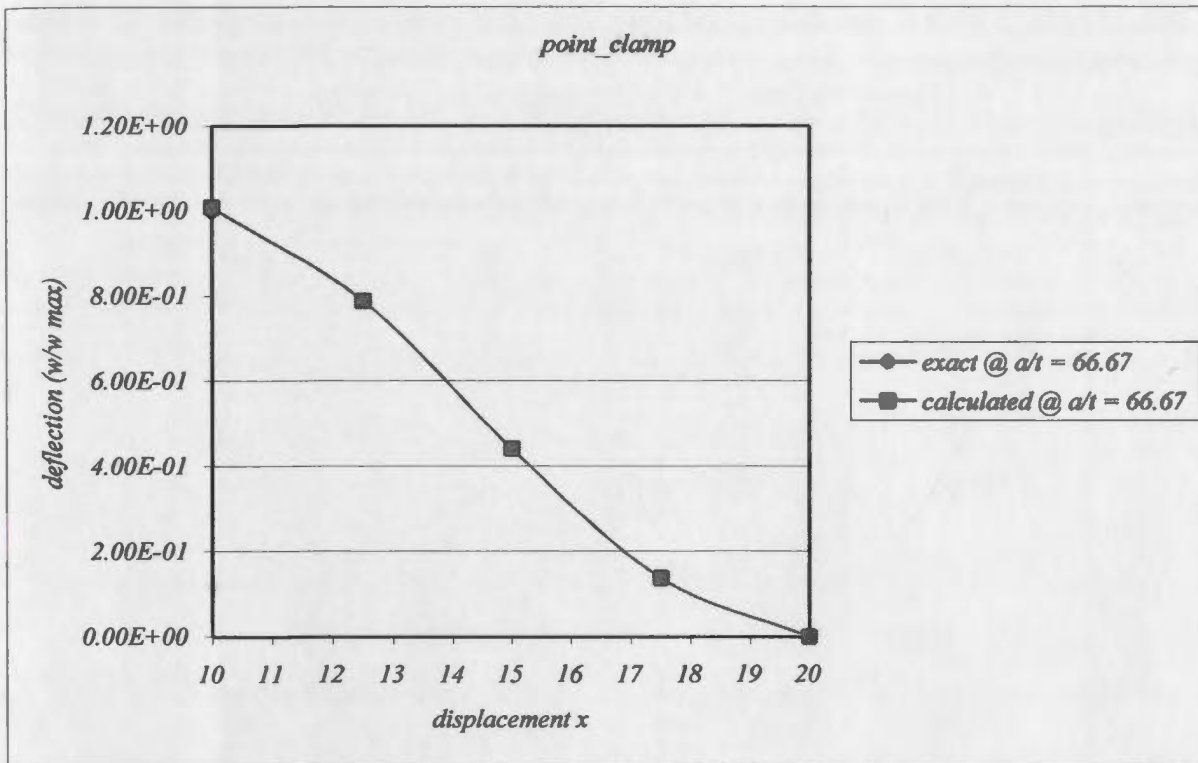


Figure 5.12: Plot of deflection of clamped plate under CL for  $a/t$  equal to 66.67 for 4x4 uniform mesh (w max is the central deflection according to thin plate theory)

Table 5.12: Clamped Plate under UDL: Displacements for different orders ( $a/t = 66.66$ )

(Hierarchical 18-node solid thick shell element)

Mesh	Order	DOF	$\alpha = \frac{W_{\max} D}{qa^4}$
2x2	2	125	0.001025
	3	205	0.001276
	4	285	0.001274
	5	365	0.001275
	6	445	0.001275
	7	525	0.001275
	3x3	2	245
3		410	0.001285
4		575	0.001285
5		740	0.001285
6		905	0.001285
7		1070	0.001285
4x4		2	405
	3	685	0.001285
	4	965	0.001285
	5	1245	0.001285
	6	1525	0.001285
	7	1805	0.001285
	Reference value [10]		

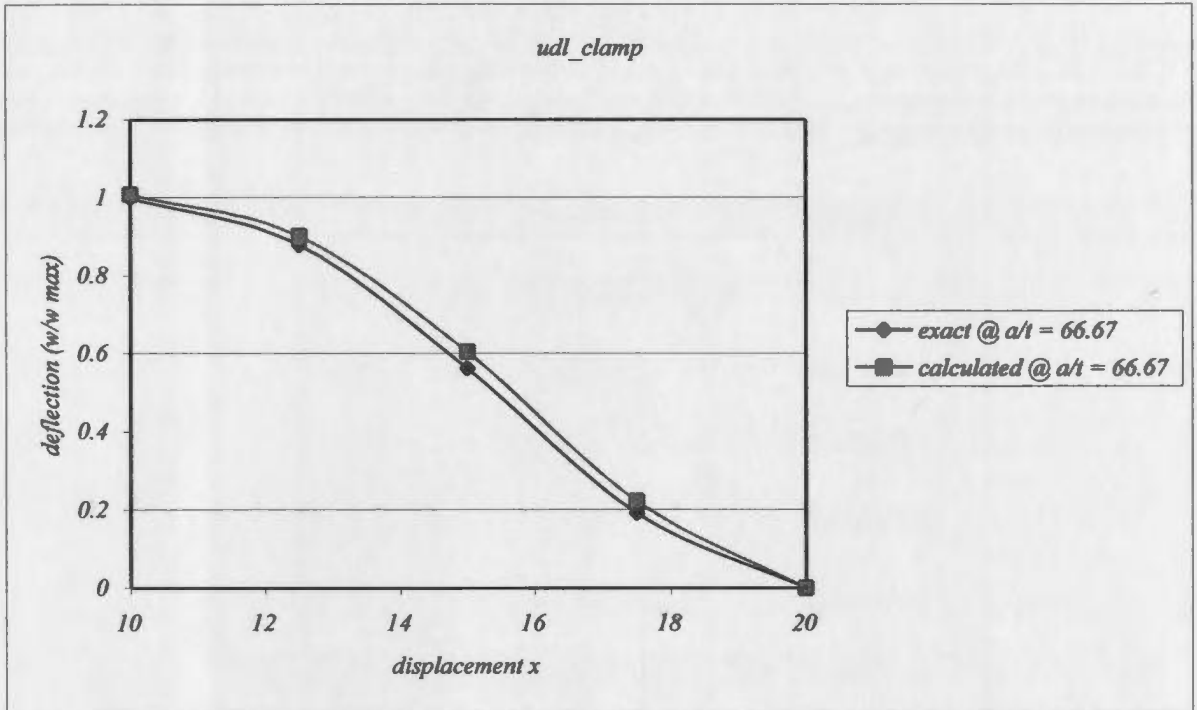


Figure 5.13: Plot of deflection of clamped plate under UDL for  $a/t$  equal to 66.67 for 4x4 uniform mesh (w max is the central deflection according to thin plate theory)

Table 5.13: SS Plate under UDL: Displacements for different orders for 2x2 mesh

(Hierarchical 18-node solid thick shell element)

$a/t$	Order	DOF	$\alpha = \frac{W_{\max} D}{qa^4}$	$a/t$	$\alpha = \frac{W_{\max} D}{qa^4}$
20	2	125	0.004278	200	0.003983
	3	205	0.004353		0.004066
	4	285	0.004368		0.004062
	5	365	0.004376		0.004065
	6	445	0.004729		0.004308
	7	525	0.004732		0.004337
10	2	125	0.005029	100	0.003993
	3	205	0.005084		0.004077
	4	285	0.005094		0.004076
	5	365	0.005096		0.004079
	6	445	0.005494		0.004343
	7	525	0.005496		0.004354
Reference value [10]					0.004062

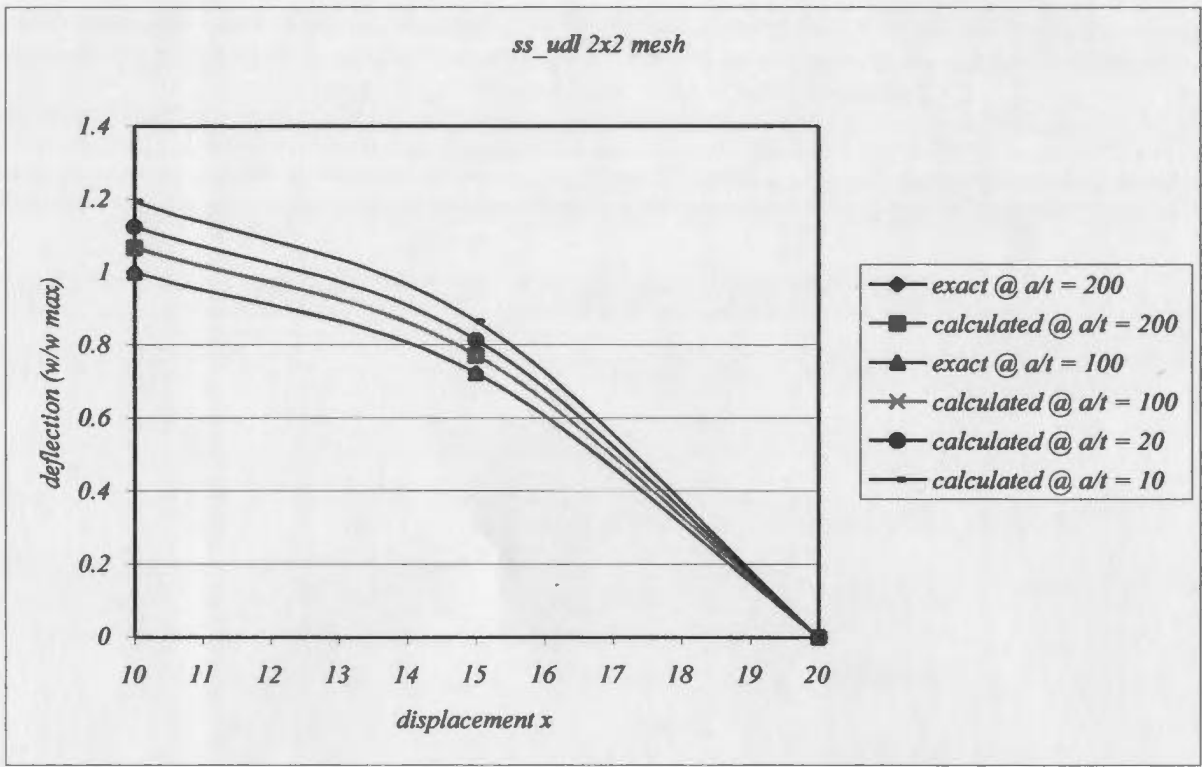


Figure 5.14: Plot of deflection of SS plate under UDL for various  $a/t$  ratios for 2x2 mesh  
 (w max is the central deflection according to thin plate theory)

Table 5.14: SS Plate under UDL: Displacements for different orders for 4x4 mesh

(Hierarchical 18-node solid thick shell element)

$a/t$	Order	DOF	$\alpha = \frac{W_{\max} D}{qa^4}$	$a/t$	$\alpha = \frac{W_{\max} D}{qa^4}$
20	2	405	0.004307	200	0.004046
	3	685	0.004321		0.004065
	4	965	0.004323		0.004066
	5	1245	0.004324		0.004067
	6	1525	0.004768		0.004326
	7	1805	0.0047707		0.004333
10	2	405	0.004979	100	0.004056
	3	685	0.004987		0.004075
	4	965	0.004988		0.004077
	5	1245	0.004988		0.004079
	6	1525	0.005511		0.004373
	7	1805	0.005513		0.004378
Reference value [10]					0.004062

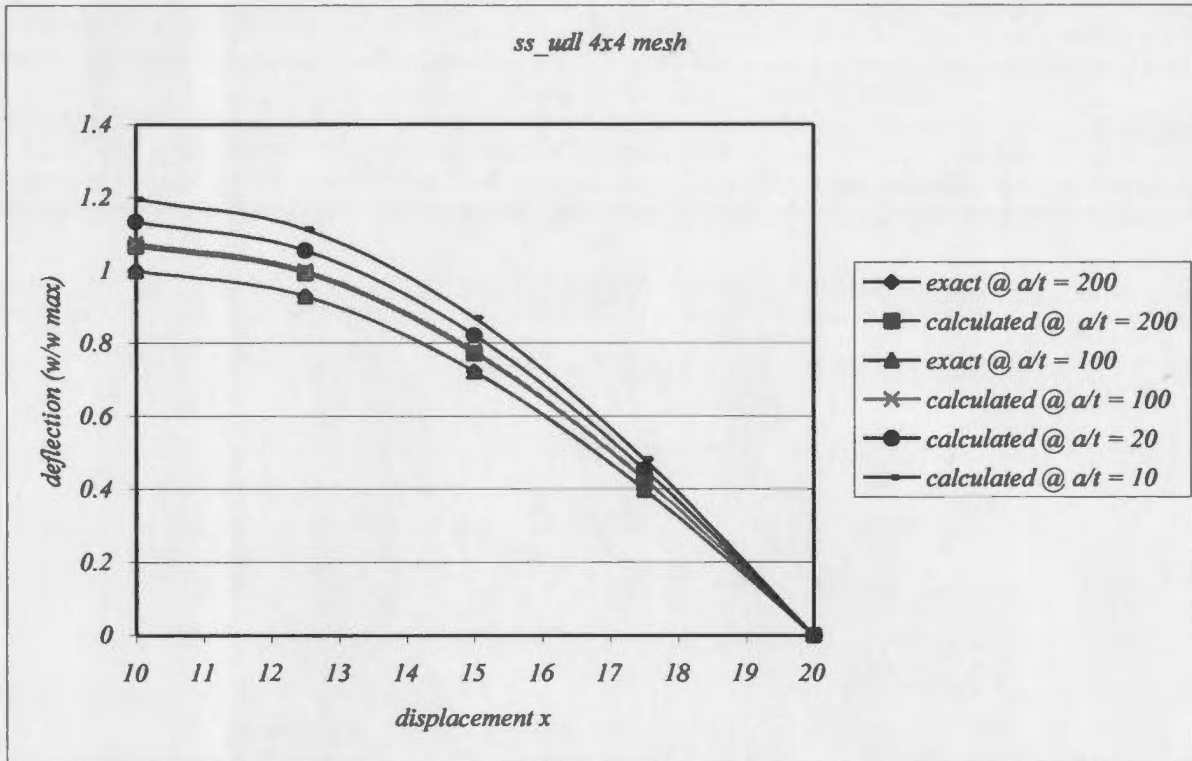


Figure 5.15: Plot of deflection of SS plate under UDL for various  $a/t$  ratios for 4x4 mesh  
( $w_{max}$  is the central deflection according to thin plate theory)

Table 5.15: Clamped Plate under UDL: Displacements for different orders for 2x2 mesh

(Hierarchical 18-node solid thick shell element)

$a/t$	Order	DOF	$\alpha = \frac{W_{\max} D}{qa^4}$	$a/t$	$\alpha = \frac{W_{\max} D}{qa^4}$
20	2	125	0.001328	200	9.9173e-4
	3	205	0.001482		0.001233
	4	285	0.001482		0.001218
	5	365	0.001482		0.0012302
	6	445	0.001519		0.001252
	7	525	0.001519		0.0012549
10	2	125	0.002071	100	0.0010044
	3	205	0.002134		0.001261
	4	285	0.002134		0.001255
	5	365	0.002134		0.001258
	6	445	0.002188		0.001281
	7	525	0.002189		0.001283
Reference value [10]					0.00126

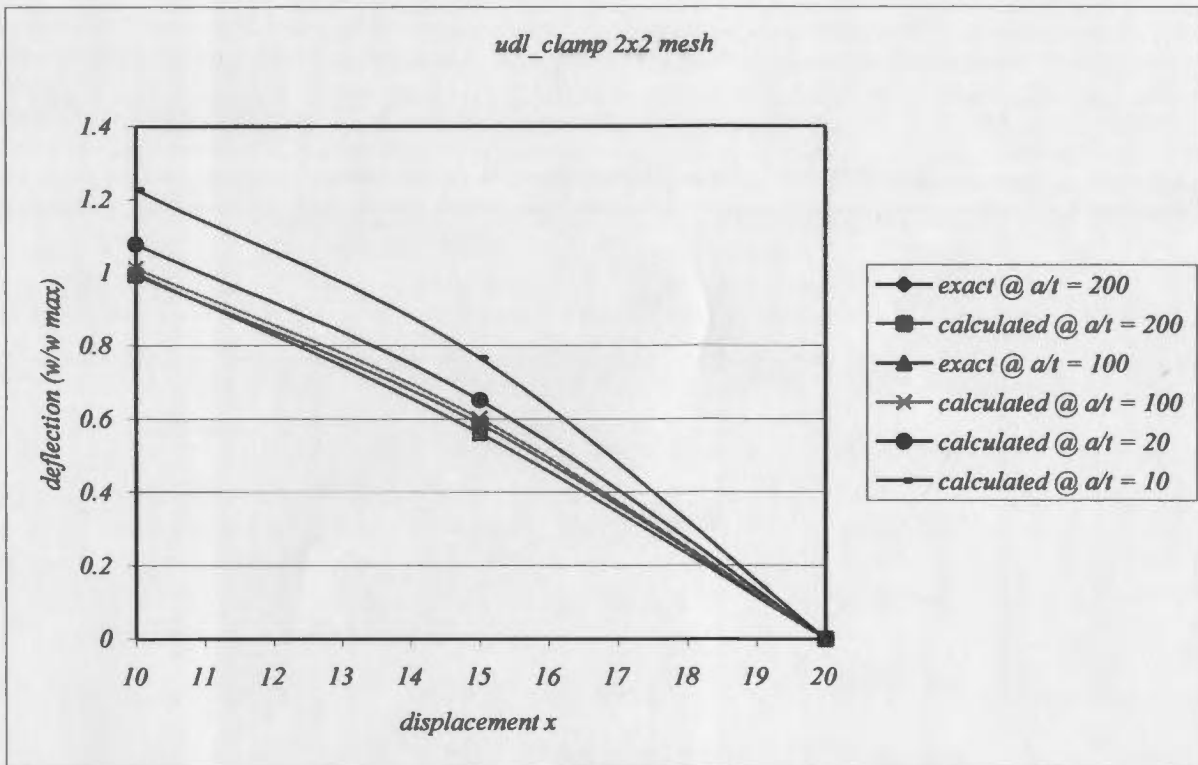


Figure 5.16: Plot of deflection of clamped plate under UDL for various  $a/t$  ratios for 2x2 mesh (w max is the central deflection according to thin plate theory)

Table 5.16: Clamped Plate under UDL: Displacements for different orders for 4x4 mesh

(Hierarchical 18-node solid thick shell element)

$a/t$	Order	DOF	$\alpha = \frac{W_{\max} D}{qa^4}$	$a/t$	$\alpha = \frac{W_{\max} D}{qa^4}$
20	2	405	0.001466	200	0.001199
	3	685	0.001485		0.001267
	4	965	0.001485		0.001267
	5	1245	0.001485		0.001267
	6	1525	0.001552		0.001304
	7	1805	0.001553		0.001304
10	2	405	0.0021306	100	0.0012109
	3	685	0.002136		0.001273
	4	965	0.002136		0.001274
	5	1245	0.002136		0.001274
	6	1525	0.002237		0.001316
	7	1805	0.002237		0.001316
Reference value [10]					0.00126

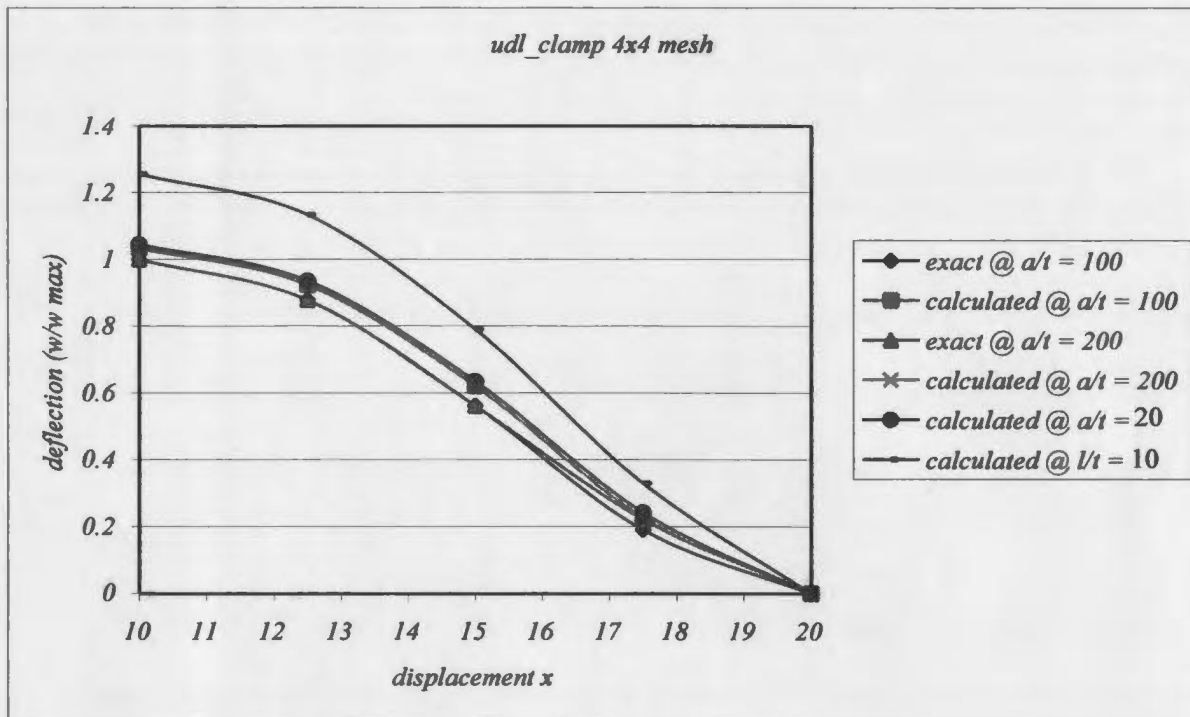


Figure 5.17: Plot of deflection of clamped plate under UDL for various  $a/t$  ratios for 4x4 mesh ( $w_{max}$  is the central deflection according to thin plate theory)

*Discussions:*

1. The results obtained are in excellent agreement with the exact values given by Zienkiewicz [10].
2. The solution converges to the exact value when a 4x4 mesh is used. 2x2 mesh gives reasonable good results with an error of 0.9 % in displacement.
3. For a particular mesh type, reasonably good results are obtained at order 3. For orders above 3, the change in the displacement solution is marginal and it converges towards a particular value.

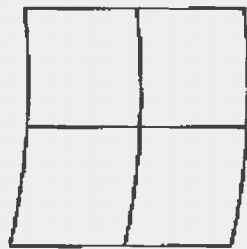
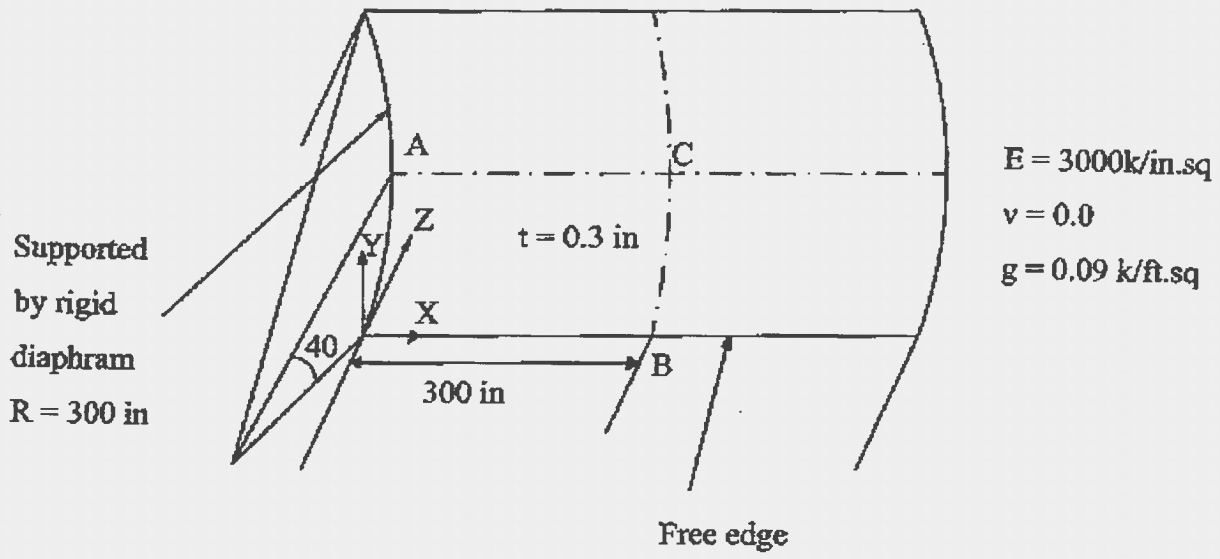
4. The solution obtained for thickness ratios 100 and 200 indicates (refer Figure 5.5) that the element gives accurate results for all the thin plate cases. This shows that the element is free of shear locking in thin plate cases. However, for obtaining accurate results, the analysis should be carried using higher orders (orders  $>3$ )
5. The solutions obtained for moderately thick plate (thickness ratios 10 and 20) deviate marginally from the exact thin plate solution. This is due to shear deformation effect in thick plates that is not considered in thin plate theory. Thus the developed element works well for both the thin and moderately thick plate analysis.
6. For the cases where central concentrated load is applied a refined mesh is necessary with degenerated plate/shell element. Where as for solid thick shell element, the refinement of mesh is not required.
7. The Hierarchical 18 noded solid element performs very well and gives the good results that agree with reference values. This element can be used for thick plates by employing higher orders in thickness direction.

## 5.2 Barrel Vault problem

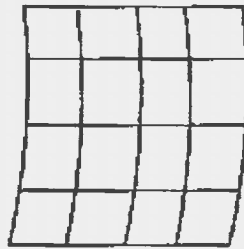
A barrel-vault supported by rigid diaphragms supported at both ends and loaded by its self-weight is shown in Figure 5.18. The diaphragm prevents the displacement in the  $Y$  and  $Z$  directions but allows displacements in the  $X$  directions. The shell is analyzed for both  $2 \times 2$  and  $4 \times 4$  meshes for different orders. The analyses were carried using both element types. The equivalent loads were obtained using mid surface and equally distributed for top and bottom nodes for plate/shell and thick solid shell elements. The numerical values for deflections obtained at points B and C shown in Figure 5.10 are compared with reference values given by Scrodelis and Lo [56]. The results are given in tables 5.17 and 5.18.

### *Discussions:*

1. The deep shell theory solution for the vertical deflection is -3.613 inches. The results obtained are in good agreement with the reference values.
2. The solution converges towards the reference values for both  $2 \times 2$  and  $4 \times 4$  cases. However, the results obtained deviates from the reference values by a margin of 1.3% for degenerated hierarchical plate/shell element and 2.4 to 5% for 18-node solid thick shell element for  $4 \times 4$  mesh for displacement at key points.
3. Improved results are obtained with lesser number of degrees of freedom compared to the references.



2x2 mesh



4x4 mesh

Figure 5.18: Barrel vault and its finite element meshes

Table 5.17: Displacements at B and C of cylindrical roof

(Hierarchical Degenerated plate/shell element)

Mesh	Order	DOF	$u_b$ (inches)	$w_b$ (inches)	$w_c$ (inches)
2x2	2	150	-2.0093	-3.8003	0.6107
	3	246	-1.9869	-3.7576	0.5796
	4	342	-1.9899	-3.7635	0.5807
	5	438	-1.9493	-3.6904	0.56709
	6	534	-1.92401	-3.6447	0.5545
	7	630	-1.9143	-3.6267	0.5462
4x4	2	486	-1.7485	-3.31609	0.4973
	3	822	-1.6797	-3.1848	0.4759
	4	1158	-1.6517	-3.1314	0.46809
	5	1494	-1.7549	-3.3279	0.4976
	6	1830	-1.8521	-3.5127	0.5252
	7	2166	-1.9309	-3.6626	0.5475
Reference value [56]			-1.904	-3.613	0.5412

Table 5.18: Displacements at B and C of cylindrical roof

(Hierarchical 18 noded solid thick shell element)

Mesh	Order	DOF	$u_b$ (inches)	$w_b$ (inches)	$w_c$ (inches)
2x2	2	150	-2.0902	-3.8569	0.5686
	3	246	-2.0366	-3.7617	0.5288
	4	342	-2.0012	-3.7028	0.51875
	5	438	-2.03165	-3.7506	0.5252
	6	534	-2.01835	-3.7276	0.5211
	7	630	-2.0215	-3.7326	0.5195
	4x4	2	486	-2.0518	-3.7906
3		822	-2.04115	-3.7713	0.5286
4		1158	-2.0398	-3.7688	0.5283
5		1494	-2.0397	-3.7686	0.5282
6		1830	-2.0385	-3.7667	0.5279
7		2166	-2.0388	-3.7671	0.5278
Reference value [56]			-1.904	-3.613	0.5412

## 5.3 Pinched Cylindrical Shell

A cylindrical shell shown in Figure 5.19 is loaded by two centrally located and diametrically opposed concentrated forces is analyzed. Two types of boundary conditions are considered.

1. The ends are covered by a rigid diaphragm, which allow displacement only in the axial direction and rotation about the tangent to the shell boundary.
2. The ends are free.

Using the double symmetry, only one eighth of the cylinder is modeled. The deflection obtained at load application point is compared with values given by Cook [24]. The results obtained are given in tables 5.19 and 5.20.

### *Discussions:*

1. The results are in good agreement with the reference values [24]. In the case of hierarchical degenerated plate shell element, 4x4 mesh gives a displacement of  $1.7093e-5$  with an error of 7.3 %. In the case of 18 node solid thick element, 4x4 mesh gives a displacement of with an error of 6.3%.
2. As seen in the previous example problems, p integration gives fairly good displacement solution at lower orders.

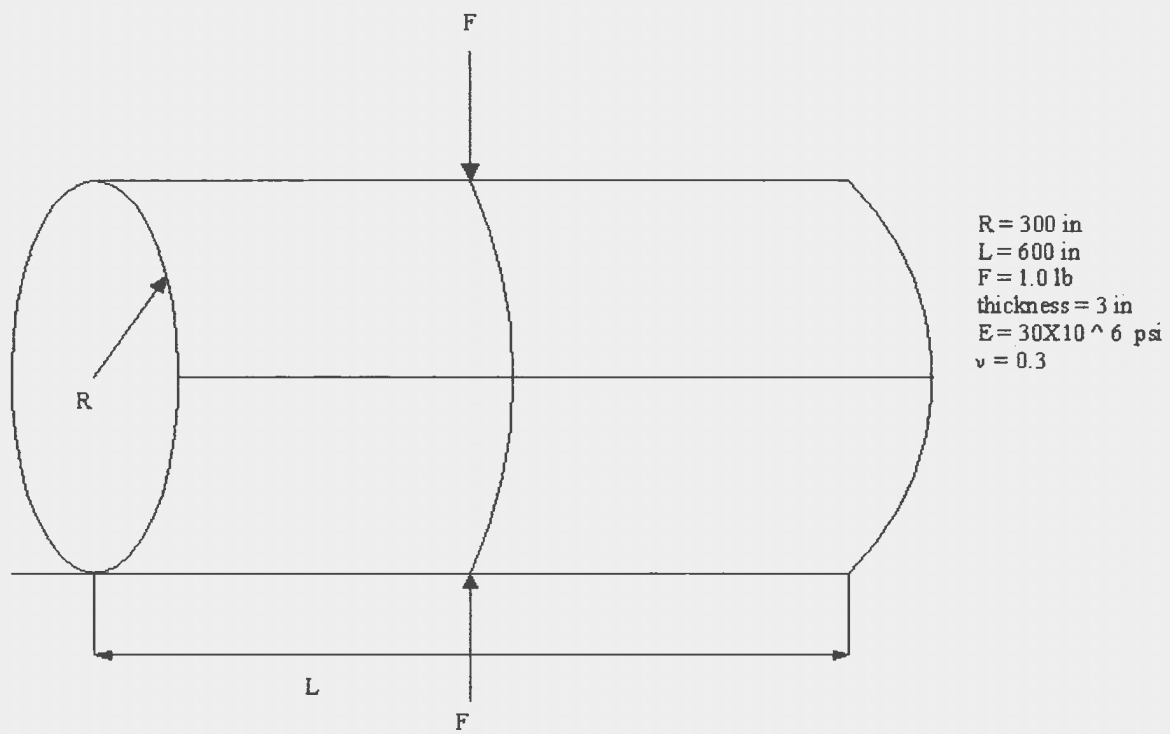


Figure 5.19: Pinched cylindrical shell, loading and dimensions.

Table 5.19: Deflection under the load of Pinched cylinder

(Hierarchical Degenerated Plate/Shell Element)

Mesh	Order	DOF	Deflection at Loaded point (inches)
2x2	2	125	2.3932e-5
	3	205	1.14904e-5
	4	285	1.2374e-5
	5	365	1.2744e-5
	6	445	1.30407e-5
	7	525	1.3243e-5
4x4	2	405	1.9129e-5
	3	685	1.7389e-5
	4	965	1.7624e-5
	5	1245	1.7345e-5
	6	1525	1.7207e-5
	7	1805	1.7093e-5
Reference value [24]			1.8248e-5

Table 5.20: Deflection under the load of Pinched cylinder  
(Hierarchical 18-node Solid thick shell element)

Mesh	Order	DOF	Deflection at Loaded point (inches)
2x2	2	125	2.55305e-5
	3	205	1.43225e-5
	4	285	1.03445e-5
	5	365	1.15779e-5
	6	445	1.2778e-5
	7	525	1.1443e-5
4x4	2	405	2.0175e-5
	3	685	1.72035e-5
	4	965	1.73481e-5
	5	1245	1.724403e-5
	6	1525	1.72595e-5
	7	1805	1.72279e-5
Reference value [24]			1.8248e-5

From the analysis of the benchmark problems, it can be seen that both hierarchical shell element and solid thick shell elements do not have shear locking and membrane locking problems.

## 5.4 Stress Intensity Factors Evaluation for Plates subjected to Bending Loads

In the previous sections, the correctness of the plate/shell elements derived and the software developed has been checked by considering some benchmark problems. In this section the accuracy of the bending stress intensity factors is examined as a function of plate thickness for a benchmark problem using the enriched crack tip plate/shell element. The material properties are assumed to be isotropic with Young's modulus  $E = 200$  GPA and Poisson's ratio  $\nu = 0.3$ .

### 5.4.1 Benchmark problem

As a benchmark problem, an infinite plate with a through thickness crack subjected to a far-field moment  $M_0$  was considered. The geometry of the problem considered is shown in Figure 5.20. In this configuration, the loading is purely mode I. To approximate an infinite plate, the plate width '2b' is taken to be 20 times the half crack length. The half crack length is taken to be  $a = 1.0$  for the results presented in this study. Taking advantage of the symmetry about y-axis only one-half of the plate is considered to analyze the problem. The problem is analyzed for various discretizations, varying size and number of elements around the crack tip. Very coarse mesh is used away from the crack tip. The obtained results are compared with the results given by Boduroglu and Erdogan [50]. The normalized  $(K_{Ib}/M_0\sqrt{a})$  values are presented for various b/h ratios (vide  $b/h = 2, 4, 6, 8,$  and  $10$ ) in the Table 5.21. From the table it can be seen that there

is an excellent correlation of the present results with reference values. Also the size of the elements near the crack tip affects the results as expected.

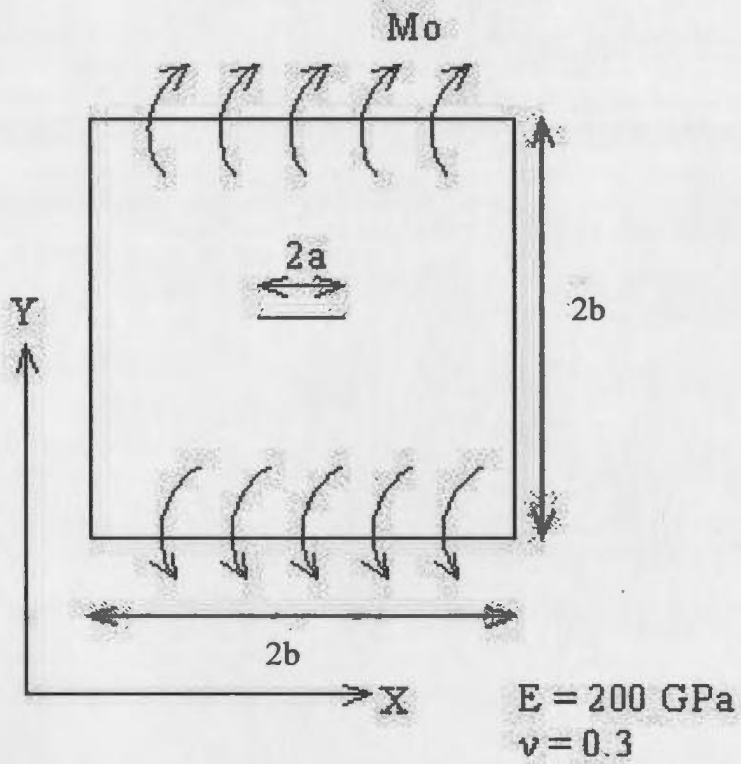


Figure 5.20: Centre crack under bending moment

Table 5.21: Normalized Stress Intensity factors in a plate containing central crack subjected to uniform bending  $M_0$  away from the crack region.  $a/b = 0.1$

b/h		10	8	6	4	2
Reference values						
Bodurogulu and Erdogan [50]		0.7526	0.7737	0.8045	0.853	0.9296
Element length near crack tip	No. of elements at the crack tip					
0.5	1	0.68461	0.717346	0.76565	0.850018	1.03089
	2	0.720625	0.7518	0.80112	0.89518	1.1079
	3	0.72867	0.7572	0.804014	0.8957	1.11401
0.4	1	0.72892	0.75469	0.790467	0.868185	1.02228
	2	0.78517	0.813304	0.85757	0.94205	1.1323
	3	0.7952	0.820511	0.86279	0.947824	1.14479
0.3	1	0.7405	0.75764	0.78925	0.84309	0.961509
	2	0.83035	0.84887	0.88368	0.95123	1.1065
	3	0.7173	0.7669	0.8375	0.94101	1.0796
0.2	1	0.703664	0.71178	0.7323	0.76973	0.850073
	2	0.82995	0.83712	0.858168	0.90334	1.01398
	3	0.85599	0.86209	0.88333	0.933574	1.0569
0.1	1	0.60181	0.60576	0.61995	0.645305	0.69066
	2	0.7414	0.74184	0.75463	0.783718	0.85026
	3	0.7739	0.77339	0.78548	0.81715	0.89339

## 5.4.2 Bending Stress Intensity factors for plate with central and edge cracks.

The bending stress intensity factors are evaluated for rectangular plate subjected an edge bending moment away from the crack region for various crack length to width ratios. The analyses are carried for two different thickness ratios. The stress intensity factors for central crack problem have been calculated by Bodurogulu and Erdogan [50]. Dirgantara and Aliabadi [49] gave numerical results for both central and edge cracks. The numerical results obtained from the present formulation along with the reference values are presented in Figures 5.21 to 5.25.

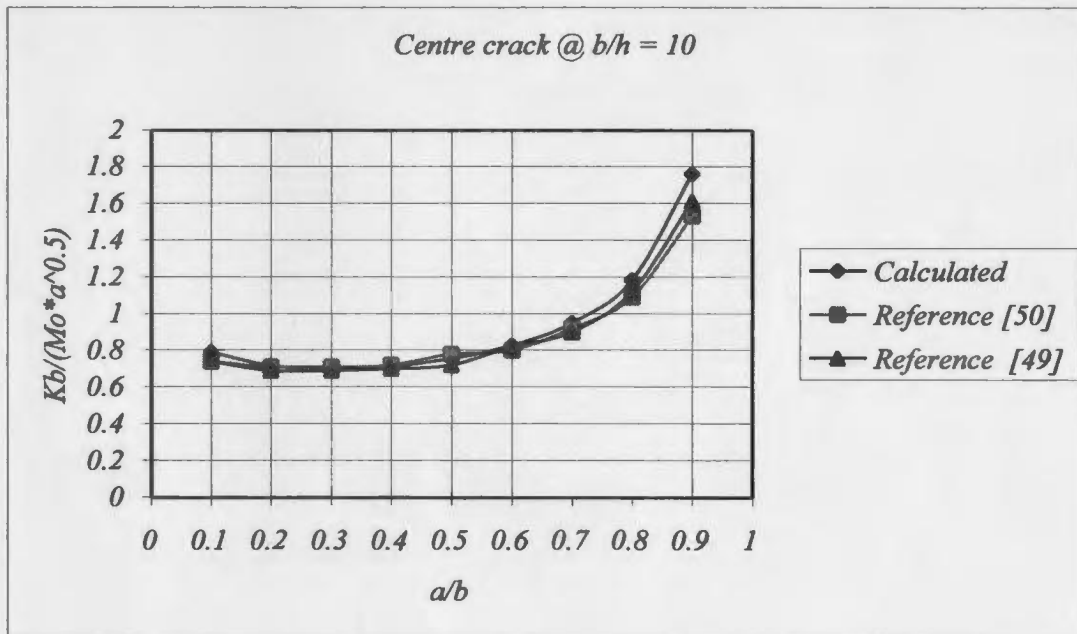


Figure 5.21: Plot of Bending Stress Intensity factor for centre-crack plate under bending moment for different crack lengths at  $b/h$  equal to 10

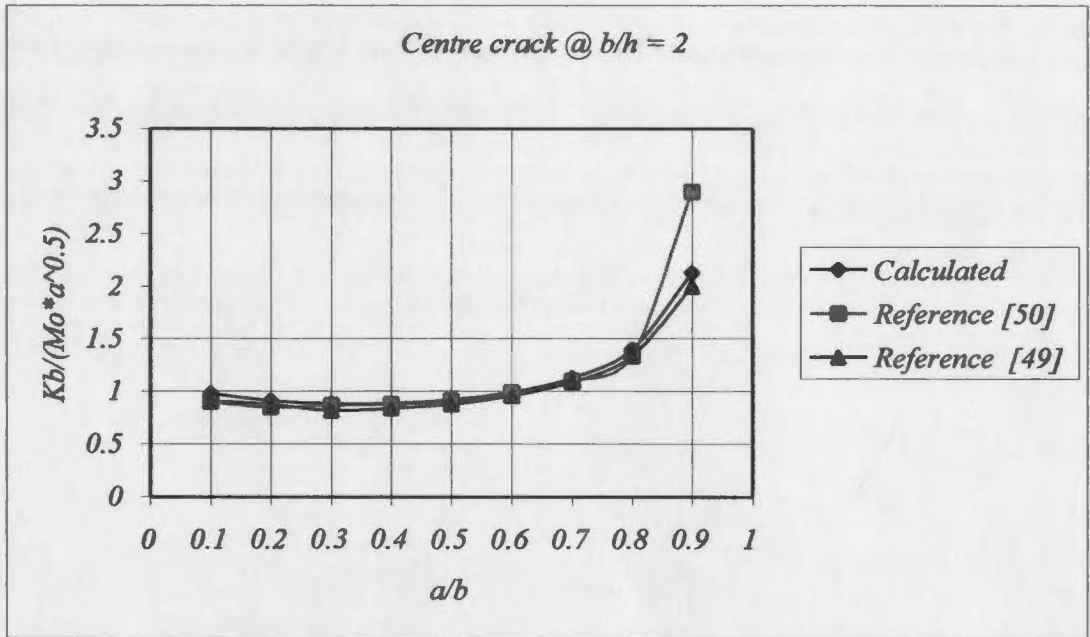


Figure 5.22: Plot of Bending Stress Intensity factor for centre-crack plate under bending moment for different crack lengths at  $b/h$  equal to 2

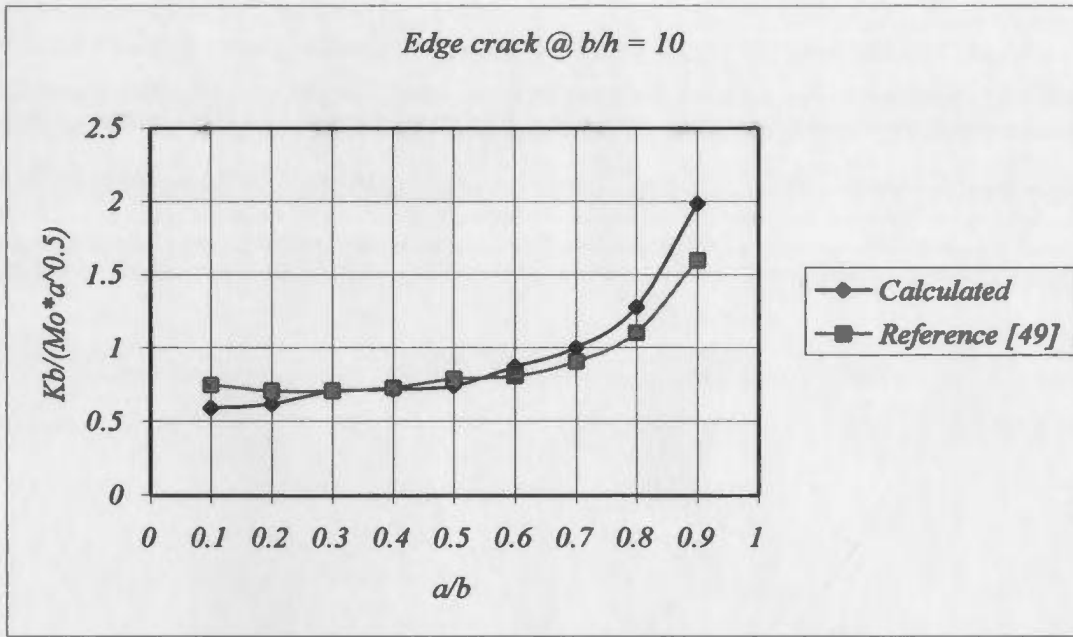


Figure 5.23: Plot of Bending Stress Intensity factor for edge-crack plate under bending moment for different crack lengths at  $b/h$  equal to 10

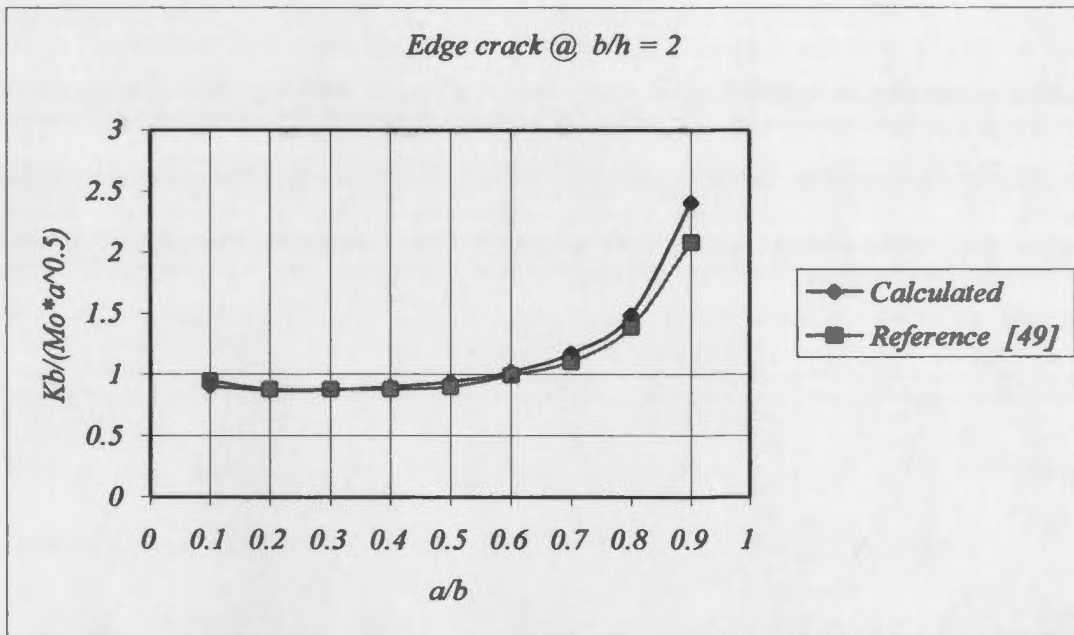


Figure 5.24: Plot of Bending Stress Intensity factor for edge-crack plate under bending moment for different crack lengths at  $b/h$  equal to 2

*Discussions:*

A benchmark problem of an infinite plate with through-thickness central crack subjected to far field end moment was analyzed. In order to study the effect of element size and mesh discretization on stress intensity factor centrally cracked plate with crack length to plate width ratio ( $a/b$ ) of 0.1 was analyzed with various mesh discretizations, varying the size and number of elements around the crack tip for different plate width to thickness ratios. The results obtained from the present analysis were compared with those reference values given by Bodurogulu and Erdogan [50] in the Table 5.21.

From this table it was observed the size of the element and number of elements surrounding the crack tip has an effect on the calculated SIF. From the analysis an element size of 0.1 with 2x2 or 3 x3 mesh surrounding the crack tip gives good results. The mesh division away from the crack tip do not affect the results.

The results obtained for central cracked and edge cracks for two plate width to thickness ratios ( $b/h$ ) for different crack length to plate width ratios are presented in the Figures 5.21 to 5.24 along with reference values. From these Figures it can be seen the results obtained from the present analysis compare very well with the reference values except for very high  $a/b$  ratios. For central crack the numerical results are in good agreement for thin and moderately thick plates. In the case of edge crack, for thin plates ( $b/h = 10$ ) the results deviate marginally from the solutions given by Dirgantara and Aliabadi [49]. For moderately thick plates, ( $b/h = 2$ ) the solutions are in excellent agreement.

From the results presented it can be concluded that the element developed in the present analysis can be used for thin and moderately thick plates.

# Chapter 6

## CONCLUSIONS AND RECOMMENDATIONS

### 6.1 Conclusions

Nine-node hierarchical degenerated plate shell element and eighteen-node hierarchical degenerated solid thick shell element are developed for analyzing the bending of plates and shells and also to perform crack analysis at centre and edge portions of the plate. The correctness of the developed formulation is verified by comparing the solutions with benchmark plate and shell problems. It is observed that both the elements perform very well and the results obtained are compared with reference values. They do not exhibit any shear and membrane locking. In closing, the following section deals with the results for the present formulation in comparison with benchmark problems available in literature.

#### Square Plate Problem

1. The numerical results obtained are in excellent agreement with the exact values available in literature for thin and moderately thick plates.
2. Refined mesh was employed for analyzing simply supported plate subjected to concentrated load for hierarchical degenerated plate shell element.
3. For hierarchical eighteen-node solid thick shell element uniform mesh gave compatible results. Therefore, it is concluded that solid thick shell element performs better than plate/shell element.

### Barrel vault problem

1. The results for the cylindrical roof cylinder show that the element formulation developed in the present work is free from shear and membrane locking for both hierarchical degenerated plate shell element and 18-node degenerated solid thick shell element.
2. The solid thick shell element converged well when compared to the reference values. Thus it is concluded that solid thick shell element performs well in comparison with hierarchical degenerated plate shell element

### Pinched Cylinder

1. Deflection at the load application point is in good agreement in correlation with the reference values
2. From the former examples it is concluded that p integration gives good results.

### Bending Stress Intensity factors for plate with central and edge crack

1. Bending Stress intensity factor obtained for infinite plate having central crack subjected to far moment are in good agreement with reference values given by Bodrogulu [50].
2. Rectangular plate with an edge crack under bending moment was analyzed. The numerical results were compared with Bodrogulu et al [50] and Dirgantara et al [49].
3. At centre crack length equal to 0.1 the hierarchical degenerated plate shell element gave excellent results for thin and moderately thick plates.
4. Also the same plate was analyzed for varying crack length from 0.1 to 0.9 for central crack and edge crack. For central crack, the numerical results are in good

agreement for thin and moderately thick plates. In case of edge crack, for thin plates ( $b/h$  equal to 10) the results deviate marginally from the solutions given by Dirgantara and Aliabadi [49]. For moderately thick plates, ( $b/h$  equal to 2) the solutions are in excellent agreement.

## 6.2 Recommendations

1. In the present work plate/shell element was used to obtain bending stress intensity factors. Solid thick shell element incorporating near crack tip displacement could be developed to obtain stress intensity factors of plates with through thickness cracks. Using thick solid element the interference of crack faces on compression side can be investigated.
2. Three dimensional crack front elements can be included along with the thick solid element to obtain stress intensity factors for part through thickness cracks in plates and shells.

## REFERENCES

1. Ottosen and Peterson, Introduction to the finite element method, (London, Prentice Hall International (UK) Ltd, 1992)
2. P-version Vs H-version – Part II cited November 4<sup>th</sup> 2004, available from [www.engineesclub.net/techpubs/ENGCLUBS8.doc](http://www.engineesclub.net/techpubs/ENGCLUBS8.doc)
3. K.S.Woo and P.K.Basu, “Analysis of singular cylindrical shells by p-version of FEM,” International Journal of Solids and Structures, 25 (1989) 151-165
4. R.H.Gallagher, “A review of finite element techniques in fracture mechanics,” Numerical Methods in Fracture Mechanics (Ed.A.R. Luxmoore and D.R.J.Owen), University College Swansea, Swansea,(1978), 1-25
5. S.B.Benzley and D.M.Parks, “Fracture mechanics,” Structural Mechanics Computer Programs (Ed.W.Pilkey, K.Saczalski and H.Schaeffer), University Press of Virginia, Charlottesville, (1974), 81-102
6. M.C.Apostal,S.Jordan and P.V.Marchal, “Finite element techniques for postulated flaws in shell structures,” Electric Power Research Institute, Palo Alto, Ca; EPRI SR-22 Special Report (1975)
7. M.L.Williams, “The bending stress distribution at the base of a stationary crack,” Journal of Applied Mechanics 28,78-82 (1961)
8. G.C.Sih, P.C.Paris and F.Erdogan, “Crack tip stress intensity factors for plane extension and plate bending problems,” Journal of Applied Mechanics 29,306-312 (1962)
9. G.C.Sih, “A review of three dimensional stress problems for a cracked plate,” International Journal of Fracture Mechanics 7, 39-59 (1971)

10. O.C.Zienkiwicz and Y.K.Cheung, The finite element method in structural and continuum mechanics Mc.Grawhill, London and NewYork, 1967
11. K.J.Bathe, Finite Element Procedure in Engineering Analysis Prentice Hall, NJ 1982
12. Barna A.Szabo and G.J.Sahramann, "Hierarchic plate and shell models based on p-extension," International Journal for Numerical Methods in Engineering, 26 (1988) 1855-1881
13. P.M.Naghdi, " On the theory of thin elastic shells," Quart. Appl. Math, XIV, 369-380 (1957)
14. S.Timoshenko and S.Woinowsky-Krieger,Theory of Plates and Shells, 2<sup>nd</sup> edn; McGraw-Hill, NewYork, 1959
15. V.V.Novozhilov, Thin Shell Theory, 2<sup>nd</sup> English translation, P.Noordhoff; Groningen, 1964
16. A.L.Goldenveizer, 'Derivation of an approximate theory of bending of a plate by the method of elasticity; Prikl Mat Mech; 26, 668-686 (1962) English translation: PMM, 1000-1025 (1964)
17. A.L.Goldenveizer, 'The principles of reducing three-dimensional problems of elasticity to two-dimensional problems of the theory of plates and shells', in H.Gortler (ed.), Proc. 11<sup>th</sup> Int. Congr. Of Theoretical and Applied Mechanics, Springer-Verlag, 1964, 306-311
18. K.O.Frederichs and R.F.Dressler, ' A boundary layer theory for elastic plates', Conm Pure Appl Math; 14, 1-33 (1961)
19. E.L.Reissner and S.Locke, 'On the theory of plane stress', Quart. Appl Math; 19, 195-203 (1961)

20. K.J.Bathe and L.W.Ho, "A Study of three-node triangular plate bending elements," International Journal for Numerical Methods in Engineering 15, 1771-1812 (1980).
21. R.W.Clough and J.L.Tocher, "Finite element stiffness matrices for analysis of plate bending," Proc. Conf. On matrix methods in Structural Mechanics, WPAFB, Ohio, 1965,515-545.
22. G.P.Bazeley, Y.K.Cheung, B.M.Irons and O.C.Zienkiwicz, "Triangular elements in plate-bending - conforming and non-conforming solutions, Proc. Conf. On Matrix Methods in Structural Mechanics, WPAFB, Ohio, 1965,547- 576.
23. T.Pian, "Element stiffness matrices for prescribed boundary stress," Proc. Conf. On matrix methods in Structural Mechanics, WPAFB, Ohio, 1965,457- 477.
24. R.D.Cook, " Four-Node 'Flat' Shell Element: Drilling degrees of freedom, membrane-bending coupling, warped geometry, and behavior," Computers and Structures 50, 549-555 (1994).
25. O.L.Roufaeil, " New Rectangular plate bending elements and their performance," Computers and Structures, 50 (1994).
26. A.Peano, "Hierarchies of conforming finite elements for plane elasticity and plate bending," Comp. And math. with Appls., Volume 1,211-224,1976
27. M.P.Rossow and I.N.Katz, "Hierarchical finite element and precomputed arrays," International Journal for Numerical Methods in Engineering, Volume 2,977-999,1974
28. O.C.Zienkiwicz, J.P.De, S.R.Gago and D.W.Kelly, "The hierarchical concept in finite element analysis," Computers and Structures, Volume 16,53-65,1983
29. B.A.Szabo, "Mesh design for the p-version of the finite element method," Computer Methods in Applied mechanics and Engineering, Volume 55,181-197,1986

30. I.Babuska, M.Griebel and J.Pitkaranta, "The problem of selecting the shape functions for a p-type finite element," International Journal for Numerical Methods in Engineering, volume 28,1891-1908,1989
31. R.B.Morris, Y.Tsuji, and P.Carnevali, "Adaptive solution strategy for solving large systems of p-type finite element equations," International Journal for Numerical Methods in Engineering, Volume 33,2059-2075,1972
32. K.S.Woo and P.K.Basu, "Analysis of singular cylindrical shells by p-version of FEM," International Journal of Solids and Structures, Volume 25,no 2,151-165,1989
33. B.A.Szabo and G.J.Sahrmann, "Hierarchic plate and shell element," International Journal for Numerical Methods in Engineering, Volume 26,1855-1881,1988
34. K.S.Surana and P.M.Sorem, "P-version hierarchical three dimensional curved shell element for elastostatics," International Journal for Numerical Methods in Engineering, Volume 31, 649-676,1991
35. Subbarayalu, " Hierarchical plate and shell elements incorporating symbolic computation", M.Engg Thesis, Memorial University of Newfoundland, 1999
36. Chandrasekhar Ganti, " Analyses of Stress Intensity for Structural Integrity in Mechanical Components", M.Engg Thesis, Memorial University of Newfoundland, 2005
37. J.Ahmad and F.T.C.Loo, " Solution of plate bending problems in fracture mechanics using a specialized finite element technique," Engineering Fracture Mechanics 11 (1979) 661-671.

38. G.Yagawa and T.Nishioka, "Finite element analysis of stress intensity factors for plane extension and plate bending problems," *International Journal for Numerical methods in Engineering* 14 (1979) 727-740.
39. O.C.Zienkiewicz, R.L.Taylor and J.M.Too, "Reduced Integration Technique in general analysis of plates and shells," *International Journal for Numerical Methods in Engineering* 3 (1971) 275-290
40. Wen-Hwa Chen and Pei-Yen Chen, "A hybrid-displacement finite element model for the bending analysis of the cracked plates", *International Journal of Fracture*, 24 (1984) 83-106.
41. T.Q.Ye and R.H.Gallagher, "A singular finite element for analysis of plate bending problem in fracture mechanics," *International Journal of Fracture*, 24 (1984) 137-147.
42. T. Watanabae, et al, "J.Integral analysis of plate and shell structures with through-wall cracks using thick shell elements," *Engineering Fracture mechanics*, 19 (1984) 1105-1112.
43. S.Ahmad, B.M.Irons and O.C.Zienkiwicz, "Analysis of thick and thin shell structures by curved finite elements," *International Journal for Numerical Methods in Engineering* 2,419-451 (1970).
44. C.G.Go, C.I.Lin, Y.S.Lin and S.H.Wu, "Formulation of a super-element for the dynamic problem of a cracked plate," *Communications in Numerical Methods in Engineering*, 14 (1998) 1143-1154.
45. R.Ehlers, "Stress Intensity factors and crack opening areas for axial through cracks in hollow cylinders under internal pressure loading," *Engineering Fracture Mechanics*, 25 (1986) 63-77.

46. G.Agnihotri, "Stress Analysis of a crack using the finite element method"  
Engineering Fracture Mechanics, 44 (1993) 109-125.
47. A.Vafai and H.E.Estekanchi, " A parametric finite element study of cracked plates  
and shells" Thin-Walled Structures, 33 (1999) 211-229.
48. M.V.V.Murthy, K.N.Raju and S.Viswanath, International Journal of Fracture 17,537-  
552 (1981).
49. T.Dirgantara, M.H.Alibadi, "Stress intensity factors for cracks in thin plates,"  
Engineering Fracture Mechanics 69 (2002) 1465-1486
50. H.Boduroglu and F.Ergodan , "Internal and Edge cracks in a plate of finite width  
under bending," Journal of Applied Mechanics 50 (1983) 621-629
51. L. N. Gifford Jr. and P. D. Hilton, "Stress Intensity Factors by enriched finite  
elements", Engineering Fracture Mechanics 10 (1978) 485-496
52. H.Sosa and G.Herman, " On invariant integrals in the analysis of cracked plates",  
International Journal of Fracture 40 (1989) 111-126
53. B.Szabo and I.Babuska, Finite Element Analysis, John Wiley and Sons, 1991
54. M.Suri, " Analytical and Computational assessment of locking in the hp finite  
element method", Computer Methods in Applied Mechanics and Engineering, 133  
(1996) 347-371
55. Y.Lieno, J.Pitkaranta, " On the membrane locking of h-p finite elements in a  
cylindrical shell problem", International Journal for Numerical Methods in  
Engineering, 37 (1994) 1053-10770
56. A.C.Scordelis and K.S.Lo, " Computer Analysis of Cylindrical Shells", Jl. Am.  
Concr. Inst; 61, May 1964

# APPENDICES

## Shape functions

### A.1 Hierarchical degenerated plate element

$$N1 = -\frac{1}{4}(1-\xi)(1-\eta)(1+\xi+\eta)$$

$$N2 = -\frac{1}{4}(1+\xi)(1-\eta)(1+\xi-\eta)$$

$$N3 = -\frac{1}{4}(1+\xi)(1+\eta)(1-\xi-\eta)$$

$$N4 = -\frac{1}{4}(1-\xi)(1+\eta)(1+\xi-\eta)$$

$$N5 = -\frac{1}{4}(1-\xi^2)(1-\eta)$$

$$N6 = -\frac{1}{4}(1+\xi)(1-\eta^2)$$

$$N7 = -\frac{1}{4}(1-\xi^2)(1+\eta)$$

$$N8 = -\frac{1}{4}(1-\xi)(1-\eta^2)$$

## A.2 Displacement field shape functions for hierarchical degenerated plate element

$$N1 = \frac{1}{4}(1-\eta)(1-\xi)$$

$$N2 = \frac{1}{4}(1-\eta)(1+\xi)$$

$$N3 = \frac{1}{4}(1+\eta)(1+\xi)$$

$$N4 = \frac{1}{4}(1+\eta)(1-\xi)$$

$$N5 = \frac{1}{4}(1-\eta)(\xi^2 - 1)$$

$$N6 = \frac{1}{4}(1+\xi)(\eta^2 - 1)$$

$$N7 = \frac{1}{4}(1+\eta)(\xi^2 - 1)$$

$$N8 = \frac{1}{4}(1-\xi)(\eta^2 - 1)$$

$$N9 = \frac{1}{4}(\eta^2 - 1)(\xi^2 - 1)$$

### A.3 Hierarchical 18 node solid plate element

$$N1 = -\frac{1}{8}(1-\xi)(1-\eta)(1+\xi+\eta)(1+\zeta)$$

$$N2 = -\frac{1}{8}(1+\xi)(1-\eta)(1+\xi-\eta)(1+\zeta)$$

$$N3 = -\frac{1}{8}(1+\xi)(1+\eta)(1-\xi-\eta)(1+\zeta)$$

$$N4 = -\frac{1}{8}(1-\xi)(1+\eta)(1+\xi-\eta)(1+\zeta)$$

$$N5 = -\frac{1}{8}(1-\xi)(1-\eta)(1+\xi+\eta)(1-\zeta)$$

$$N6 = -\frac{1}{8}(1+\xi)(1-\eta)(1+\xi-\eta)(1-\zeta)$$

$$N7 = -\frac{1}{8}(1+\xi)(1+\eta)(1-\xi-\eta)(1-\zeta)$$

$$N8 = -\frac{1}{8}(1-\xi)(1+\eta)(1+\xi-\eta)(1-\zeta)$$

$$N9 = -\frac{1}{4}(1-\xi^2)(1-\eta)(1+\zeta)$$

$$N10 = -\frac{1}{4}(1+\xi)(1-\eta^2)(1+\zeta)$$

$$N11 = -\frac{1}{4}(1-\xi^2)(1+\eta)(1+\zeta)$$

$$N12 = -\frac{1}{4}(1-\xi)(1-\eta^2)(1+\zeta)$$

$$N13 = -\frac{1}{4}(1-\xi^2)(1-\eta)(1-\zeta)$$

$$N14 = -\frac{1}{4}(1+\xi)(1-\eta^2)(1-\zeta)$$

$$N15 = -\frac{1}{4}(1-\xi^2)(1+\eta)(1-\zeta)$$

$$N16 = -\frac{1}{4}(1-\xi)(1-\eta^2)(1-\zeta)$$

## A.4 Displacement field shape functions for hierarchical 18 node solid plate element

For corner nodes

$$N1 = \frac{1}{8}(1-\eta)(1-\xi)(1+\zeta)$$

$$N2 = \frac{1}{8}(1-\eta)(1+\xi)(1+\zeta)$$

$$N3 = \frac{1}{8}(1+\eta)(1+\xi)(1+\zeta)$$

$$N4 = \frac{1}{8}(1+\eta)(1-\xi)(1+\zeta)$$

$$N5 = \frac{1}{8}(1-\eta)(1-\xi)(1-\zeta)$$

$$N6 = \frac{1}{4}(1-\eta)(1+\xi)(1-\zeta)$$

$$N7 = \frac{1}{8}(1+\eta)(1+\xi)(1-\zeta)$$

$$N8 = \frac{1}{8}(1+\eta)(1-\xi)(1-\zeta)$$

for mid side nodes and central node

$$N9 = \frac{1}{8}(1-\eta)(\xi^2 - 1)(1+\zeta)$$

$$N10 = \frac{1}{8}(1+\xi)(\eta^2 - 1)(1+\zeta)$$

$$N11 = \frac{1}{8}(1+\eta)(\xi^2 - 1)(1+\zeta)$$

$$N12 = \frac{1}{8}(1-\xi)(\eta^2 - 1)(1+\zeta)$$

$$N13 = \frac{1}{8}(1-\eta)(\xi^2 - 1)(1-\zeta)$$

$$N14 = \frac{1}{8}(1+\xi)(\eta^2 - 1)(1-\zeta)$$

$$N15 = \frac{1}{8}(1+\eta)(\xi^2 - 1)(1-\zeta)$$

$$N16 = \frac{1}{8}(1-\xi)(\eta^2 - 1)(1-\zeta)$$

$$N17 = \frac{1}{8}(\eta^2 - 1)(\xi^2 - 1)(1+\zeta)$$

$$N18 = \frac{1}{8}(\eta^2 - 1)(\xi^2 - 1)(1-\zeta)$$



